HIGH SPIN STATES OF SOME XENON AND TELLURIUM ISOTOPES

by

ERIC BARNABY RAMSAY B.Sc

A thesis submitted to the faculty of Graduate Studies and Research in partial fulfillment of the requirements for the degree of Master of Science.

Foster Radiation Laboratory

McGill University, Montreal

Quebec, Canada

ABSTRACT

High spin states in $^{126,128}Xe$ and ^{116}Te have been studied in the (α,4nγ) reactions on enriched Tellurium and Tin targets using in-beam gamma-ray spectroscopic methods. For both Xenon nuclei, new levels at high spins have been proposed. The occurrence of backbending in the $^{126,128}Xe$ nuclei is also examined. For the ^{116}Te nucleus, two new levels have been tentatively assigned.

RESUME

Les états de spin élevé des isotopes $^{126,128}Xe$ et ^{116}Te ont été étudiés, par des méthodes de spectro-scopie gamma en ligne, lors de réactions (α,4nγ) sur des cibles de Tellure et d'Etain enrichies. Dans le cas des deux noyaux du Xénon, de nouveaux niveaux de spin élevé ont été proposés. La possibilite que le phénomène de "backbending" se produise, pour les noyaux $^{126,128}Xe$ a également été considérée. Pour le noyau ^{116}Te, deux nouveaux niveaux ont été proposés a titre d'essai.

ACKNOWLEDGEMENTS

It is a pleasure for me to express my sincere gratitude to my thesis supervisor, Prof. J.E. Kitching, for his guidance during the course of this work and for his unlimited patience in the face of my many missed deadlines.

It would be impossible to list the numerous favors done for me by Prof. J. Crawford while this work was in progress. I offer my deepest thanks for all his help.

I wish to thank the director of the lab, Prof J.K.P. Lee, for providing the necessary stimuli to keep the writing of this thesis going at a constant pace.

My colleagues Mr. Shlomo Kovalski and Mr. Ali Alousi are also thanked. The former for the exciting discussions had, the latter for his help with the more pragmatic matter of finding useful research papers. I also wish to thank Mr. Richard Turcotte for the French translation of the abstract.

Dr. Ken Oxorn and Dr. Kamilia Sofia are kindly thanked for their roles as tutors during the early part of this work.

Special thanks go to Mr. Leo Nikkenen and Mr. Mario Della Neve for working their black art and keeping the cyclotron in working condition while the experiments were in progress.

Finally, I wish to thank my parents for their never failing encouragement and support.

The award of a Carl Reinhardt Bursary during the course of this work is gratefully acknowledged.

TABLE OF CONTENTS

LIST OF TABLES

LIST OF FIGURES

Chapter I: Introduction

In the field of human endeavours, research in the natural sciences provides one of the most stimulating and challenging occupations available for the interested individual. The scientific method has proven to be most efficacious in bringing to light the underlying form and processes of nature responsible for the diversity of phenomena we see around us. It has been the author's good fortune to have worked in one interesting area of research, namely that of In Beam Gamma-Ray Spectroscopy (I.B.γ.), conducted here at McGill. The work to be presented concerns itself with the experimental determination of the excited states of three nuclei: ^{126}Xe, ^{128}Xe, and ^{116}Te. To understand the purpose and nature of this work a brief background is given.

Nuclear physics effectively began in 1911 when Lord Rutherford and his associates discovered that the scattering of alpha particles by gold atoms could be best explained if atoms consist of a small, massive, positively charged core surrounded by orbiting electrons. The magnitude of this core, called the nucleus, was estimated by Rutherford to be on the order of 10^{-14} m. Since then, the nucleus has been found to be constituted of nucleons of two types: the zero charged neutrons and the positively charged protons. The force which holds the nucleus together against the proton-proton repulsion is called the 'strong' force.

Studies of nuclei indicate that the strong force has a short range, on the order of the average distance between nucleons in the nucleus i.e. between 1 and 2 fermis. Further, the nuclear force saturates leading to nuclei which all have similar internal densities and which have radii

proportional to $A^{1/3}$ where A is the number of nucleons. Further understanding of the strong force has come mainly from an examination of the two body nucleon-nucleon interaction. The results of studying these nucleon-nucleon systems indicate that any description of the nuclear force needs to include the following(1):

a) Terms depending on the spin degree of freedom:

A direct spin-spin interaction of the form:

$$\vec{\sigma}_1 \cdot \vec{\sigma}_2 V(|\vec{r}_1 - \vec{r}_2|)$$

a spin orbit interaction:

$$[(\vec{\sigma}_1 + \vec{\sigma}_2) \cdot (\vec{r}_1 - \vec{r}_2) \times (\vec{p}_1 - \vec{p}_2)] V(|\vec{r}_1 - \vec{r}_2|)$$

and a tensor interaction:

$$\{3[\vec{\sigma}_1 \cdot (\vec{r}_1 - \vec{r}_2)][\vec{\sigma}_2 \cdot (\vec{r}_1 - \vec{r}_2)] - (\vec{r}_1 - \vec{r}_2)^2 \vec{\sigma}_1 \cdot \vec{\sigma}_2\} V(|\vec{r}_1 - \vec{r}_2|)$$

b) Charge symmetry and charge independence. The former referring to the fact that the nuclear force is known to be the same for n-n and p-p interactions, the latter referring to evidence that for p-n interactions where the space-spin states are the same as for n-n and p-p reactions the interactions are also the same.

c) An exchange potential to allow for exchange of charge.

d) A repulsive core.

Despite these known attributes of the nuclear force, mathematical descriptions for the force which differ from each other can be found which satisfy the experimental data equally well. Because of this lack of precise knowledge of the nuclear force, in addition with its evident complexity, it becomes very difficult to derive the properties of nuclei

using a fundamental approach. As a result, to gain any understanding of nuclei at all, experimental data on nuclei are interpreted in terms of various nuclear 'models' that are invented to fit the facts.

Depending upon the number of nucleons in the nucleus being studied, some models become more appropriate than others in describing nuclear behaviour. It may even happen that more than one model is invoked to describe different aspects of the same nucleus. One of the most successful models to be used is the shell model introduced independently by M.G. Mayer (2) and Haxel,Jensen and Suess (3). This model was suggested by the experimental evidence that, similar to the case of electrons in atoms, the nucleons filled up nuclear orbitals in a definite sequence which lead to shell effects. These 'shells' occur independently for neutrons and protons when their numbers in nuclei reach 2, 8, 20, 28, 50, 82, 126 and 184. When both neutron and proton number equals a shell closure, the nucleus is found to be especially stable, in analogy to the inert elements. The shell model considers particle motion in a spherical potential with strong L-S coupling forces. In this way the model is able to reproduce the shell sequence for nuclei found above.

In addition to the evidence for shell structure it was also known that nuclear behaviour indicated the effects of collective nuclear motion (4,5,6,7,8,9). Bohr(7) in 1952 proposed a collective model to explain collective behaviour and then with Mottelson(9) in 1953 proposed a unified model where the nucleus is described in terms of particle and collective degrees of freedom.

Nilsson(10) in 1955 introduced a model, since named the Nilsson model, where the nuclei were treated by considering particle motion in a deformed well. More recently, Stephens(11) has interpreted nuclei showing

collective behaviour in terms of the Coriolis effects introduced as a result of their rotation.

The abundance of possible viewpoints from which to describe nuclear structure thus necessitate experiments which can indicate which theoretical approach is most suited to which nucleus and over what energy range. Also, further experimental work may also lead to more general models which unify these theoretical approaches. As is evident, one of the most useful experimental datum is to have a precise knowledge of the level schemes of the excited states of nuclei to as high a spin as is experimentally possible. We want to obtain high spins since a proper description of the levels over a greater range requires that the models be made more refined. It is to satisfy this need that the experimental method of In Beam Gamma-Ray Spectroscopy proves useful. By performing (α,xnγ) reactions one is able to project out of the many nuclear states certain of them which are amenable to study using simple models. Other nuclear reactions, (p,γ) etc., will, over the same energy range, project out a different set of states in general. Thus by selecting the probing reaction one may select states associated with one or possibly two models.

Historically, I.B.γ. began in 1963 when Morinaga and Gugelot(12) observed that discrete gamma-rays can be detected during the de-excitation of nuclei produced by (α,xn) reactions. Many of the basic features of this type of reaction have since been understood and an outline is provided here:

When an incoming projectile, such as an α-particle, collides with some target nucleus then, providing the projectile has sufficient kinetic energy to overcome the Coulomb repulsion of the target a new system may be formed called the compound nucleus. For medium heavy target nuclei the

cross-section for the compound nucleus normally dominates the cross-section for other reactions for projectile energies moderately above the Coulomb barrier (13). The compound nucleus exists in a very excited state and immediately begins to 'evaporate' off neutrons, protons and alpha particles(14). Generally, however, the Coulomb barrier suppresses the emission of charged particles and neutron evaporation predominates. Depending on the energy of the projectile, one type of (α,xn) reaction predominates. For example, at an α-particle lab energy of 59 MeV the $^{126}Te(\alpha,4n)^{126}Xe$ reaction has the highest cross-section for occurring over other possible reaction channels. After the final neutron is emitted we are left with what is called the residual nucleus. The residual nucleus exists in an excited state where its energy is less than the neutron binding energy. De-excitation of the residual nucleus takes place through the emission of gamma-rays and internal conversion electrons. The initial de-excitation consists of gamma-rays from what is called the statistical region(15). This region represents the high density of levels at high excitation. The gamma-rays from this region register in the gamma-ray spectrum as a continuous background with individual gamma-rays being unresolved. Because gamma-rays are inefficient at removing angular momentum from the residual nucleus, there is a tendency for the gamma cascade to reach first to the lowest energy state for a given spin and then to cascade down further along the lowest energy, highest spin level sequence. This latter sequence is called the Yrast line(16). It is these gamma-rays from the Yrast line which stand out in a spectrum above the unresolved background of statistical gamma-rays. This cascade of gamma-rays is referred to as the ground band. Examination of a spectrum, however, usually shows a number of discrete gamma-rays which are not part

of the ground band. These gamma-rays come from side-bands which receive their feeding also from the statistical region and then they in turn feed members of the ground band. Figure 1 offers an overview of the transitions taking place. For all electromagnetic transitions, except those between states of zero angular momentum, γ-ray emission and internal conversion compete. In the latter case, the available energy and angular momentum changes are transferred to an orbital electron which is then ejected.

The highest spin state that one may expect to observe depends on the amount of angular momentum brought in by the projectile. Classicaly, the maximum angular momentum is(17):

$$L_{max} \approx 0.25\sqrt{M(E - Eb)}\ (A^{1/3} + M^{1/3})$$

where A is the atomic mass of the target, M the projectile mass, E the projectile's energy in MeV and Eb the Coulomb barrier in MeV. Eb is found from $Eb \approx zZ/A^{1/3}$ where z and Z are the target and projectile atomic numbers. For the nuclei studied in this work we have:

^{126}Xe with E = 48 MeV, $L_{max} \approx 17$

^{128}Xe with E = 48 MeV, $L_{max} \approx 17$

^{116}Te with E = 59 MeV, $L_{max} \approx 20$

In 1971 and 1972 Johnson et al. (18,19) studying the ^{160}Gd(α,4n)^{160}Dy reaction plotted $2\,\mathcal{J}_I / \hbar^2$ where $\mathcal{J}_I$ is the effective moment of inertia for a transition I→ I-2, versus $\hbar^2\omega^2 = 4(I^2 - I+1)(E_I - E_{I-2}/4I-2)^2$ and found that below I=10 , $\mathcal{J}_I$ increases smoothly with ω^2, but above I=12 sudden jumps take place. This effect is called 'back-bending' because of its shape. The satisfactory explanation of this effect forces further refinements to be made to nuclear models and since its discovery much

Figure 1

Flow diagram for gamma-rays produced in (α,xnγ) reactions.

Taken from Morinaga(15)

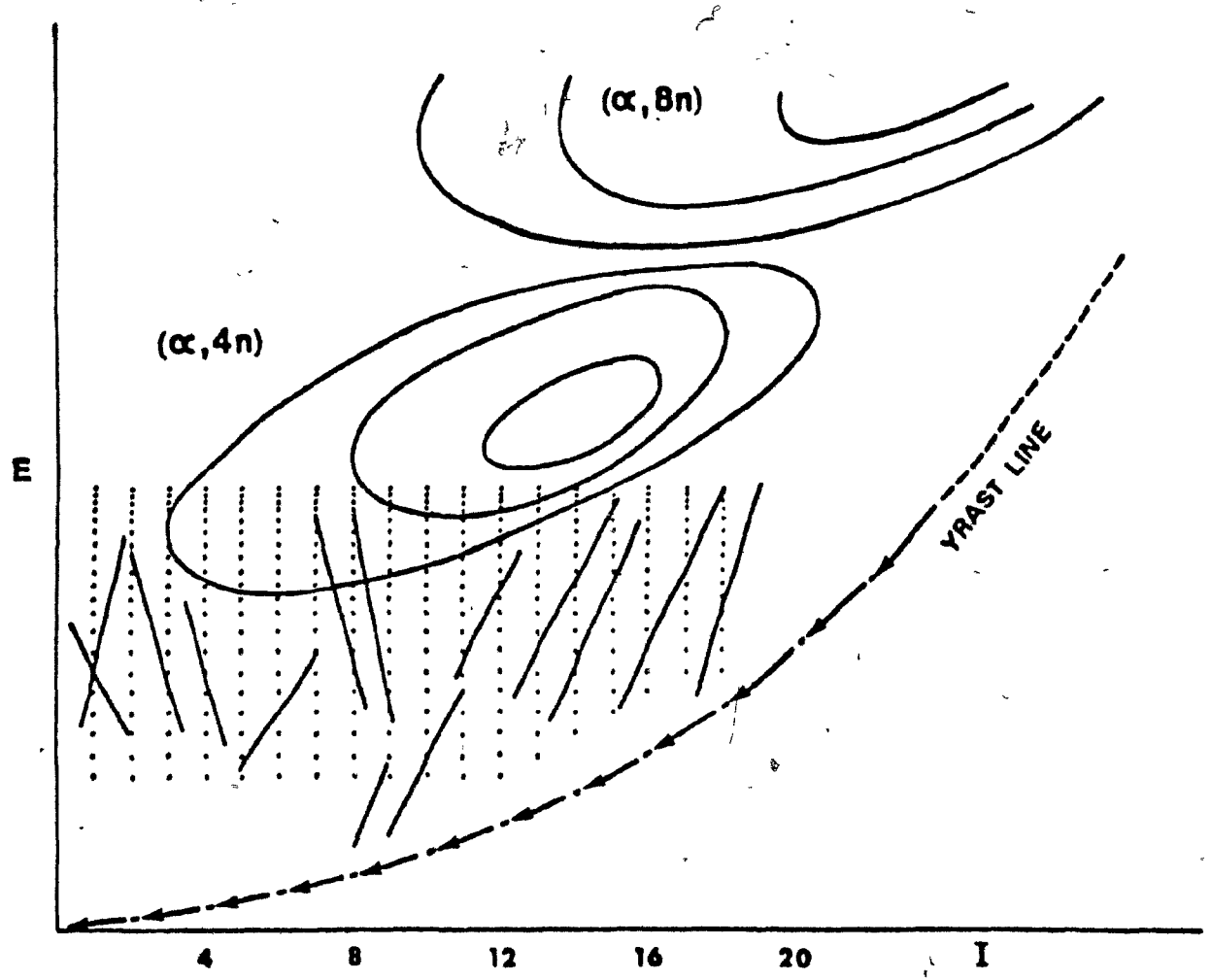
(α,8n)
(α,4n)
E
YRAST LINE
4
8
12
16
20
I

effort has been made in the investigation of high spin rotational levels(13,20,21). Since high spin states are expected from the (α,xn) reactions in this work, this phenomenon will also be examined.

In-beam gamma work began at McGill in 1979. Since that time, many nuclei have been successfully studied using this technique. Since it becomes more difficult to do pioneering work using alpha particles, this thesis represents the last experiments to be carried out in this field using the McGill equipment.

Chapter II - Experimental Apparatus

A) Cyclotron:

The alpha particle beam required for I.B.Y. work is produced by the McGill synchrocyclotron. This machine was commissioned for use in 1949 and now bears the distinction of being the oldest working cyclotron in Canada. However, like a fine wine, the performance of this machine has improved with age. At present, alpha paricles, deuterons, protons and $^{3}He^{++}$ may be accelerated to maximum energies of 100, 50, 100 and 133 MeV respectively.

The requirement for a source of alpha particles is met by a radial ion P.I.G source (Figure 2). Referring to the figure, helium gas is fed in from the top of the anode and is subsequently ionized by means of a discharge between the anode and the two cathodes, the latter being located at the top and bottom of the ion source. The helium ions, both singly and doubly charged, as well as unionized helium atoms, exit radially through a slit in the anode. The body of the ion source is water cooled so that heat released in the discharge (about 2 kw.), may be dissipated. The ion source is maintained at a positive potential of +3 kv. so as to repel the positive ions. This is necessary since the placement of the water pipes block the trajectory of the ions on their first orbit.

Having so obtained a source of alpha particles, it is now necessary to accelerate them. Figure 3 shows the principal components of the synchrocyclotron, including the Dee. The Dee has a radio frequency high voltage of approximately 15 kv applied to it. This allows for acceleration of the alpha particles by alternately attracting and repelling the particles as they enter and exit the Dee in their spiral orbit. The spiral

Figure 2:

Radial Ion Source

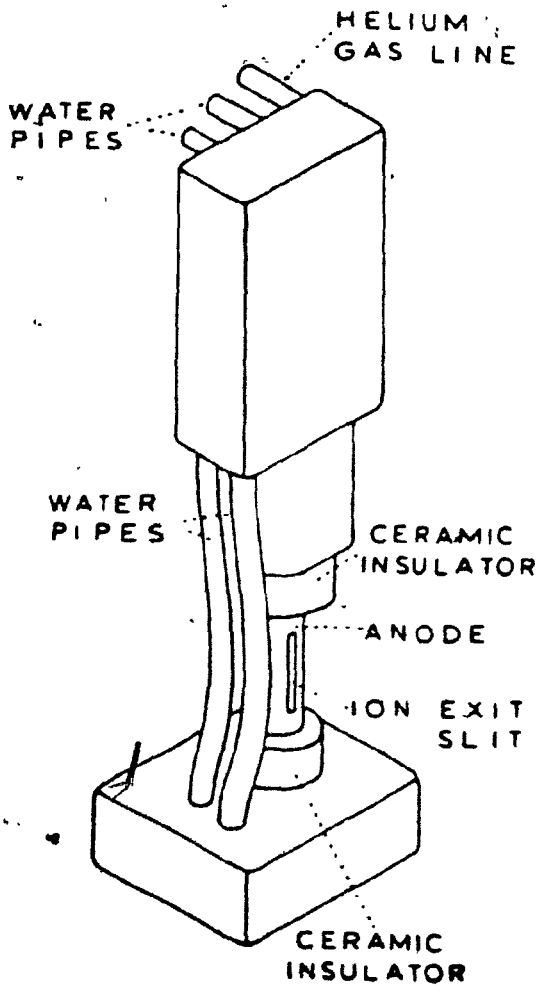
HELIUM
GAS LINE
WATER
PIPES
WATER
PIPES
CERAMIC
INSULATOR
ANODE
ION EXIT
SLIT
CERAMIC
INSULATOR

Figure 3:

The Synchrocyclotron

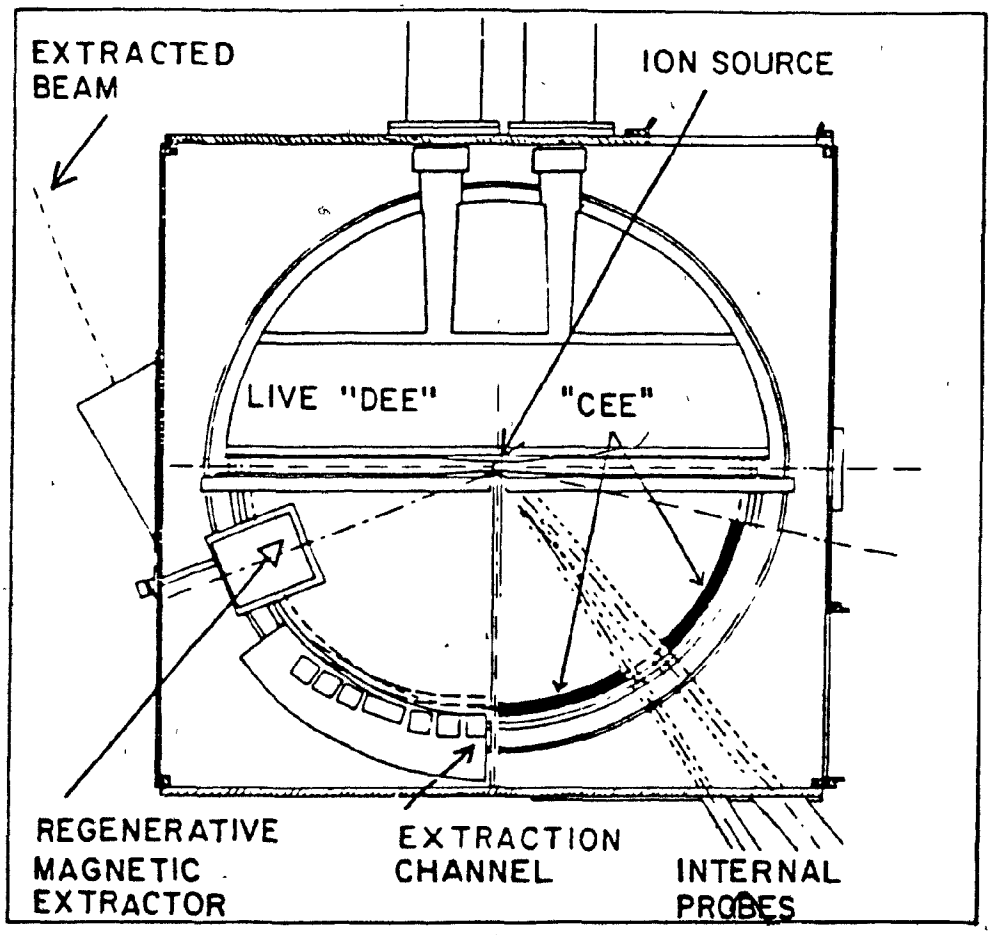
EXTRACTED
BEAM
ION SOURCE
LIVE "DEE"
"CEE"
REGENERATIVE
MAGNETIC
EXTRACTOR
EXTRACTION
CHANNEL
INTERNAL
PROBES

motion is brought about by a large electromagnet , the pole faces of which cover the top and bottom of the Dee and defines the maximum radius of the orbiting particles. The magnetic field is cylindrically symmetric and falls off with the radius. The field strength at the centre of the magnet is approximately 17 KGauss. The alpha particle may be selectively accelerated by exploiting the charge to mass ratio difference between it and other ions present. As the alpha particles increase in velocity, they undergo a relativistic mass increase. This increase in mass is a function of increasing orbit radius and, coupled with the shaped magnetic field, causes the particles' orbital velocity to decrease. To compensate for this, the frequency of the radio frequency voltage applied to the Dee is lowered appropriately so as to provide phase stability to the accelerating particles. At an orbit radius of 36 inches, the particles have their maximum energy and are then extracted. The time taken for the beam to travel from the ion source at the centre of the cyclotron to the point of extraction is 600 μs. The beam is represented by bunches of particles 25 μs long.

Stretcher:

For reasons that will be dealt with later, it is more useful to have a continuous beam of alpha particles rather than the pulsed beam the cyclotron gives. The 'Cee' shown in figure 3 enables us to do this. This changing of the beam profile from a pulsed to a continuous mode is accomplished as follows:

At a radius of approximately 32 inches, the radio frequency to the Dee is turned off. To obtain further acceleration to the 36 inch extraction orbit, an oscillating voltage of -5 kv is applied to the Cee. The Cee is simply two 'c' shaped copper sheets separated by Teflon

supports to a distance of 4 inches. It is also electrically isolated from the rest of the cyclotron. The radio frequency voltage applied to the Cee is out of phase with the radio frequency that was applied to the Dee and contains random frequency components equivalent to noise. This has the effect of destroying the phase stability of the bunched beam and the particles are smeared out over the time interval between beam packets thus giving a D.C. beam. This apparatus is called the 'stretcher' and was built by Mr. Leo Nikkinen of this laboratory. The stretcher gives us a duty cycle of 100% as compared to 0.2% to 0.4% for the unstretched beam.

Regenerative Magnetic Extractor

The last thing to be dealt with in the cyclotron is the regenerative magnetic extractor shown in figure 3. This bit of hardware is a piece of iron which causes an increase in the local magnetic field, perturbing the orbit of the particles passing by. The orbit perturbation of the particles takes the form of an unstable radial oscillation which grows exponentially with each orbit. Eventually, the orbit amplitude carries the particles into the extraction channel from where they exit the cyclotron. The extraction efficiency is typically 10% and is a strong function of ion source placement.

B) Beam Transport

Having obtained an alpha beam from the cyclotron, it is now necessary to transport this beam to the experimental area. Figure 4 shows the positional relationship between the cyclotron, control room and experimental area.

After leaving the cyclotron, the beam goes through a self excited sextupole magnet to correct for spatial distortion in the beam caused by the method of extraction. Next, the beam encounters a pair of two inch

Figure 4:

Foster Radiation Lab. facility layout

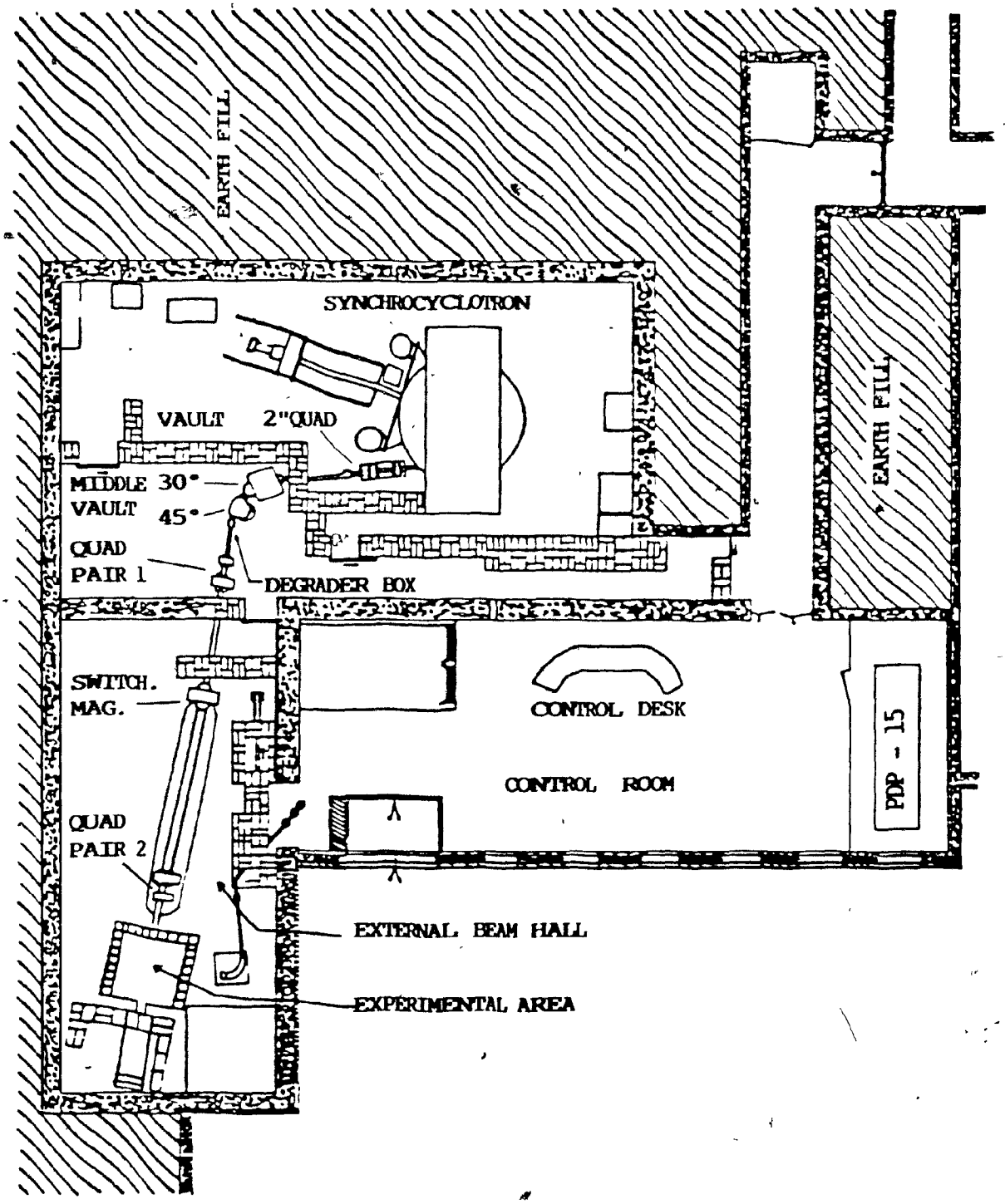
EARTH FILL
SYNCHROCYCLOTRON
VAULT
2"QUAD
MIDDLE 30°
VAULT 45°
QUAD
PAIR 1
DEGRADER BOX
EARTH FILL
SWITCH.
MAG.
CONTROL DESK
CONTROL ROOM
PDP - 15
QUAD
PAIR 2
EXTERNAL BEAM HALL
EXPERIMENTAL AREA

quadrupole magnets, used for focussing, and from there is bent by two separate magnets through angles of 30° and 45° . Following the 45° magnet is the degrader box. The beam can be degraded to more suitable energies at this point. How this is done will be explained later. After the degrader box the beam is refocussed as necessary by a pair of four and six inch quadrupoles and then enters the beam hall. The beam may be steered to different experimental sites in the beam hall by means of a switching magnet. The beam, after leaving the switching magnet, is refocussed once more by another pair of quadrupoles and then enters the target area. At the target site the beam may be focussed anywhere from 3 to 7 mm., depending on beam energy. The poorer focussing occurs because of the beam spread resulting from the method of beam degradation.

C)Degraders

Since the (α,xn) reactions of interest may have their optimum occurrences at energies less than 100 MeV it becomes necessary to find means by which to lower the beam energy. This is accomplished by placing beryllium degraders in the path of the beam. These degraders are flat circular pieces of Be. which vary in thickness from 1.52 to 3.38 mm. On passing through the degrader, the beam ionizes Be. atoms in the vicinity of its path, giving up some of its energy in the process. The process of ionisation is statistical in nature and gives rise to a distribution skewed to high energies. This latter effect is known as the Landau-Symons effect and the distribution is known as the Landau distribution(22,23).

The energy of the degraded beam versus degrader thickness was calculated from stopping power tables as tabulated by Williamson et al.(24). The beam divergence as well as the degree of straggling is proportional to the atomic number Z of the degrading material. The spread

in energy is calculated to be less than 5 MeV for a degradation of 50 MeV. Figure 5 shows the alpha particle beam energy as a function of the Be. thickness (calculated). Table 1 gives a table of energy versus the different Be. thicknesses available. The position of the degrader box was chosen for two reasons: 1) the beam could be focussed at the degrader site 2) neutrons produced at the site could be adequately shielded from the experimental area. The concern with neutrons will be dealt with in detail later on.

D)Experimental Area

Having directed the beam to where it is wanted, a description of the experimental area is now given. Figure 6 shows the area layout.

The motivation behind the design of the experimental area is to allow for the optimum detection of gamma-rays over extended time periods with as little signal interference as possible. The experimental shed, which is built on a raised platform in order to bring target and detectors level with the beam, demonstrates this design philosophy:

First, the shed structure consists of aluminium; walls, roof, door and floor(of anodized aluminum) with dimensions 1.85 m x 1.85 m x 2.0 m. Also, the portion of the beam pipe in the shed is isolated from the part outside by means of an insulating teflon flange. These precautions effectively make the shed into a Faraday cage and eliminate radio frequency waves given off by the cyclotron, especially those carried along the beam pipe, from the interior of the shed. As a further precaution, the shed is insulated from the concrete floor since R.F. noise may be transmitted through the floor material. Next, the shed and all the internal electronics are isolated from each other. The electronic apparatus receive power from an outlet where the ground pin has been

Figure 5:

Alpha Beam Energy vs. Degrader Thickness

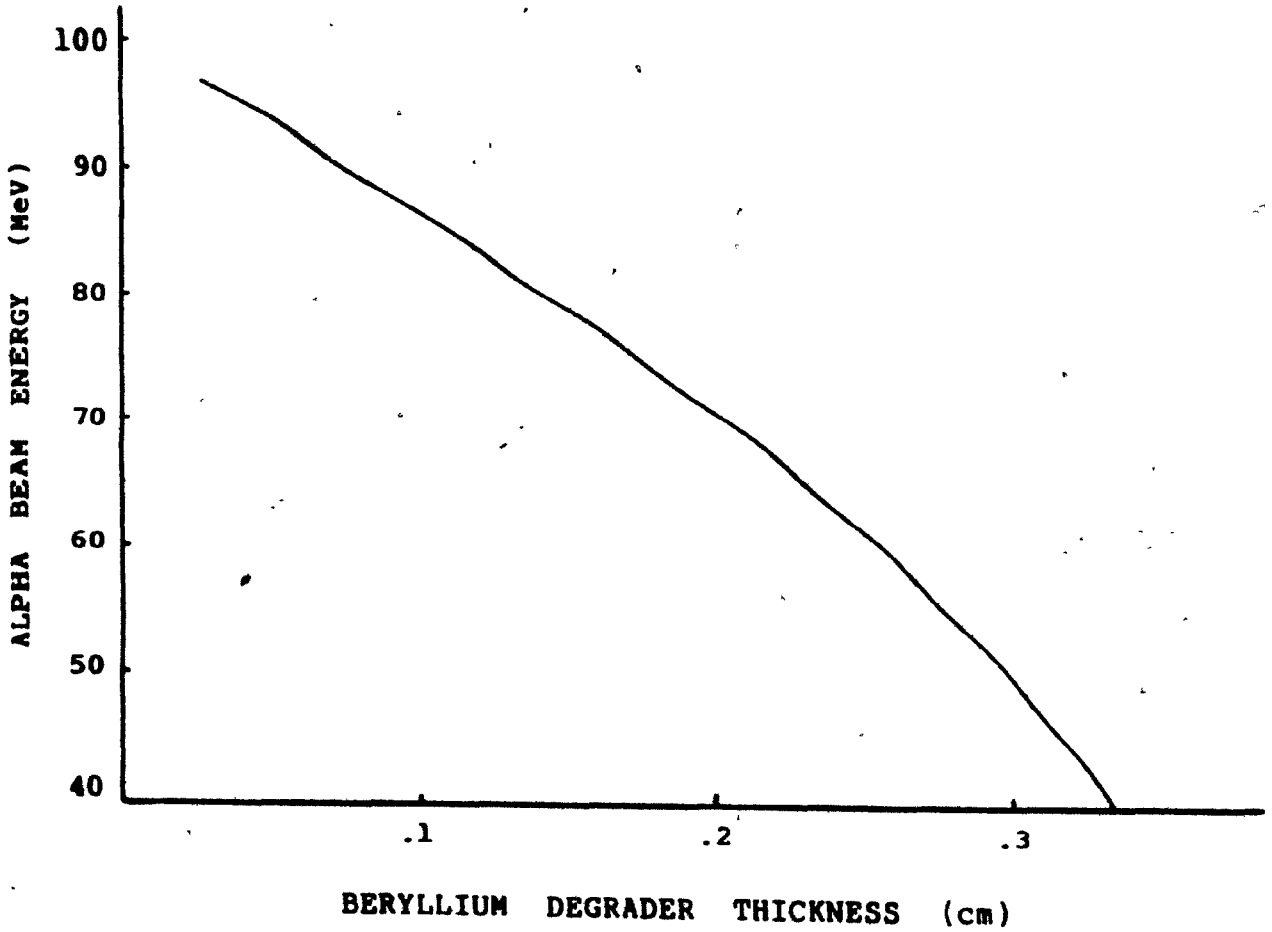
100
90
80
70
60
50
40
ALPHA BEAM ENERGY (MeV)
.1
.2
.3
BERYLLIUM DEGRADER THICKNESS (cm)

Table 1

Alpha beam energy as a function of Be. degrader thickness.

Incident energy = 100 MeV.

Thickness (cm)	Thickness (mg/cm^2)	Energy (Mev)
0.152	281.6	78.2
0.206	380.2	69.0
0.231	427.1	64.3
0.259	478.7	59.0
0.284	525.7	54.1
0.305	563.3	49.3
0.338	624.3	42.0

removed, thus leaving the electronics at a floating ground. All electrical signals are carried from the shed to the data accumulation computer through triaxial cables. The outer shield of the cable is connected to the shed and the inner shield is connected to the casing of all electronic modules. This cable is then grounded locally at the computer site. All these steps are necessary since the detectors will pick up R.F or other spurious electrical noise, superimpose it on the electrical pulses representing gamma-ray detection and lead to poor detector resolution.

The next problem to be dealt with is that of the high neutron background present in the experimental area. The neutron background poses a problem since, as will be dealt with in the section on detectors, the resolution of Germanium detectors degrades over time when exposed to high energy neutrons. High energy neutrons here may be anything from 1 MeV upwards. To enhance detector lifetime it then becomes necessary either to eliminate the neutrons in the experimental area or to thermalize them. The protection methods used involve a combination of both these requirements.

One source of high energy neutrons is, as stated before, the degrader box. The degraders, however, are located on the other side of a 3 foot thick concrete wall which thermalises the neutrons and captures most of them. The degraders, however, increase the beam divergence causing beam scattering into the switching magnet, leading to more neutron production. The solution to this problem was to surround the switching magnet with concrete blocks, leaving only sufficient space for the beam pipe to get through. This same solution is also used for the 'beam dump'. This is the area, located about 12 feet from the experimental shed, where the beam is stopped. As a final effort to reduce the fast neutrons in the shed, the shed is surrounded by one foot cubic containers filled with water and

boric acid. The water serves to thermalize the neutrons which are then absorbed by the Boron. Inside the target chamber itself, neutrons are produced by collision of the beam with the target and surrounding beam pipe material. By focussing the beam as tightly as possible the beam is prevented from hitting the sides of the beam pipe during its journey to the target. By making the target sufficiently thin, 50 mg/cm^2 , and by using larger exit pipes, the amount of interaction of the dispersed beam with the beam pipe is reduced.

Since the high energy neutrons produced in the (α,xn) reactions are emitted predominantly in the direction of the beam (25,26), the Germanium detectors are always positioned at angles greater than or equal to 90° with respect to the beam direction. Measurements were made to determine the levels of neutrons present in the hut for the targets used in this work. The neutron detector used was a Victoreen model 488A. This detector is most sensitive to 5 MeV neutrons and only tells the flux of neutrons around this energy. The average flux found was 110 fn/cm^2 taken in the forward angle direction relative to the beam. The letters 'fn' stand for 'fast neutrons'. To put this number in context, Germanium detectors begin to show damage at fluences of 10^9 - 10^{10} fn/cm^2 (see section on detectors).

E)Detectors:

Four types of detectors were used for this work: Lithium drifted Germaium [Ge(Li)], high purity Germanium [Ge(HP)], Bismuth Germanate (BGO), and Sodium Iodide [NaI(Tl)] detectors. For gamma-ray detection where the resolving power of the detector is critical, the Germanium detectors were used. In timing applications where we are only interested in the detection of a gamma-ray irrespective of its energy, the NaI(Tl)

Figure 6:

Experimental Area

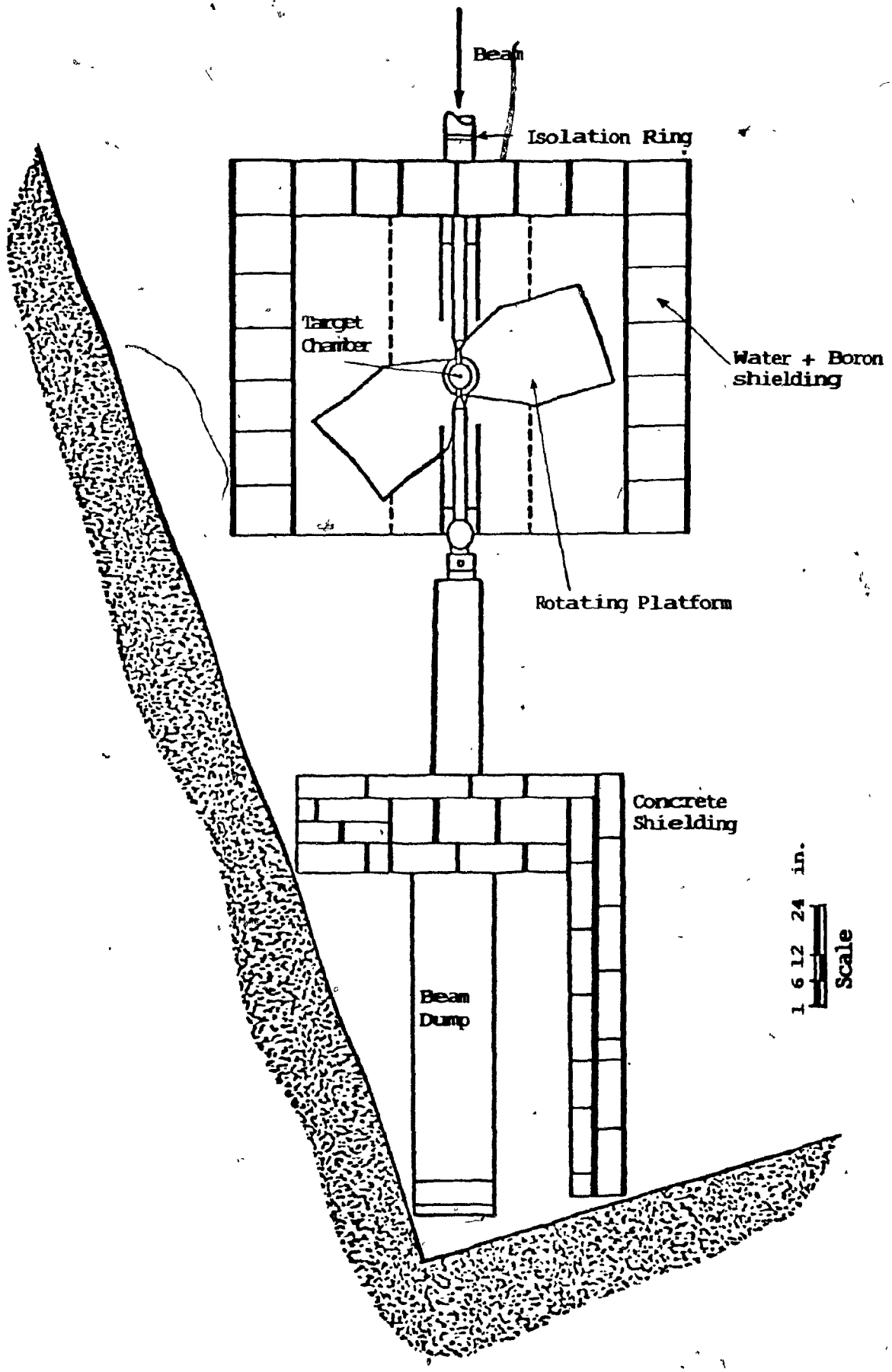
Beam
Isolation Ring
Target Chamber
Water + Boron shielding
Rotating Platform
Concrete Shielding
Beam Dump
1 6 12 24 in.
Scale

and BGO detectors were used. Table 2 lists all the detectors used and their specifications. The operation of the solid state Germanium detectors and that of the scintillation NaI(Tl) and BGO are well known and may be found in references such as Goulding and Pehl (27). A brief summary of the main principles of these detctors will be given.

Scintillation detectors:

A scintillation phosphor is a material able to convert energy lost by ionizing radiation into pulses of light. In most scintillation applications, the ionizing radiations of interest are in the form of gamma-rays, electrons, neutrons and alpha particles. The absorption of the energy of any of the above particles leaves the atoms of the scintillator in excited states which subsequently decay by emitting light. These light pulses are then detected by a sensitive photocathode. Electrons are emitted from the photocathode via the photoelectric effect and are amplified in a photomultiplier tube. The amplification in the photomultiplier tube occurs via a series of dynodes which multiply the electron flow by secondary emission. The output voltage of the photomultiplier is directly proportional to the energy deposited in the scintillator.

The use of NaI as a scintillator began with the discovery of Hofstader(28) in 1948 of the luminescent properties of NaI. Later, an improvement in scintillation was obtained by adding thallium halide to give NaI(Tl). The thallium halide shifts the absorbed particle energy into the region of visible light to which the crystal is most transparent. The wavelength of maximum scintillation intensity is 420 nm. More recently, the use of BGO as a scintillation detector stems from the discovery of Weber and Monchamp(29) in 1973 that BGO, when exposed to X-rays, undergoes

Table 2

Table of detectors used

Quantity	Type	Efficiency*	Range (MeV)	Resolution**
1	Ge(Li)	10%	0.03 - 4	2.4 keV
1	p-type Ge.	16%	0.03 - 4	2.2 keV
1	n-type Ge.	19%	0.005 - 4	2.1 keV
1	n-type Ge.	28%	0.005 - 4	2.1 keV
2	NE 213		1 - 20	
4	NE 213		1 - 10	
1	BGO			
8	NaI(Tl)			

* - relative to a 3"x3" NaI(Tl)

** - at 1.3 MeV

luminescence. The actual chemical structure of the BGO crystal is $Bi_4Ge_3O_{12}$ and the light emitted in scintillation comes from the $^3P_1 - {}^1S_0$ electronic transition within the Bi^{3+} ions. For applications where the energy of a gamma-ray is not important, BGO's are more suitable than NaI's because of their greater detector efficiency. This higher efficiency results, in part, from the greater density of the BGO material.

Solid State Detectors:

Semi-conductor detectors were first introduced in the mid-sixties and quickly gained in popularity because of their superior energy resolution over NaI's. These detectors may be used to measure the energies of photons, electrons and heavier charged particles. Essentially, the detector is a piece of solid material whose nature and size is matched to the absorption characteristics of the radiation to be measured. When a photon or particle is absorbed, electrons and holes are produced. These are then collected by an electric field in the material to provide an electrical signal that is a direct measure of the energy of the photon or particle. In our case, we are specifically interested in detecting photons in the energy range ~20 keV to ~3 MeV. The material most suited for this application is Germanium. The band gap from the valence to the conduction band is 0.79 eV, allowing for the creation of electron-hole pairs with relative ease. In fact, the Germanium crystal has to be cooled to liquid nitrogen temperature to reduce the amount of thermally generated electron-hole pairs.

A number of processes occur when a gamma-ray enters the detector which in turn lead to the production of electron-hole pairs. One process is the photoelectric effect. This effect exhibits a Z^5 dependence on the atomic number, Z, of the detecting material. Germanium has an atomic

number of 32 whereas Silicon, the next best material, has an atomic number of 14, thus making Ge. more suitable for high energy gamma-ray spectroscopy. Apart from the photo-electric effect, photons entering the Germanium crystal may undergo Compton scattering, with the secondary photon frequently exiting the detector. As a result, only a fraction of the total energy of the photon is deposited, leading to the familiar Compton background in the subsequent spectrum. The last process by which photons may be absorbed is by pair production. Photons with energies equal to or greater than 1.02 MeV may give rise to an electron-positron pair. The positron eventually annihilates in the detector material and the 1.02 MeV energy reappears as a pair 511 keV gamma-rays emitted in opposite directions, one or both of which may escape from the detector. Thus we find that high energy gamma-ray spectra contain single and double escape peaks along with the full energy peak.

The first type of Germanium detector to become available was of the Lithium drifted variety. With this type of detector, a loaf, normally cylindrical, of high resistivity p-type germanium is prepared. Lithium ions are then introduced onto the surface of the Ge. bar and permitted to drift into the Ge. under the influence of a strong electric field. The lithium ions then compensate, or neutralize, the p-type impurities in the Germanium. After the drifting process is completed, there still remains a high concentration of lithium ions at the surface, providing a n contact. In operation, the detector is reversed biased to a voltage of the order of 1000 V.

The number of impurity ions in the Ge(Li) detector is $\sim 10^{12}$ /cm^3. Impurities act as charge trapping sites and it is to neutralize this effect of these impurities why lithium compensation is used. More

recently, however, the problem of impurity ions has been overcome by the development of Ge. crystals of 10^9 - 10^{12} impurities per cm^3. These so called 'high-purity' detectors undergo fabrification methods similar to those of lithium drifted detectors except that the lithium drifted step is omitted. A lithium diffused n^+ surface layer is still used but in this case it merely provides the n^+ contact and is not drifted into the germanium. Of the high purity detectors used in this work both n and p-type coaxial detectors were utilized. With p-type material the lithium diffused n^+ contact is put on the outside of the germanium and a metal surface barrier in the core. For n-type material the contacts are reversed with the lithium diffused contact in the core and the p^+ contact on the outside.

Our earlier preoccupation about getting rid of fast neutrons can now be explained. A fast neutron entering a Ge. crystal, because it is neutral, does not ionize the detector material but instead loses energy by collision with Ge. ions, displacing them from their lattice sites. The Ge. ions, toward the end of their range, become neutral and knock further lattice atoms from their sites. Consequently, a fast neutron colliding with a lattice nucleus can produce thousands of displaced atoms and will seriously damage the crystal in the vicinity of the initial collision. Lithium drifted Ge. detectors suffer the additional problem that, due to precipitation of lithium ions at damage sites, the compensation of acceptors in the original material is destroyed. These defects act as trapping sites for the signal charge carriers. Since the location of the initial charge production and variations in the concentration of traps at different points in the detector cause the loss of the signal to change from one event to another, a fluctuation in output results. This

translates to poor energy resolution. Hence the effort to reduce to a minimum the presence of fast neutrons at the detector site. Even so, one detector, a p-type Ge(HP) from Princeton Gamma Tech., suffered neutron damage during the early course of the experiments and had to be replaced. It has been determined by Kraner et al.(30) that dose levels of 10^{10} fast neutrons/cm^2 lead to measurable neutron damage.

Of all the species of germanium detectors detectors available, it has been found that n-type coaxial Ge(HP) detectors are the most resistant to neutron damage, being some 30 to 60 times more resistant than the corresponding p-type. The reason for this stems from the placement of the p^+ contact on the outside of the germanium in the case of the n-type detector. Most particle interactions occur near the outer portions of the detector so that the holes produced have a short distance to travel to the p^+ contact. Since hole trapping is the predominant degrading effect on energy resolution, then the probability for trapping to occur is reduced in the n-type detector.

One vital piece of information required with the Ge. detectors is their detection efficiency. This is needed so that the number of events detected can be related to the number actually occurring . This in turn enables us to determine the intensities of observed gamma-rays. Figure 7 shows the relative efficiency of a 28% n-type high purity Ge. detector manufactured by Ortec. Efficiency varies with detector position and is usually quoted in comparison to the absolute efficiency of a NaI(Tl) crystal. The 28% efficiency of the n-type detector refers to how it compares with a 3"X 3" NaI(Tl) when both detectors are held at a distance of 25 cm from a ^{60}Co source where the 1.3 MeV gamma-ray is the one being measured.

Figure 7:

Efficiency curve of 28% Ge(HP)

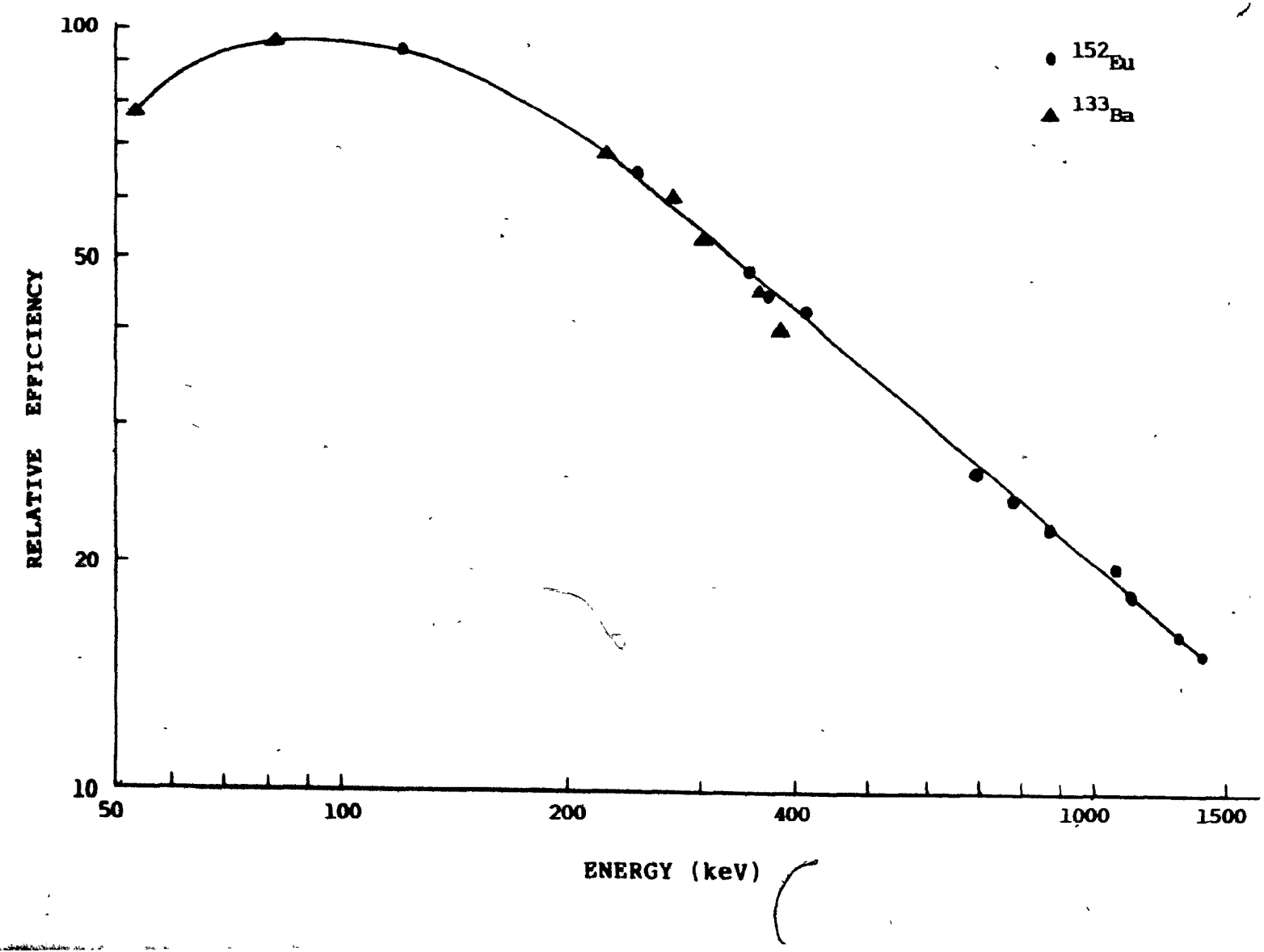
100
50
20
10
RELATIVE EFFICIENCY
50
100
200
400
1000
1500
ENERGY (keV)
152Eu
133Ba

F)Targets

The targets used for all experiments were prepared by one of two methods, depending on the nature of the target material.

In the case of the ^{126}Te and ^{128}Te targets, which were in the form of Tellurium powder, the powder was compressed to a pressure of 800 lbs/sq. cm to form a flat target of density 50 mgms/sq. cm. The targets were then glued to strips of mylar of density 100 μgms/cm^2 . The glue used was diluted Polystyrene Q-dope. Q-dope produces a very low level of activity under α bombardment and the in beam gamma-rays from mylar are well known(31). The mylar with target is then glued to a target holder. The various target holders and target chambers will be discussed in the chapter on Experimantal Techniques. In the case of the ^{116}Sn target, the procedure was similar except that the target came in oxide powder form and could not be compressed. Instead ~50 mg of the finely ground powder was sprinkled onto a thin base of Q-dope of area 1 cm^2 . Of course, the density of the resulting target will not be perfectly uniform, but this is not considered a problem.

G)Data Acquisition:

Data acquisition varies from experiment to experiment but there are features which are common to all. We present these features here and leave specific details to when the experiments are treated.

Data acquisition is handled by a Digital PDP-15 computer. The spectrum enters the computer via a Tracor Northern TN-1212 analogue to digital converter and from there is stored in the memory of the computer as data counts in 4096 channels. The data accumulated on the PDP-15 is analysed on a PDP-11 computer for which a number of analysis programs have been written.

Earlier the remark was made that it was necessary to convert the cyclotron beam from a pulsed mode to that of a continuous D.C beam. The reason for doing this is as follows: In the (α,xn) reaction, the lifetimes of the nuclear states are usually on the order of pico-seconds. This means that for a pulsed alpha beam an enormous amount of gamma-rays are produced in bursts lasting 25 μsec and occurring every 600 μs, these figures corresponding to the time profile of the beam. This has a number of consequences: If the 'flash' of gamma-rays exposed to the Ge. detector is sufficiently intense, the resulting accumulation of signal currents become almost like a D.C. current burst and blocks the conventional FET pre-amplifier for a long time - from 100 μsec to 1 msec, even after the gamma-ray flash ceases. A milder beam flash results in pile-up where two gamma-rays enter the detector crystal in a time interval shorter than the decay time of the first detected gamma-ray. This results in peaks whose energies do not convey any useful information and are rejected by the associated electronics. Hence our efficiency is down. Also, the ADC's on the PDP-15 require on the order of 5 to 10 μsec to process a gamma-ray signal during which time the input is blocked. Thus our efficiency is down again. The solution to this, then, is to stretch the beam as previously explained. This gives us a continuous flow of information to the computer, boosting the efficency of the detection system.

Chapter III: Experimental Techniques

A) Singles:

Prior to other experiments, it is necessary to know at what energy the (α,xn) reaction of interest is optimally produced. This information is obtained from an excitation function experiment.

We first obtain a theoretical prediction of the cross section for production of the isotope of interest, using the code 'Alice'(32), to see if the reaction is possible in the range of alpha beam energies available. For pre-equilibrium emission of neutrons, the calculation is done by the Geometry Dependent Hybrid Model (33). For equilibrium emission the calculation follows the method of Weisskopf and Ewing (34,35).

Once satisfied that the experiment is possible, the excitation function is experimentally determined. The excitation function so obtained is represented by a plot of relative gamma-ray intensity versus bombarding energy. This experiment is the simplest to execute. The target chamber, figure 8, is a vertical cylinder into which two openings have been drilled and fitted with entry and exit ports for the passage of the beam. Also on the cylinder are openings to allow a video camera to see the target location. This camera is used to properly align the target and beam by observing the luminescence given off by a piece of phosphor fitted at the target site. The top of the cylinder is fitted with a transparent plexiglass cap, the centre of which has a hole drilled in it for the insertion of a solid aluminum cylinder to which the target holder is mounted (figure 9). The cylinder in the cap can be moved up and down to adjust the target position. Only one detector, a Ge(HP), is used in this experiment and it is placed at an angle of 125° relative to the beam

Figure 8:

Singles and Angular Distribution Target Chamber

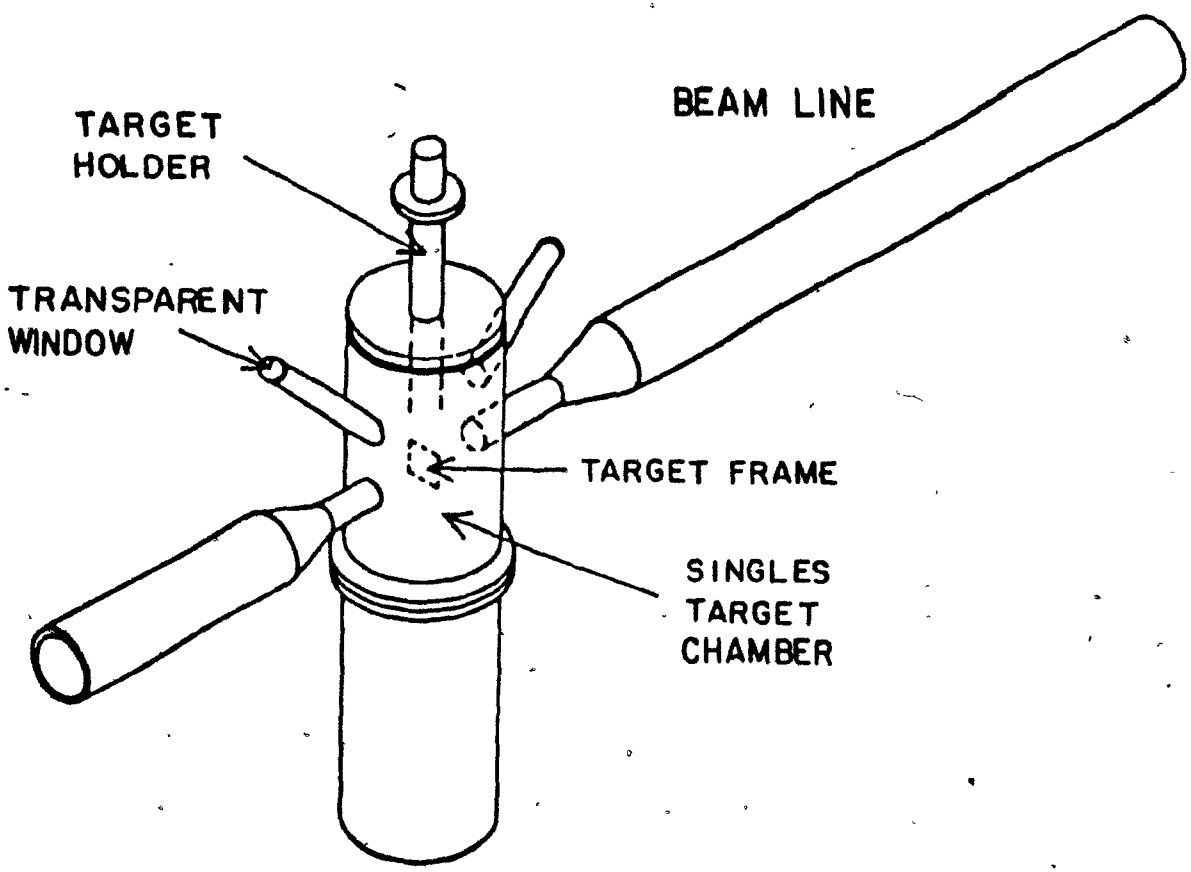
TARGET
HOLDER
BEAM LINE
TRANSPARENT
WINDOW
TARGET FRAME
SINGLES
TARGET
CHAMBER

Figure 9

Target Holder and Target Frame

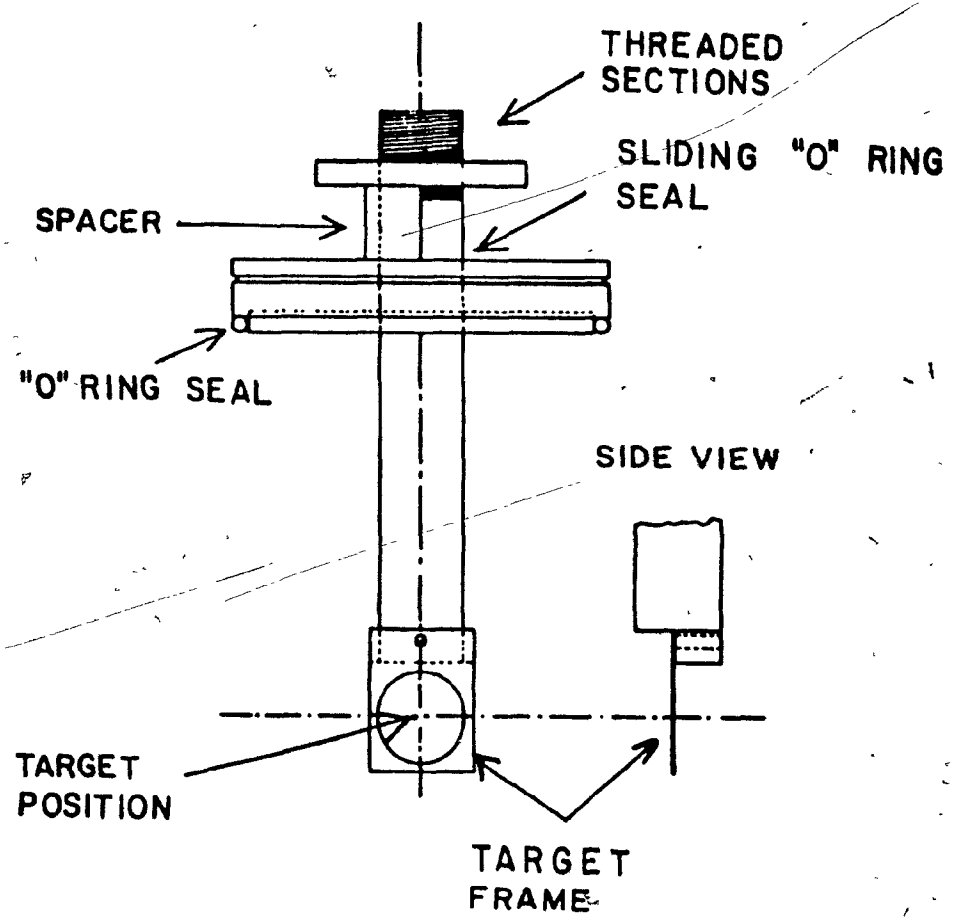
THREADED SECTIONS
SLIDING "O" RING SEAL
SPACER
"O" RING SEAL
SIDE VIEW
TARGET POSITION
TARGET FRAME

direction:

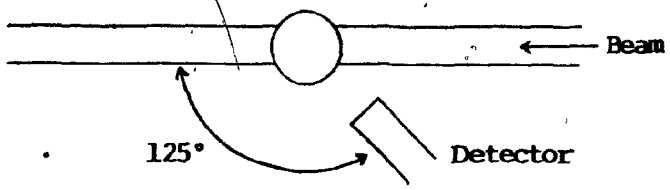

Normalization of the peaks in the acquired spectrum is with respect to the total intensity of the spectrum. This is a reasonable thing to do since although the peaks of interest have different production cross-sections with different bombarding energies, the total production cross-section remains fairly constant.

The set-up being complete , the targets are then bombarded at energies of 42, 49, 54, 59, 64, 69 and 78 MeV. A digital representation of the spectrum (chapter II) accumulated at each energy is written on dec-tape by the PDP-15 computer using a general purpose accumulation program. The excitation function for each reaction channel is normally very distinct and it becomes possible to assign gamma-rays, on a tentative basis, to specific isotopes if the excitation functions for known gamma-rays are used for comparison. More positive identification is got with the multiplicity filter experiment to be discussed later.

B)Angular Distribution:

Part of the essential information needed to construct useful level schemes is to know the spin and parity of the energy levels. One technique for obtaining the spin of levels and, by deduction , their spin parity, is that of angular distribution.

The excited states of nuclei are subject to decay to lower states with simultaneous emission of electromagnetic radiation. Electromagnetic

radiation can be classified according to the angular momentum (the multipole order) carried by each photon. For each multipole order there are two possible classes of radiation:

Electric 2^λ - pole ($E\lambda$) radiation

Magnetic 2^λ - pole ($M\lambda$) radiation

The term 'multipolarity' is used to specify the kind of radiation as to both class and multipole order.

Conservation of angular momentum for the system of nucleus + gamma-ray imposes a selection rule for transition between two states of specified angular momentum (J_i, J_f):

$$|J_i - J_f| \leq \lambda \leq J_i + J_f$$

Coservation of parity further restricts the class of radiation. For $E\lambda$ radiation $\pi_i \pi_f = (-1)^\lambda$ and for $M\lambda$ radiation $\pi_i \pi_f = (-1)^{\lambda+1}$. π_i and π_f refer to the parity of the initial and final states of the nucleus emitting the gamma-ray. One further requirement, a consequence of photons having helicity $h = \pm 1$, is that no radiation of multipole order zero can occur. Now, for each multipole radiation of order λ, the radiation field displays a characteristic angular distribution. The intensity of emitted photons is given by the Poynting vector:

$$\vec{P} = (c/4\pi)\vec{E} \times \vec{H}$$

the magnitude of which is given by:

$$|\vec{P}| = c/4\pi|E|^2 \quad \text{or} \quad |\vec{P}| = c/4\pi|H|^2$$

and the angular distribution for $E\lambda$ and $M\lambda$ radiations will be identical. The angular distribution of photons of multipolarity λ and component μ is

given by:

$$Z'_{\lambda\mu}(\theta) = \frac{(-1)^{\mu-1}}{4\pi} \sum_k \langle \lambda 1 \lambda \; -1 | k0 \rangle \langle \lambda \mu \lambda \; -\mu | \; k0 \rangle \; P_k(\cos\theta) \; ,$$

k is an even integer of maximum value 2λ . $P_k(\cos\theta)$ are Legendre Polynomials.

Under ordinary circumstances the radiation from a collection of arbitrarily oriented nuclei would be isotropic. However, if it becomes possible to align these radiating nuclei with respect to some axis, then measurement of the intensity of the radiation field at various angles with respect to the symmetry axis will reveal this angular distribution. This alignment of nuclei is obtained as follows: In our experimental set-up, the incoming alpha paricle transfers a large orbital angular momentum to the compound nucleus. For an even-even target with spin zero, this angular momentum acts in a direction perpendicular to the beam direction and the compound nucleus is completely aligned. For targets with non-zero spin, the angular momentum of the compound nucleus is the vector sum of the momentum brought in and the spin of the original target. If the initial spin of the target is small compared with the angular momentum of the alpha particle, then the alignment will be almost complete.

If the isotope that we are interested in is produced, for example, by the $(\alpha,4xn)$ reaction then the neutrons and gamma-rays given off in going from the compound nucleus to the residual nucleus will remove some of the angular momentum making the final alignment partial.

The full mathematical treatmemt of this topic may be found in Morinaga and Yamazaki (36). Here we give the mathematical results of importance which allows us to understand the situation. To treat the excited states of the residual nuclei we take a statistical approach. In

general, the angular momentum j of a state has $2j + 1$ components m along some quantization axis. If we consider an assembly of such systems where the assembly is composed of pure states, then we can define the population parameter P(m) which gives the probability of each state with respect to a suitable symmetry axis as the quantization axis. In our case this is the axis defined by the alpha beam. The probability that a gamma-ray of order λ and component μ is emitted from an oriented state of population parameters $P(m_1)$ is then:

$$a_{\lambda\mu} = \sum_{m_i} |\langle j_i m_i \lambda\mu | j_f m_f \rangle|^2 P(m_1)$$

where j and m refer, of course, to the angular momentum of the nuclear levels involved. If we multiply the equation given earlier governing the angular distribution of multipole radiation by $a_{\lambda\mu}$ then we get the angular distribution of gamma-rays given off by our aligned nuclei:

$$W(\theta) = \sum_{m_1,\mu} |\langle j_1 m_1 \lambda\mu | j_f m_f \rangle|^2 P(m_1) Z_{\lambda\mu}(\theta)$$

This equation can be re-written so as to express $W(\theta)$ in terms of the Legendre Polynomials present in $Z_{\lambda\mu}(\theta)$. The result is:

$$W(\theta) = \sum_k \rho_k(j_1) F_k(j_f \lambda j_1) P_k(\cos\theta)$$

the term ρ_k is called the statistical tensor and is defined in terms of the population parameters:

$$\rho_k(j) = \sqrt{2j+1} \sum_m (-1)^{j-m} \langle jmj - m | k0 \rangle P(m)$$

$$k = 0, 1, \ldots, 2j$$

The expression $F(j_f \lambda j_1)$ takes care of the remaining terms:

$$F(j_f \lambda j_1) = (-1)^{1+j_1-j_f} \sqrt{2j+1}(2\lambda+1) \langle \lambda 1 \lambda - 1 | k0 \rangle W(j_1 j_i \lambda\lambda; k j_f)$$

where $W(J_1 J_1 \lambda\lambda; k J_f)$ is a Racah coefficient.

Since an electromagnetic transition between two nuclear levels may proceed via mixed multipole radiation, this possibility must be taken into account. If the function F_k is re-defined as:

$$F_k(J_f \lambda\lambda' J_1) = (-1)^{1+J_1-J_f}[(2\lambda + 1)(2\lambda' + 1)(2J_1 + 1)]^{1/2} \langle \lambda 1 \lambda' - 1 | k0 \rangle W(J_1 J_1 \lambda\lambda'; k J_f)$$

then $W(\theta)$ becomes:

$$W(\theta) = \sum_k A_k(J_1 \lambda\lambda J_f) P_k(\cos\theta)$$

with

$$A_k(J_1 \lambda\lambda' J_f) = \rho_k(J_1) \frac{1}{1+\delta^2}[F_k(J_f \lambda\lambda J_1) + 2\delta F_k(J_f \lambda\lambda' J_1) + \delta^2 F_k(J_f \lambda'\lambda' J_1)]$$

The quantity δ is called the mixing ratio and is given by:

$\delta^2 = \frac{T(\lambda')}{T(\lambda)}$, where T is the transition amplitude.

Finally, all our discussions to this point has assumed complete alignment of nuclei. To take care of the more usual case of partial alignment we define the attenuation coefficient due to incomplete alignment:

$$\alpha_k = \frac{\rho_k}{B_k} = \frac{\rho_k}{A_k^{max}}$$

$B_k = A_k^{max}$ is the statistical tensor for complete alignment.

We then get:

$$W(\theta) = \sum_k^{2\lambda} \alpha_k A_k^{max} P_k(\cos\theta)$$

Numerical tables for F_k and $B_k F_k$ have been tabulated by Yamazaki (37) and Der Mateosian and Sunyar (38).

Diamond et al. (39) found a Gaussian distribution of substates formed by heavy ion induced reactions. This being so, the population parameter takes the form:

$$P(m) = \exp(-m^2/2\sigma^2) / \sum_{m'=-J}^{J} \exp(-m^2/2\sigma^2)$$

where σ gives the characteristic width of the distribution. Andersson and Sawa (40) found, by studying 130 cases for six spins from J_1 = 5/2 to 15/2 that σ, as a function of J, has an almost constant value. These results were parameterized by J. E. Kitching (McGill) giving:

$$\frac{\sigma}{J} = \frac{1.8}{J + 0.5}$$

With the above expression for P(m) Der Mateosian and Sunyar have tabulated the α_k as a function of J and σ/J.

Experimentally, the procedure for obtaining the angular distribution is simple. The target chamber is the same as that for the singles experiment (fig. 8) but in this case two detectors are utilised. One detector, the monitor, is placed at an angle of 125° with respect to the beam axis. This angle is chosen since at 125.26° the Legendre polynomial $P_2(\cos\theta)$ term is zero and makes the determination of relative intensities straightforward since one does not have to worry about angular effects. The second detector sits on a movable platform which allows it to be rotated uniformly about the target. Experiments are conducted with this detector successively placed at six different angles ranging from 90° to 150°. Data is accumulated at each angle for both detectors and subsequently written on dec-tape. Because of the finite size of the detector and target, the result for the angular distribution has to be modified to take into account the finite solid angle subtended. This is

done by introducing a solid angle correction factor Q_k into our equations:

$$W(\theta) = \sum_k a_k Q_k A_k {}^{max}P_k(\text{Cos } \theta)$$

To keep the effect of Q_k on the results small, the target was made as small in diameter as was practical and the detector pulled back as far from the target as considerations for collection efficiency would allow.

To determine Q_k a program written by Krane (41) was used. In this program, only detector size is considered, the target being considered a point source. To determine the coefficients A_k a Legendre fitting routine found in Bevington (42) was used. Examples of the fitted results will be given in the chapter on experimental results.

C)Gamma-gamma Multiplicity

As stated earlier, the results of the excitation function experiments allows one to make a tentative assignment of gamma-rays belonging to the nucleus of interest. To supplement this finding and to allow for the placement of gamma-rays in a level scheme, a further experiment is executed. This is the gamma-gamma multiplicity experment. In gamma-gamma multiplicity, we are able to record events where two or more, three or more etc. gamma-rays are in coincidence up to a total of eleven or more in coincidence. Using this method, any gamma-ray found in coincidence with a known gamma-ray from the nucleus of interest may be positively assigned as belonging to the same nucleus. Knowing which gamma-rays are in coincidence, coupled with a knowledge of their relative intensities, we can construct a level scheme. The gamma-gamma multiplicity also alleviates the problem of a high background in the gamma-ray spectra. During alpha bombardment of the target, a number of radioactive products are formed. These radioactive nuclei beta decay to some daughter nuclei

which is formed in an excited state. The daughter then de-excites by alpha emission. The cascade gamma-rays given off by the daughter are of low multiplicity since the process of beta decay only feeds low lying levels. The in-beam residual nuclei on the other hand, as discussed in Chapter I, de-excite through a long cascade of gamma-rays to the ground state. Thus, in the coincidence set-up, recording events where, say, only three or more gamma-rays are detected simultaneously, will result in the in-beam cascades being detected with greater probability over that of the radioactive nuclei.

The equipment required for this experiment is the most elaborate. In this case a different target chamber from that of the singles and angular distribution is used. The target is mounted in a cylindrical target chamber of diameter 2.5 cm. which has a slot cut in it for target placement (figure 10). The tube is fitted with a plexiglass sleeve which, when in place over the target, forms a vacuum sealed unit. The clear plexiglass sleeve is used since this allows for a video camera to see a phosphor target placed in the chamber to allow for beam alignment. Suspended above and below the target chamber are two large lead collimators, each weighing 150 lbs. The two lead pieces form the two halves of a hemisphere and each has five holes symmetrically drilled into it. Into these holes are placed 3" X 3" NaI(Tl) or BGO detectors. In the experiments with ^{126}Te and ^{128}Te targets, six NaI(Tl)'s and one BGO were used. In the case of the ^{116}Sn target, the number of NaI(Tl)'s was increased by one. The holes in the top piece of lead are placed so that they do not look at holes in the bottom piece. The main purpose of the lead is to reduce the amount of spurious coincidences caused by Compton scattering between the detectors. Sandwiched with the target

Figure 10:

Multiple Coincidence Target Chamber

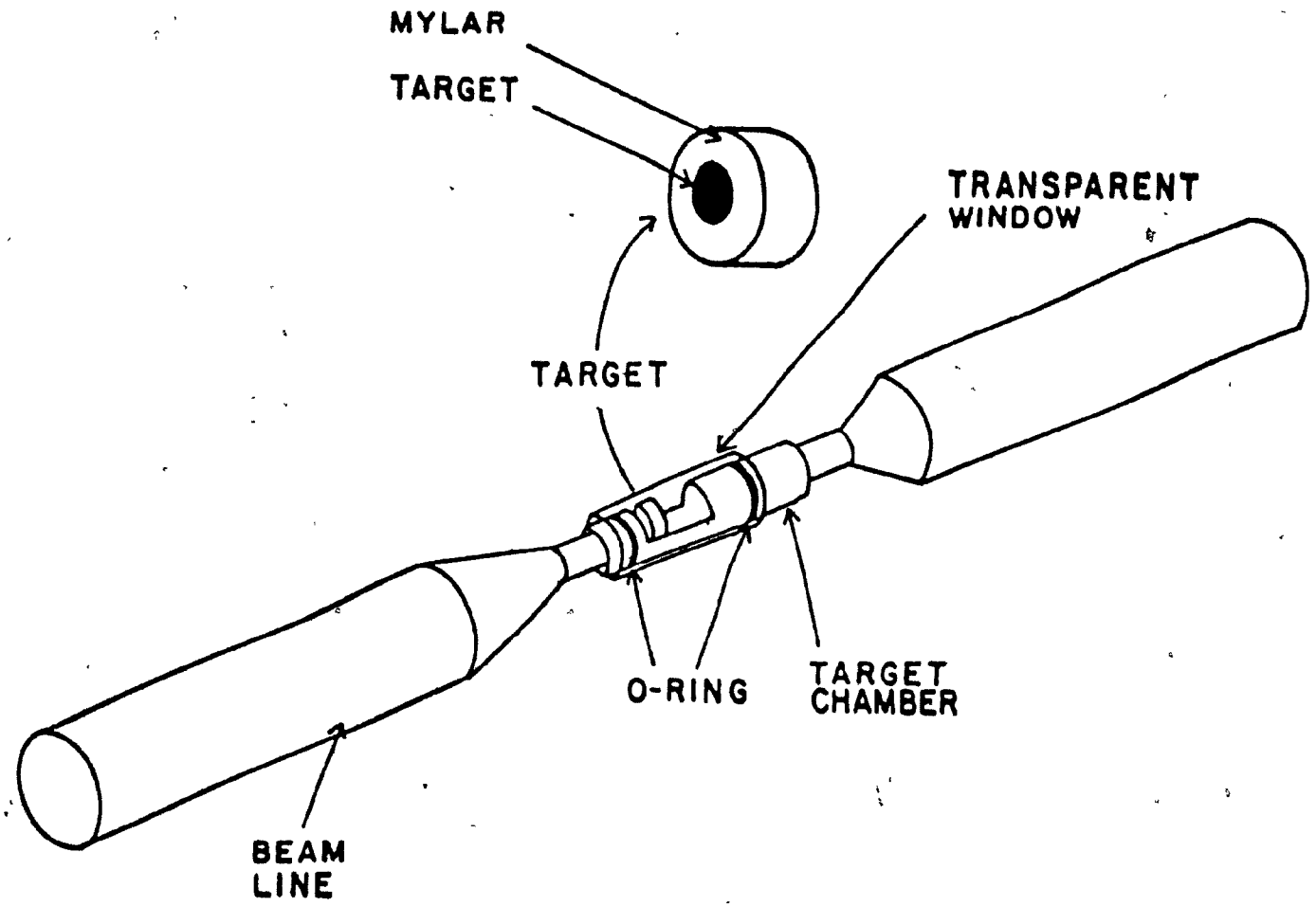
MYLAR
TARGET
TRANSPARENT WINDOW
TARGET
O-RING
TARGET CHAMBER
BEAM LINE

chamber between the lead pieces are two Ge. detectors. To reduce exposure to fast neutrons, the detectors are placed at backward angles to the beam direction. To reduce Compton scattering between the Ge. detectors, a 1/4" thick piece of lead was bent and fitted around the beam pipe, shielding the detectors from each other. The electronics for this experiment were located on an overhead rack stretching the length of the experimental shed. Figure (11) gives a photograph of the complete set-up as well as a close-up of the target chamber. Figure (12) shows a drawing labelling the main components.

The electronic circuitry used for this experiment is shown schematically in figure (13). The output of the scintillation detectors are first sent to a twelve channel photomultiplier amplifier (Lecroy 612A) and from there to an eight channel fast discriminator (Lecroy 620CL). Since for two targets there were nine detectors, the signal from the ninth detector was sent to a quad. discriminator. From this point the signals for each detector are delayed as necessary to bring them all into coincidence. The coincidence between the detectors was established by using a ^{60}Co source and comparing one detector with another till all were in mutual coincidence. This being done, the signals are fed to a sixteen fold register(Lecroy 2341A). This register gives out pules, the amplitudes of which vary directly, in discrete steps, with the number of inputs fired. Thus we are able to tell for each event the multiplicity of the event. A further input to the 16 fold register comes from one of the Ge. detectors so that in the event that none of the NaI's fire there will still be an output from the register. The register only accepts pulses at its inputs while it sees a gating pulse. This gating pulse is derived from a Ge. detector the signal of which is stretched to ~70 ns by a fast gate

Figure 11 (in two parts):

A) Photograph of Experimental set-up

B) Close-up of Target Chamber

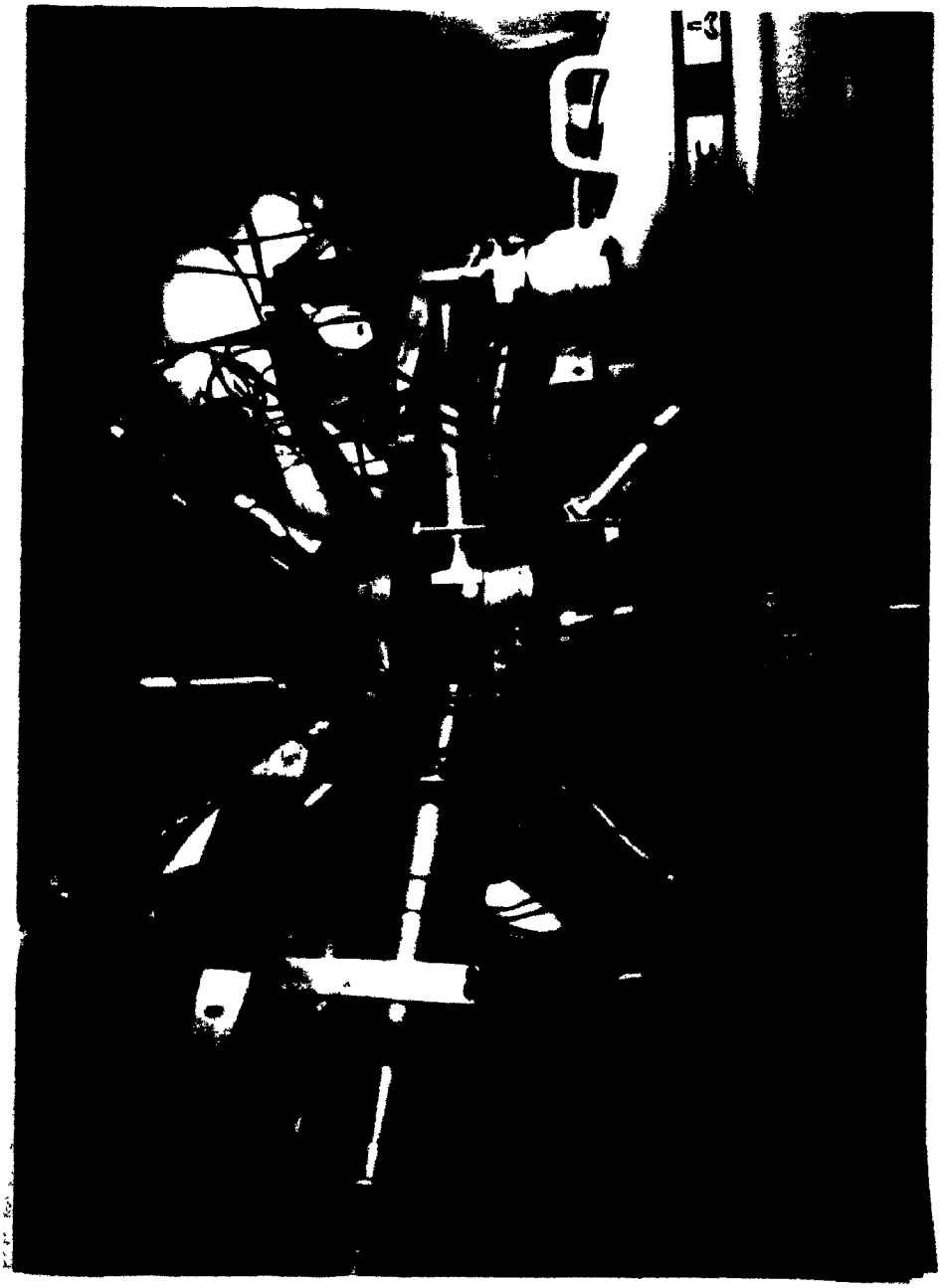

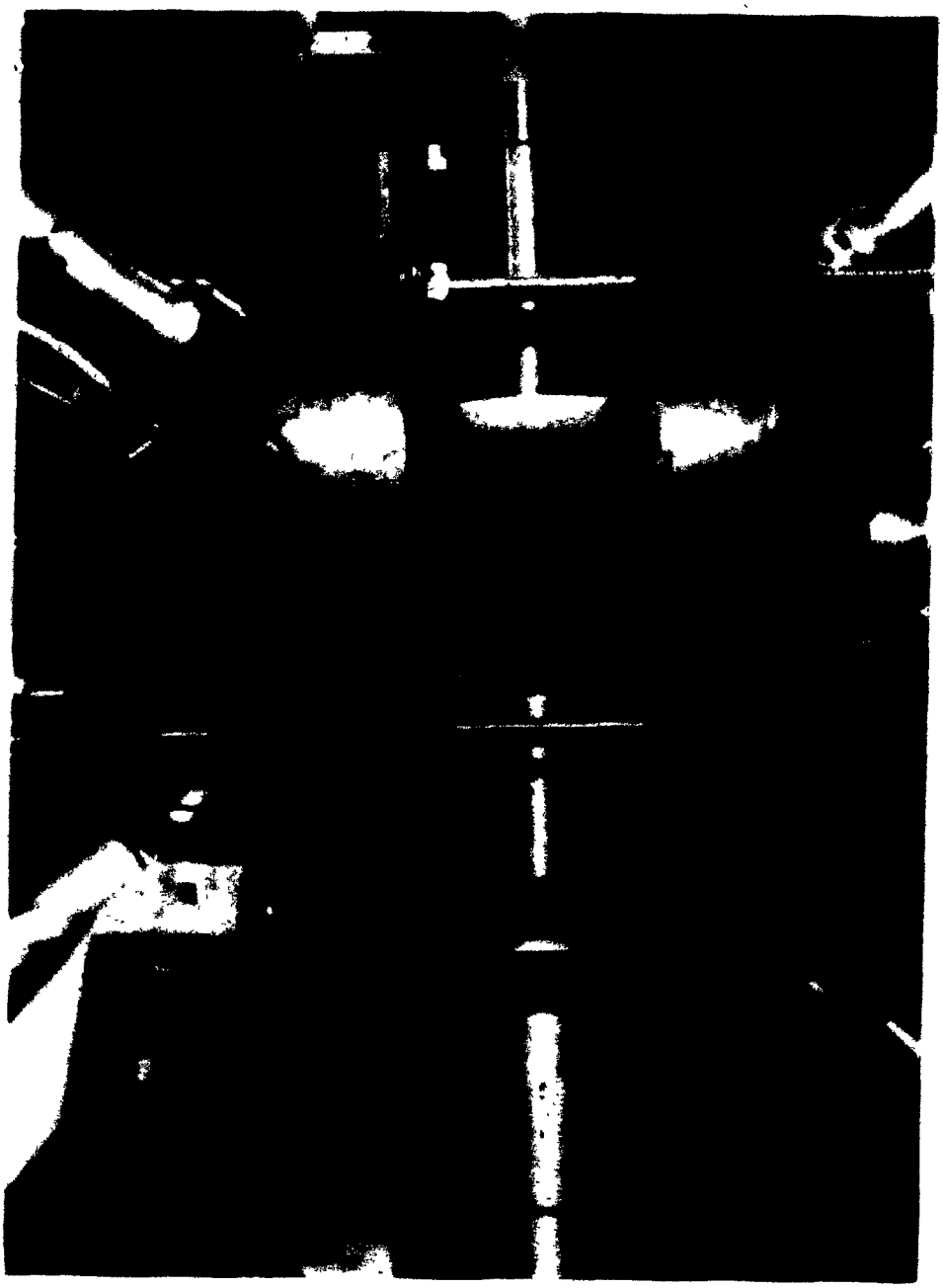

Figure 12:

Labelled Drawing of Coincidence Equipment

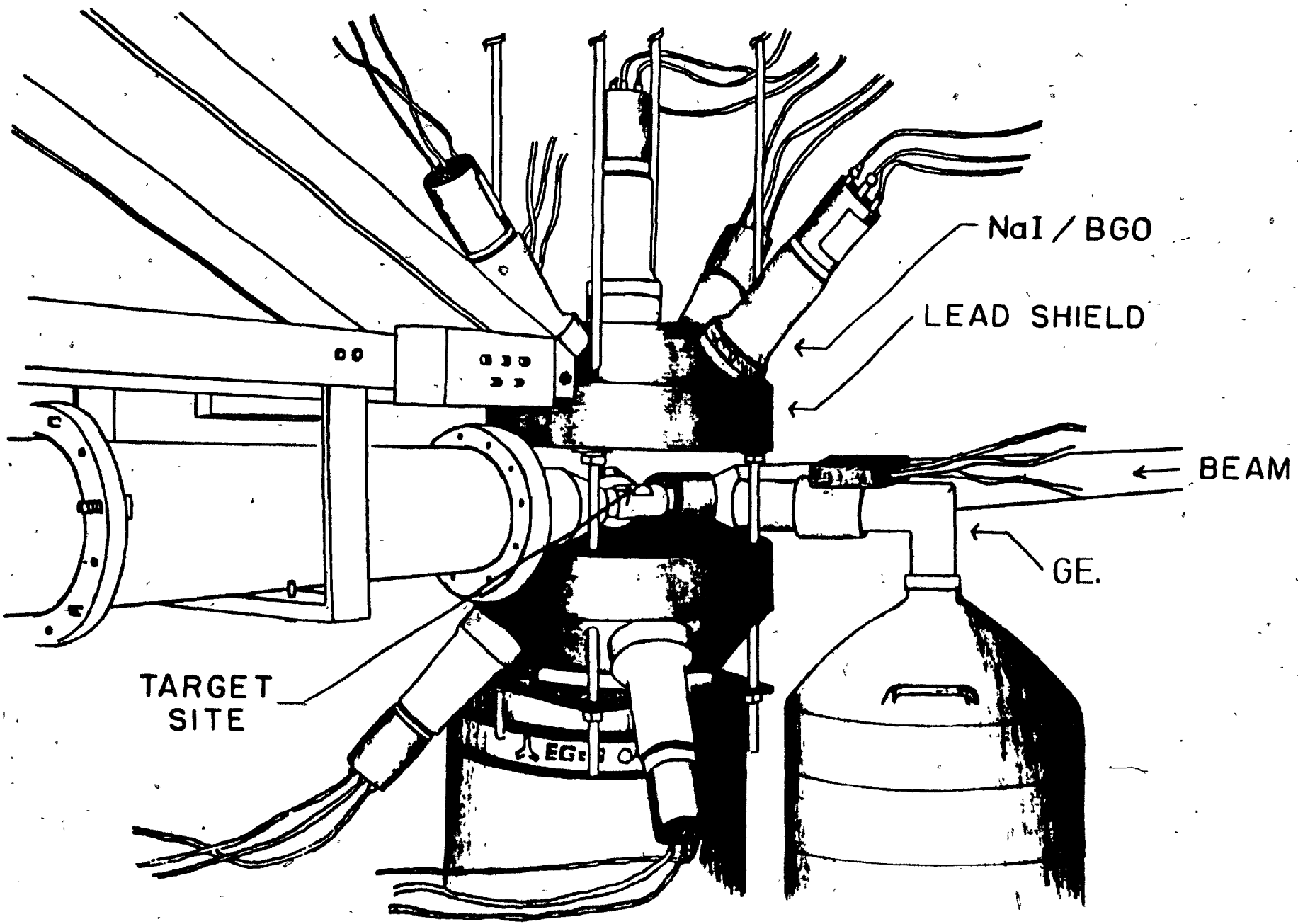
NaI / BGO
LEAD SHIELD
BEAM
GE.
TARGET
SITE

Figure 13

Circuit diagram for the gamma-multiplicity experiment

Explanation of symbols:

ARC: Amplitude and Risetime Compensated Discriminator, Canberra 1427

AMP: Spectroscopy Amplifier, Ortec 572

TAC: Time to Amplitude Converter, Ortec 467

SCA: Single Channel Analyser, Ortec 455

Fast GS: Fast Gate Stretcher(built by author)

SIA: Sum-Invert Amplifier, Ortec 433

GDG: Gate and Delay Generator, Ortec 416A

LGS: Linear Gate Stretcher, Ortec 442

DSI: Dual Summer and Inverter, Tennelec TC-212

16 FOLD REG:16-Fold Register, Lecroy 2341A

8 CHAN FAST DISC: 8-Channel Fast Discriminator, Lecroy 620CL

12 CHAN PM AMP: 12-Channel Photomultiplier Tube Amplifier, Lecroy 612A

GE: Germanium Detector

SCIN: NaI(Tl) or BGO detector

UNI: Unipolar output

INH: Pile-up output

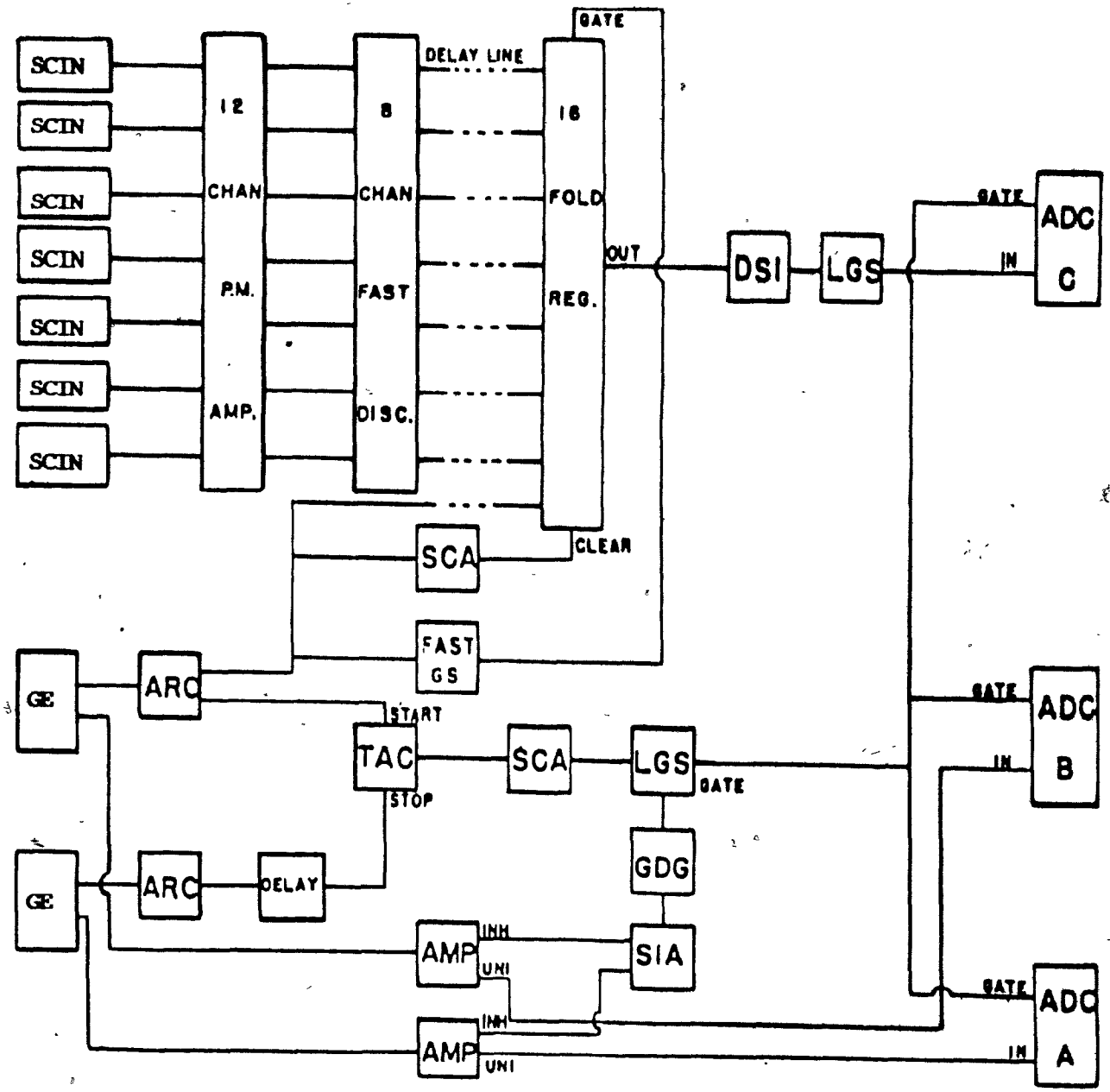
SCIN
SCIN
SCIN
SCIN
SCIN
SCIN
12
CHAN
P.M.
AMP.
8
CHAN
FAST
DISC.
DELAY LINE
16
FOLD
REG.
GATE
OUT
CLEAR
SCA
FAST
GS
DSI
LGS
GATE
IN
ADC
C
GE
ARC
START
TAC
STOP
SCA
LGS
GATE
GDG
GE
ARC
DELAY
AMP
INH
UNI
SIA
AMP
INH
UNI
GATE
IN
ADC
B
GATE
IN
ADC
A

stretcher. The fast gate stretcher originally used was built by another researcher previously at this lab (Dr. B. J. Varley). However, due to erratic and unreliable behaviour as well as poor pulse shape of the gate stretcher, a new model with overall better performance was built by the author. After each gate, the register is cleared by a signal also taken from one of the Ge. detectors. The output of the register is inverted to make it positive, sent through to a linear gate stretcher and then to an ADC on the PDP-15. The signals from the Ge. are of two types, a positive signal from the pre-amplifier used for energy and a fast negative signal taken from the anode and used for timing. The energy signals are amplified using Ortec 572 amplifiers. These amplifiers were chosen for their excellent stability over long periods of time. The amplified energy signals are sent to two more ADC's on the PDP-15. The timing outputs are used as start and stop pulses for a time to amplitude converter (Ortec 467) the output of which will eventually be used to gate all three ADC's. The output width of the TAC signal was set at 25ns. The amplifiers for the energy signals have an inhibit output which gives a pulse whenever pile-up occurs on the input. This inhibit pulse is used in anti-coincidence with the TAC pulse to prevent pile-up events being recorded.

Data is recorded event by event on magnetic tape. Typically, a run is considered complete when at least 8 magtapes worth of information have been accumulated. Depending on count rate this takes from twelve to sixteen hours. The experimental equipment and all the related power supplies generate a lot of heat which has to be dissipated. This is accomplished by cooling the experimental hut with an air conditioner.

D)Neutron Multiplicity:

The three experiments just described represent the usual method by

which I.B.γ data is acquired. However, for one isotope, ^{128}Te, because of the availability of six liquid scintillators (NE 213) on loan from the University of Manchester, a neutron multiplicity experiment was also carried out. The equipment is shown in figure 14. Briefly, four of these detectors, mounted so as to form a circle were placed in the forward direction of the beam in front of the target. The beam pipe passed through an opening at the centre of this detector defined circle. By this placement, neutrons, which are expected to be emitted in the forward direction prior to the compound nucleus reaching equilibrium (Chap.II), will be detected. The other two detectors are placed above and below the target at 90 to the beam. The isotropic neutron distribution given off by the compound nucleus after reaching equilibrium would be mainly what these detectors register. One Ge. detector was then placed at a back angle with respect to the beam.

The schematic of the electronics associated with this set-up is shown in figure 15. Pulses from the neutron detectors are sent to pulse shape discriminators (PSD's) made by Link systems #5010. The liquid scintillator used in the neutron detector is able to detect both neutrons and gamma-rays. The response of the scintillator to these two radiations result in different decay times for the output pulses; 500ns for neutrons, 10 ns for gammas. The discriminators work on this difference in fall time to tell between gamma-rays and neutrons. The outputs from the PSD's were then delayed using Quad discriminators (Lecroy 821) so that all pulses would arrive simultaneously at an eight channel fast discriminator (Lecroy 620CL). To get pulses from the detectors in order to set them in coincidence, a radium-beryllium neutron source was used. From the discriminator the signals were sent to the same 16 fold register used in

Figure 14:

Labelled Drawing of Neutron Multiplicity Equipment

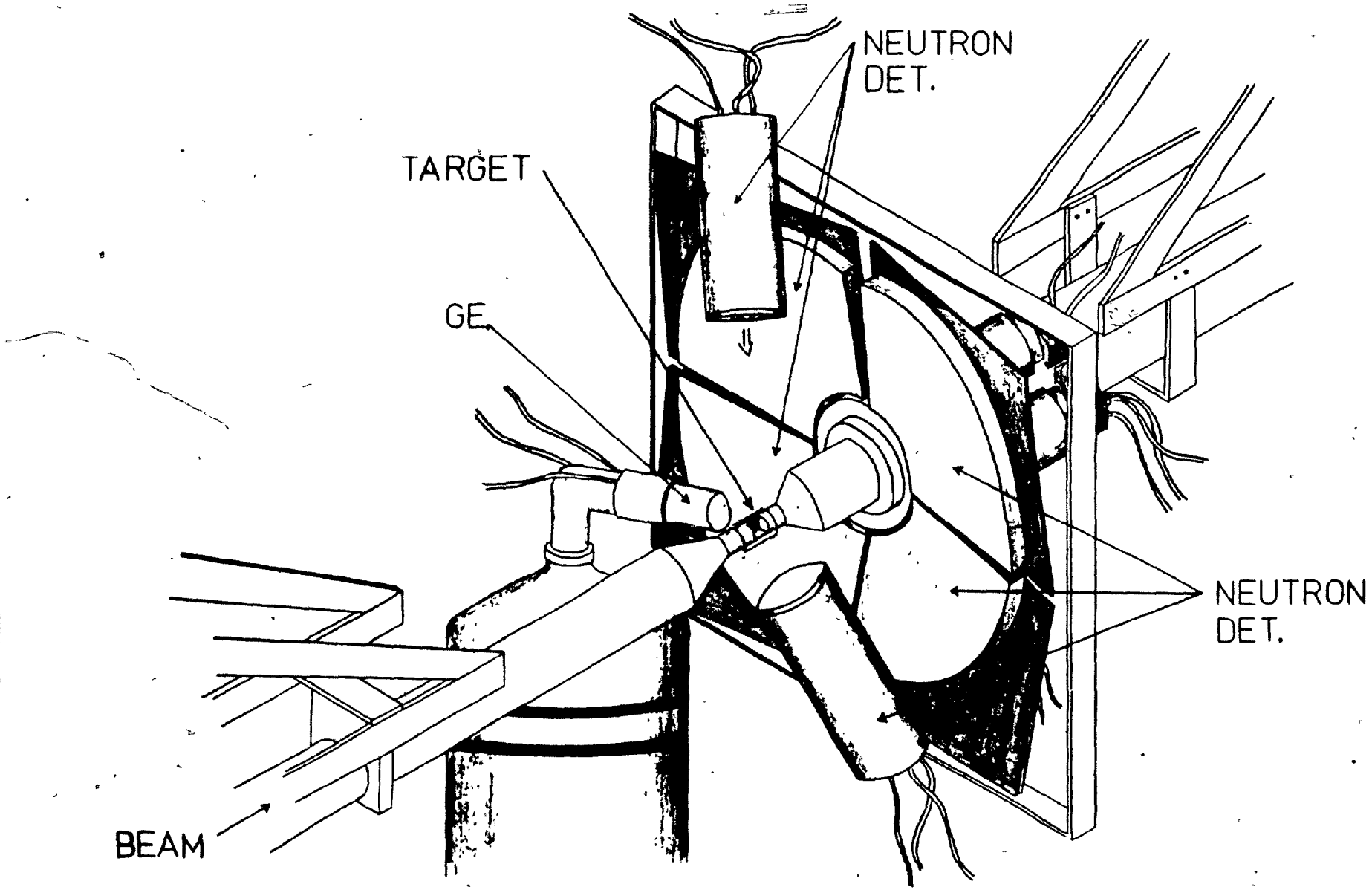
NEUTRON
DET.
TARGET
GE
NEUTRON
DET.
BEAM

Figure 15

Circuit diagram for the neutron-multiplicity experiment.

Explanation of symbols

LS: NE213 liquid scintillator

PSD: Pulse Shape Discriminator, Links 5010

Quad Disc: Quad Discriminator, Lecroy 821

8 CHAN FAST DISC: 8-Channel Fast Discriminator, Lecroy 620CL

16 FOLD REG: 16-Fold Register, Lecroy 2341A

TFA: Timing Filter Amplifier, Ortec 454

CFD: Constant Fraction Discriminator, Ortec 463

GDG: Gate and Delay Generator, Ortec 416A

SC: Slow Coincidence, Ortec 409

AMP: Spectroscopy Amplifier, Ortec 572

LGS: Linear Gate Stretcher, Ortec 442

DSI: Dual Summer and Inverter, Tennelec TC-212

SCA: Single Channel Analyser, Ortec 455

: Neutron channel output

GE: Germanium detector

INH: Pile-up output

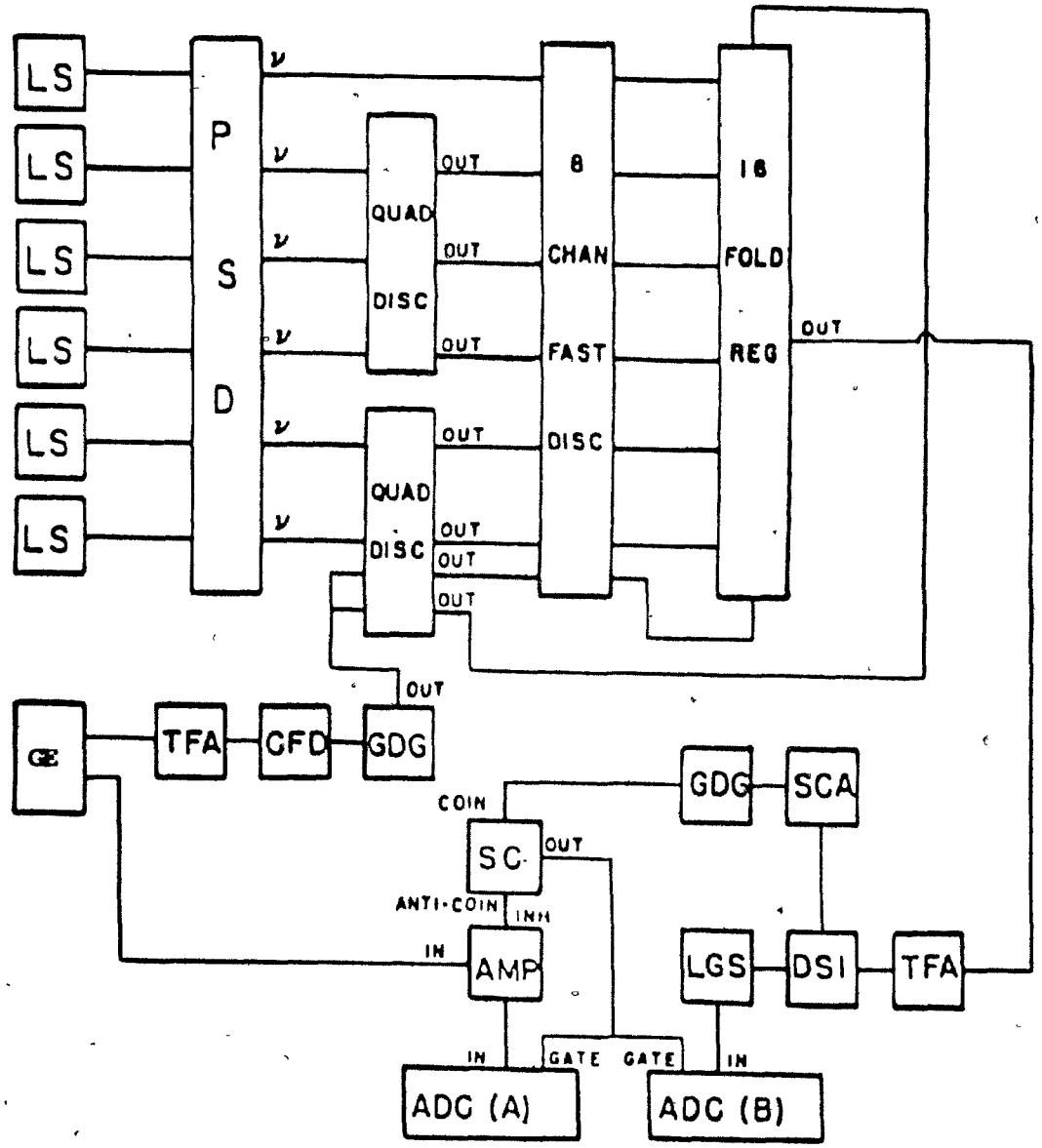
LS
LS
LS
LS
LS
LS
P
S
D
ν
ν
ν
ν
ν
ν
QUAD
DISC
QUAD
DISC
OUT
OUT
OUT
OUT
OUT
OUT
OUT
8
CHAN
FAST
DISC
16
FOLD
REG
OUT
OUT
GE
TFA
CFD
GDG
GDG
SCA
COIN
SC
OUT
ANTI-COIN
INH
IN
AMP
LGS
DSI
TFA
IN
GATE
GATE
IN
ADC (A)
ADC (B)

the gamma-gamma multiplicity experiment. The gate and clear pulses were, as before, taken from the timing output of the Ge. detector. The pulses from the register were then inverted, stretched and sent to one of the ADC's on the PDP-15. The energy signal from the Ge. was amplified using an Ortec 572 amplifier and sent to a second ADC. Both ADC's were gated using a pulse derived from a slow coincidence unit (Ortec 409). The inhibit pulse from the Ortec 572 fed the anti-coincidence input and a pulse teed off from the dual summer and inverter module used to invert the scintillator signal, fed the coincidence input.

The usefulness of doing a neutron multiplicity experiment results from the fact that it becomes possible to discriminate between different reaction channels, whether they be $(\alpha,3n)$, $(\alpha, 4n)$ etc. Its greatest use would thus be as an aid for placing gamma-rays in nuclei for which no level scheme exists. In the present case, the wealth of information already existing on the ^{128}Xe nucleus nullifies this use of the equipment. For assigning gamma-rays for which the ordinary gamma-gamma coincidence results are ambiguous the results from neutron multiplicity may prove useful.

Chapter IV: Results

A) The ^{126}Xe isotope

Previous Work:

The first published work on the level structure of ^{126}Xe appeared in 1949. Mitchell et al.(43) produced radioactive ^{126}I by bombarding metallic antimony with 23 MeV alpha particles. The ^{126}I so formed subsequently decayed by beta emission to ^{126}Xe. A 395 keV conversion electron was measured and interpreted as evidence for a first excited state in ^{126}Xe at 395 keV. Perlman and Friedlander(44) in 1951, also studying the decay of ^{126}I, substantiated this finding. In 1954 Kalkstein and Hollander(45) presented their results on the investigation of the decay of ^{126}Cs produced by nitrogen ion bombardment of indium. Here it was shown that a 385 keV gamma-ray followed positron decay in ^{126}Cs from which it was inferred that this gamma-ray came from the first excited state of ^{126}Xe. From log ft measurements the ground and first excited state were assigned spin and parity of 0^+ and 2^+ respectively. Another study of the decay of ^{126}I in 1955 by Koerts et al.(46) verified the $2^+ \rightarrow 0^+$ transition in ^{126}Xe and added a second 2^+ level at 860 keV. No further investigations into the level structure of ^{126}Xe was forthcoming until 1965 when Morinaga and Lark(47) published the first I.B.Y. investigations of this isotope. By bombarding separated metallic tellurium targets with alpha particles ^{126}Xe was produced via the reaction $^{124}Te(\alpha,2n)^{126}Xe$. Levels in ^{126}Xe up to 8^+ and a possible 10^+ state were reported. Also published in 1965 were the results of internal conversion electron measurements from the $^{127}I(p,2n)^{126}Xe$ reaction by Sakai, Yamazaki and Ejiri(48). These researchers established again the existence of three levels at 385, 872

and 929 keV in ^{126}Xe. These levels were assigned spin and parities of 2^+, 2_2^+ and 4^+ respectively. In 1966 Betigeri and Morinaga(49) published the first study of the level structure of ^{126}Xe in which a Ge(Li) detector was used. The ^{126}Xe isotope was produced by the ^{126}Te(^{3}He,3nγ)^{126}Xe reaction. No new levels for ^{126}Xe were reported in that work, but better energy measurements of the levels up to 6^+ were made. Ejiri et al.(50) in 1966 published work done using the angular distribution of conversion electrons coming from the ^{127}I(p,2n)^{126}Xe reaction. A new level at 829 keV was tentatively reported, the evidence being a gamma-ray of transition energy 439 keV going from an assigned 0_2^+ state to the first 2^+ state at 390 keV. The next work on ^{126}Xe to appear came out in 1969 and was published by Bergstrom, Herrlander and Kerek(51). They performed an I.B.γ. study on ^{126}Xe through the ^{124}Te(α,2n)^{126}Xe reaction. In that work levels up to 10^+ were definitely established as well as a tentative 5^- level at 2003 keV. The energy of the levels, via precise gamma-ray measurements, were also more accurately determined. In 1970 Singh and Taylor(52) published their investigations on the decay of ^{126}I. No new levels were proposed but better energy level determination of the 2^+ and 2_2^+ levels were made, these being 388.6 ± 0.2 and 879.8 ± 0.4 respectively. In 1974 Kusakari et al.(53) published their their study of the ^{127}I(p,2n)^{126}Xe reaction. Five new low lying levels were reported, one of which, at 2561.7 keV, was not seen in this present work. A second 6_2^+ level was tentatively assigned at 2214.3 keV and a second 4_2^+ level at 1488.2 keV. A level at 1317.3 keV was assigned spin and parity 3^+ whilst two levels at 1903.1 and 2561.7 keV were tentatively assigned values of 5^+ and 7^+. A more in-depth study of the decay of ^{126}Cs was published in 1976 by Pathak, Lessard, Nikkinen and Preiss(54). Seven new low lying levels for ^{126}Xe were reported, none of

which are produced in I.B.Y. work. Droste et al.(55) in 1978 published their findings on the level structure of ^{126}Xe studied by means of the decay of ^{126}Cs. No new levels were reported in that work. Finally, in 1979 Singh et al.(56) reported an assignment 0^+ to a level at 1313 keV found from the decay of ^{126}Cs.

I.B.Y. Spectroscopy:

The target used in this this experiment was Tellurium 126 of 98.7% isotopic purity. An excitation function was measured with the 28% Ge(HP) detector at lab bombarding energies of 42, 49, 54, 59, 64, 69 and 78 MeV. Figure 16 shows the excitation functions for six of the stronger peaks in ^{126}Xe. As may be seen from the figure, the excitation function peaks at 48 MeV and all experiments were subsequently carried out at this energy. Most of the peaks assigned to ^{126}Xe exhibit an excitation function similar to that in figure 16. Exceptions occurred when the peaks were too weak to have their intensities properly determined or when the peaks were doublets associated with peaks from other isotopes. Figure 17 shows the singles spectrum obtained in the ^{126}Te(α,xn)^{126}Xe reaction at 48 MeV. The peaks identified as belonging to ^{126}Xe are labelled. Energy calibration was carried out by placing standard sources of ^{152}Eu, ^{133}Ba and ^{60}Co at the target site. In order to correct for radioactivity from the beta-decay of product nuclei, a singles spectrum was taken immediately after turning off the alpha beam. The intensities of gamma-rays determined to be coming from ^{126}Xe, of which there were 25 in all, were determined from the singles spectrum. Table 3 lists all the gamma-rays and their relative intensities.

The multiplicity filter experiment was conducted as described in chapter III. The data was written event by event on magnetic tape on the PDP-15 computer and subsequently analysed on the PDP-11 computer. A total

Figure 16

Excitation Function for ^{126}Xe

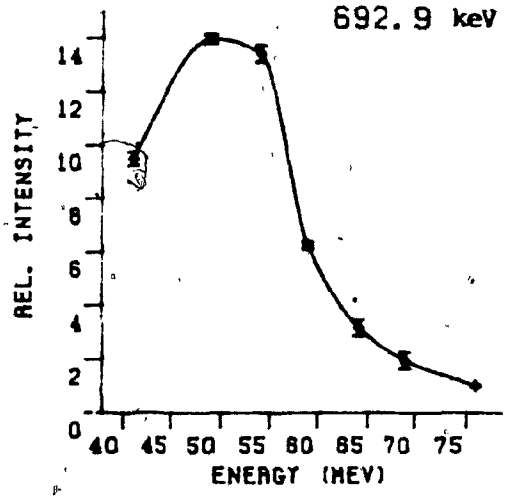
692.9 keV
REL. INTENSITY
ENERGY (MEV)

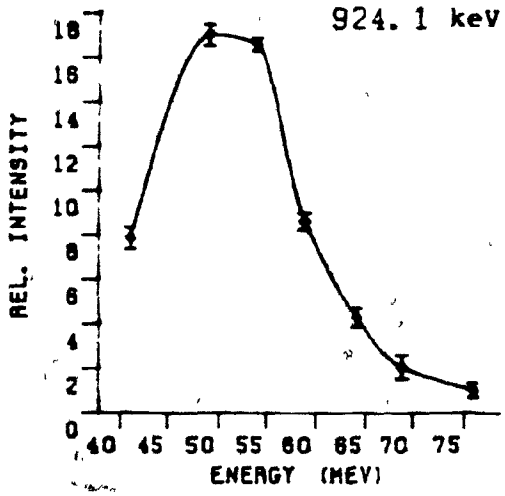
924.1 keV
REL. INTENSITY
ENERGY (MEV)

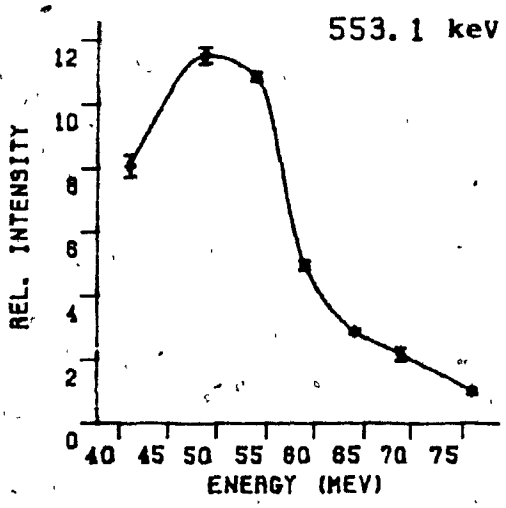
553.1 keV
REL. INTENSITY
ENERGY (MEV)

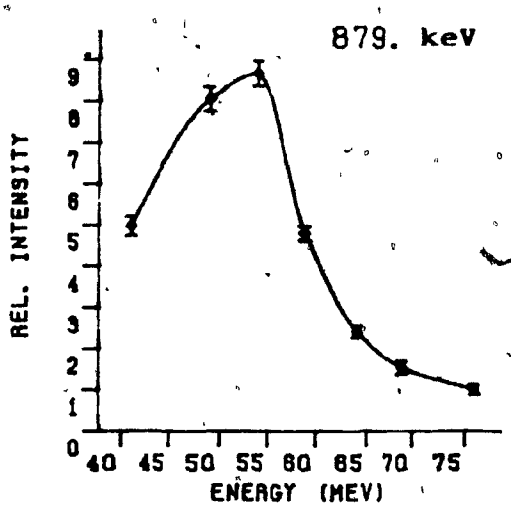
879. keV
REL. INTENSITY
ENERGY (MEV)

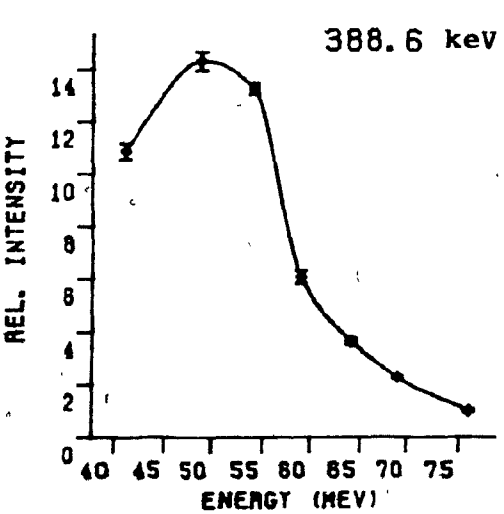
388.6 keV
REL. INTENSITY
ENERGY (MEV)

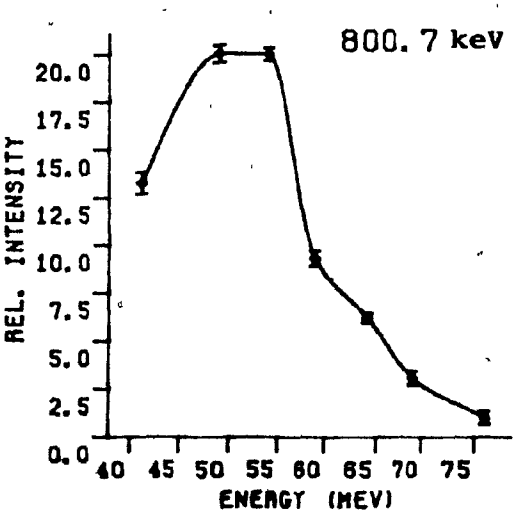
800.7 keV
REL. INTENSITY
ENERGY (MEV)

Figure 17

Singles Spectrum for ^{126}Xe

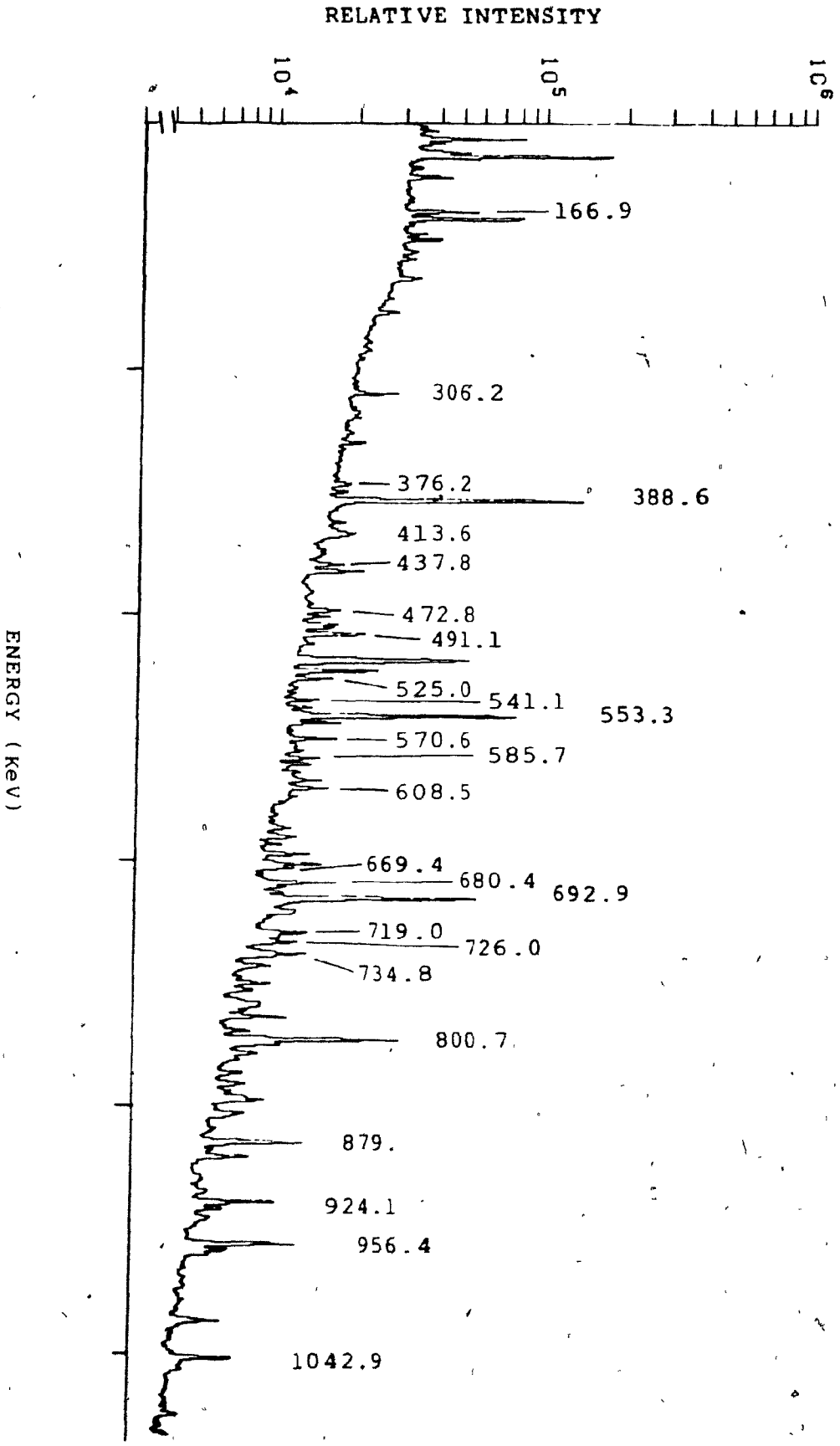
RELATIVE INTENSITY
10⁴
10⁵
10⁶
ENERGY (KeV)
166.9
306.2
376.2
388.6
413.6
437.8
472.8
491.1
525.0
541.1
553.3
570.6
585.7
608.5
669.4
680.4
692.9
719.0
726.0
734.8
800.7
879.
924.1
956.4
1042.9

Table 3

Energies and relative intensities of gamma rays assigned to transitions in Xenon 126. The numbers in parentheses indicate the uncertainties in the last digit(s).

Energy (kev)	Rel. Intensity	Energy (kev)	Rel. Intensity
166.8 (1)	131 (3)	800.7 (1)	362 (7)
306.1 (1)	27 (1)	879.7 (2)	137 (4)
388.62 (2)	1000 (12)	924.1 (1)	95 (3)
413.6 (2)	37 (6)	956.4 (1)	189 (4)
437.8 (1)	31 (2)	1042.9 (2)	87 (3)
472.9 (2)	41 (3)		
491.1 (1)	110 (4)		
525.1 (1)	43 (3)		
541.1 (1)	25 *		
553.3 (1)	789 (16)		
570.5 (1)	57 (5)		
585.7 (1)	40 (4)		
608.5 (2)	54 (5)		
669.4 (1)	36 (5)		
680.7 (1)	40 (4)		
692.9 (1)	707 (19)		
719.0 (1)	64 (7)		
726.0 (1)	59 (7)		
734.8 (1)	82 (10)		

* = upper limit

of 94 gates were set, 52 of which were on peaks, the rest being gates set on the spectrum background. Fifty two spectra with background subtracted were then obtained. For peaks close in energy, the same background was used. Figure 18 shows examples of background subtracted spectra with eight different gates. Table 4 shows the coincidence results for all the gamma-rays established as belonging to ^{126}Xe. Most gates were set with the condition that that only events where three or more gamma-rays were in coincidence were to be projected. For weak gammas the condition was changed to two or more gamma-rays in coincidence. The results of the coincidence experiment allowed the determination of gamma-rays belonging to ^{126}Xe. All the gammas indicated by the excitation function as belonging to ^{126}Xe were verified by the coincidence results. The intensities found from the singles spectrum were used to set up a level scheme, gamma-rays with less intensity being considered to precede more intense gammas with which they are in coincidence.

Angular Distribution Results

The spin and parity of the levels assigned to ^{126}Xe were deduced principally from the data of gamma-ray angular distribution. The intensities of the peaks in the angular distribution spectra were analysed and then normalised to the intensities of the main transitions in ^{126}Xe as measured by a stationary detector set at 125 degrees. The normalised intensities were fitted to fourth order Legendre polynomials as a function of detector angle. The A2 and A4 coefficients so obtained were then corrected for the finite solid angle subtended by the detector. The correction terms were calculated to be Q2 = .94 and Q4 = .81. The plotted Legendre functions for the gamma rays in ^{126}Xe are shown in figure 19. Table 5 lists the solid angle corrected A2 and A4 coefficients, the

Figure 18(in two parts)

Examples of Gamma Multiplicity Spectra

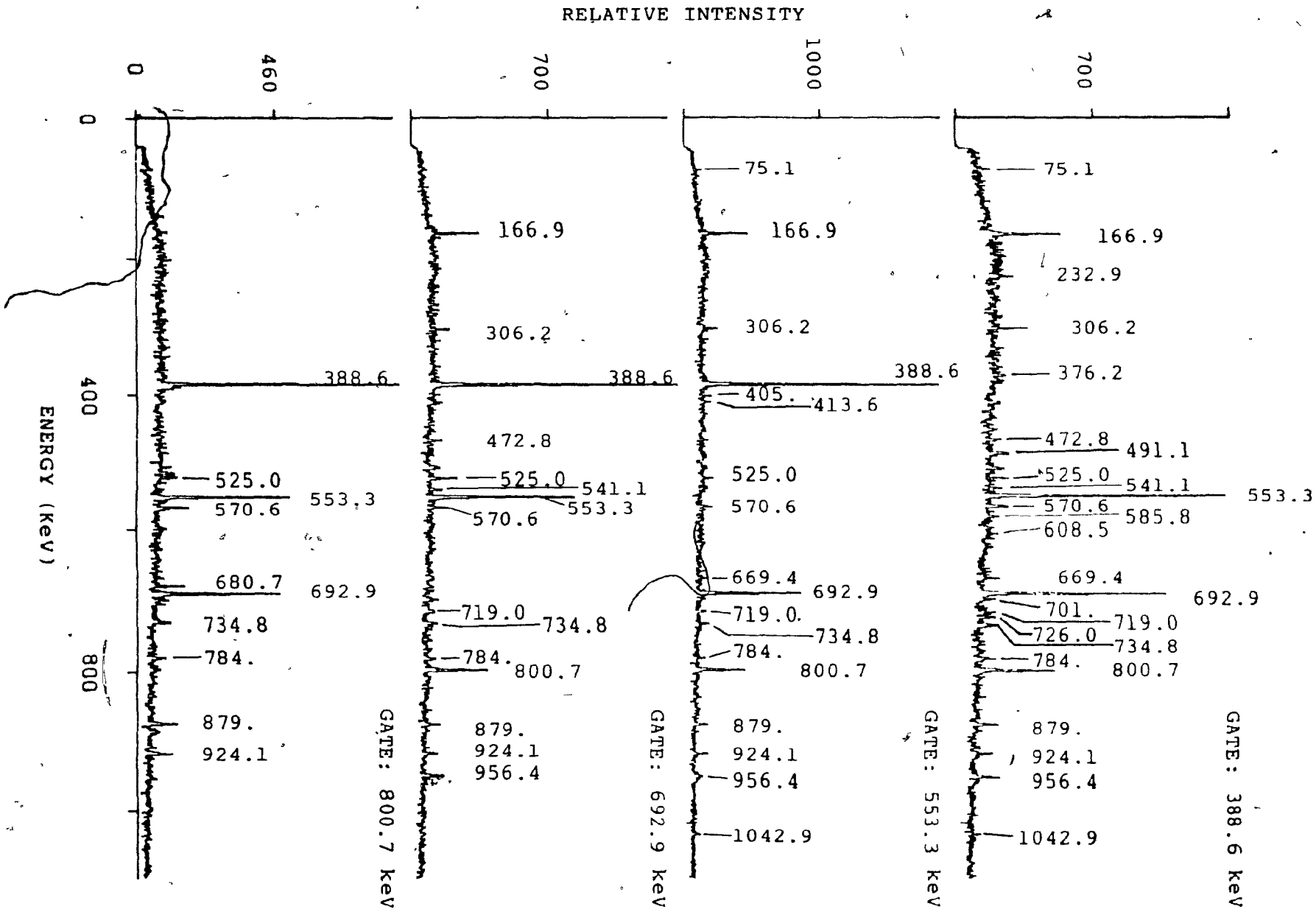
RELATIVE INTENSITY
0
460
700
1000
700
0
400
800
ENERGY (KeV)
388.6
525.0
570.6
553.3
680.7
692.9
734.8
784.
879.
924.1
GATE: 800.7 keV
166.9
306.2
388.6
472.8
525.0
541.1
570.6
553.3
719.0
734.8
784.
800.7
879.
924.1
956.4
GATE: 692.9 keV
75.1
166.9
306.2
388.6
405.
413.6
525.0
570.6
669.4
692.9
719.0
734.8
784.
800.7
879.
924.1
956.4
1042.9
GATE: 553.3 keV
75.1
166.9
232.9
306.2
376.2
472.8
491.1
525.0
541.1
553.3
570.6
585.8
608.5
669.4
692.9
701.
719.0
726.0
734.8
784.
800.7
879.
924.1
956.4
1042.9
GATE: 388.6 keV

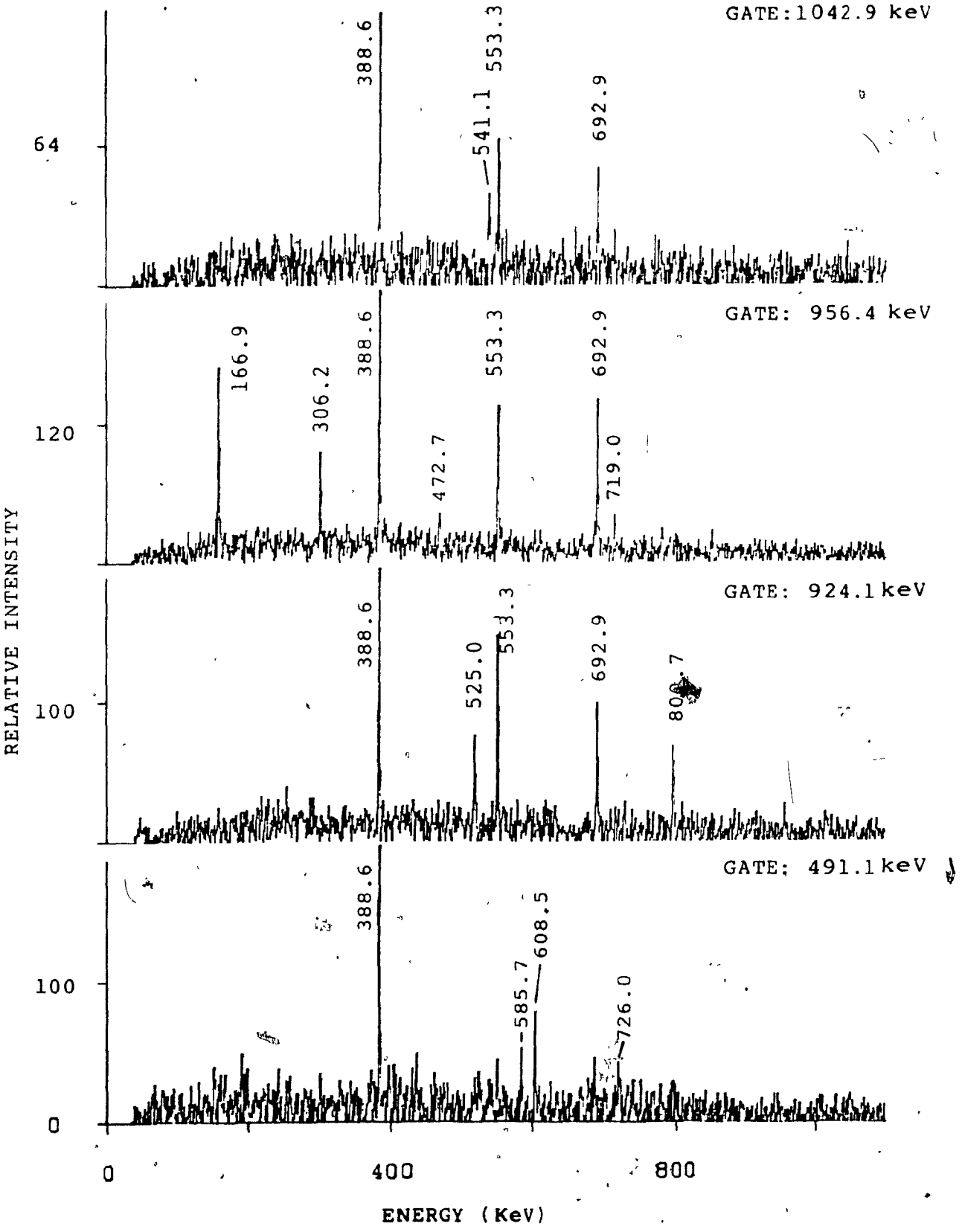
GATE:1042.9 keV
388.6
541.1
553.3
692.9
64
GATE: 956.4 keV
166.9
306.2
388.6
472.7
553.3
692.9
719.0
120
GATE: 924.1keV
388.6
525.0
553.3
692.9
806.7
100
GATE: 491.1keV
388.6
585.7
608.5
726.0
100
0
RELATIVE INTENSITY
0
400
800
ENERGY (KeV)

TABLE 4

Multiplicity Filter Results.

Gate (keV)	Coincident Gamma Rays (keV)
166.8	388.6, 553.3, 692.9, 956.4, 306.1, 719.0
306.1	103.0*, 166.8, 381.0*, 388.6, 393.1*, 553.3, 692.9, 719.0, 956.4
388.6	75.0*, 166.8, 233.1*, 306.1, 376.0*, 472.9, 491.1, 525.1, 541.1, 553.3, 570.5, 585.7, 608.5, 669.4, 692.9, 701.1*, 719.0, 726.0, 734.8, 800.7, 879.0, 924.1, 956.4, 1042.9
413.6	388.6, 553.3, 669.4, 692.9
437.8	388.6, 491.1, 585.7
472.9	343.0*, 376.2*, 388.6, 553.3, 603.1*, 692.9
491.1	388.6, 437.8, 585.7, 608.5, 680.7, (726.0)
525.1	84.0*, 388.6, 553.3, 692.9, 734.8, 800.7, 924.1
541.1	223.3*, 388.6, 553.3, 633.0*, 692.9, 1042.9
553.3	75.0*, 166.8, 306.1, 388.6, 413.6, 472.9, 525.1, 570.5, 669.4, 692.9, 719.0, 734.8, 784.0, 800.7, 879.0, 924.1, 956.4, 1042.9
570.5	388.6, 392.0, 553.3, 692.9, 734.8, 800.7, 979.0
608.5	388.6, 491.1, 726.0, 879.0
669.4	388.6, 392.0*, 413.6, 553.3, 692.9
680.7	388.6, 519.0*, 553.3, 692.9, 800.7
692.9	166.8, 306.1, 388.6, 472.9, 525.1, 541.1, 553.3,

Gate (keV)	Coincident Gamma Rays (keV) (cont'd)
	570.5, 719.0, 734.8, 784.0*, 800.7, 879.0, 924.1, 956.4
726.0	75.0*, 306.1, 388.6, 491.1, 608.5, 738.0*
734.8	388.6, 525.1, 553.3, 570.5, 680.7, 692.9, 726.0, 800.7, 879.0
800.7	388.6, 392.0*, 525.1, 553.3, 570.5, 680.7, 692.9, 734.8, 784.0*, 879.0, 924.1
924.1	388.6, 525.1, 553.3, 692.9, 800.7, 961.0*, (734.8)
956.4	166.8, 306.1, 388.6, 472.9, 553.3, 692.9, 719.0
1042.9	388.6, 541.1, 553.3, 692.9

* = not placed in level scheme

( ) = possible coincidence

Figure 19(in 6 parts)

Angular Distributions for ^{126}Xe

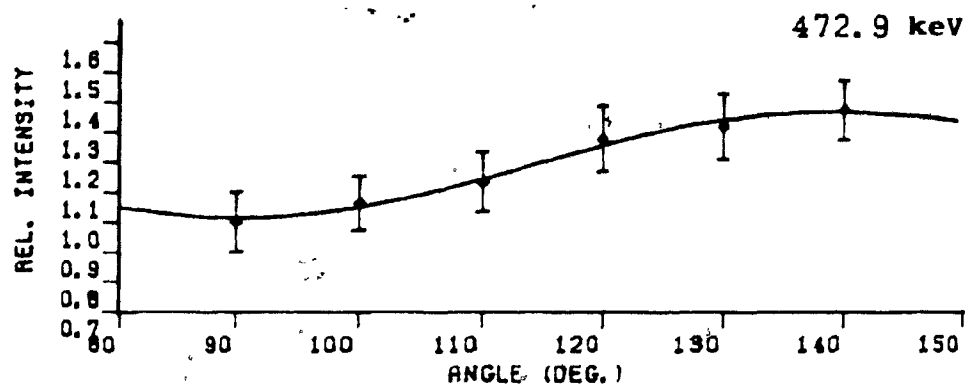
472.9 keV
REL. INTENSITY
1.6
1.5
1.4
1.3
1.2
1.1
1.0
0.9
0.8
0.7
80
90
100
110
120
130
140
150
ANGLE (DEG.)

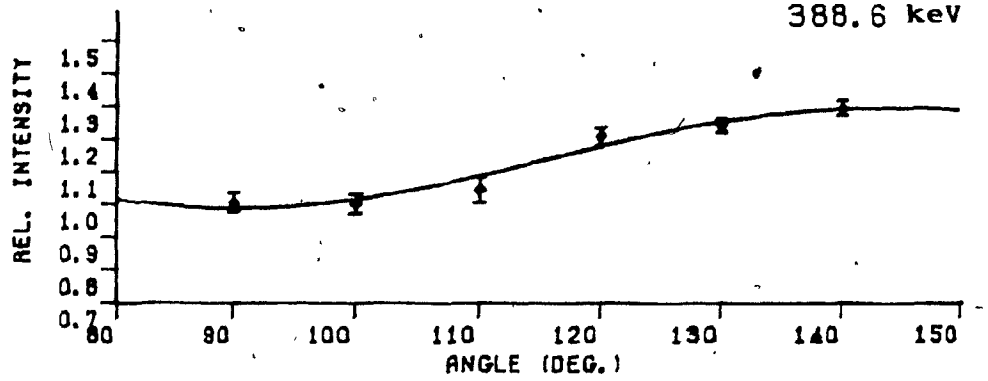
388.6 keV
REL. INTENSITY
1.5
1.4
1.3
1.2
1.1
1.0
0.9
0.8
0.7
80
90
100
110
120
130
140
150
ANGLE (DEG.)

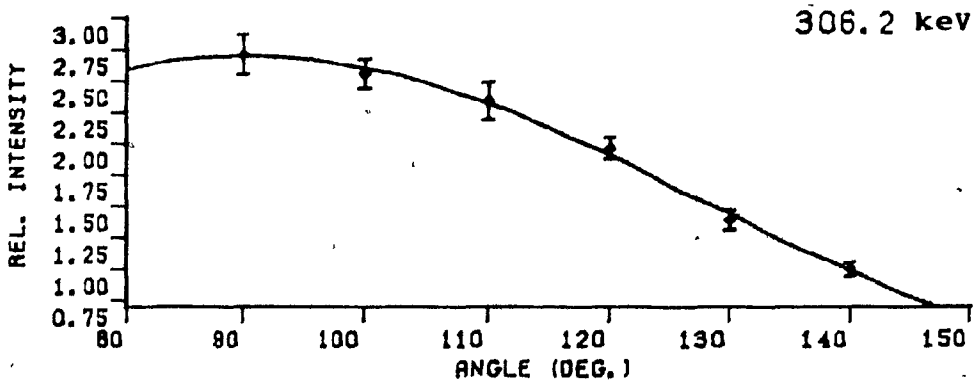
306.2 keV
REL. INTENSITY
3.00
2.75
2.50
2.25
2.00
1.75
1.50
1.25
1.00
0.75
80
90
100
110
120
130
140
150
ANGLE (DEG.)

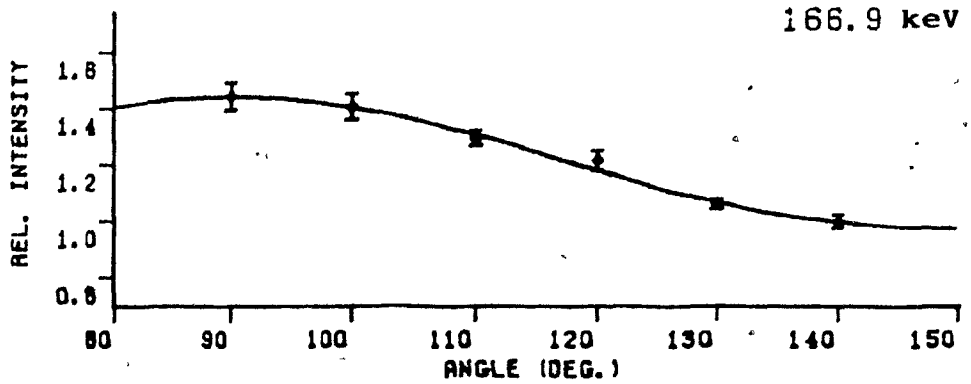
166.9 keV
REL. INTENSITY
1.6
1.4
1.2
1.0
0.8
80
90
100
110
120
130
140
150
ANGLE (DEG.)

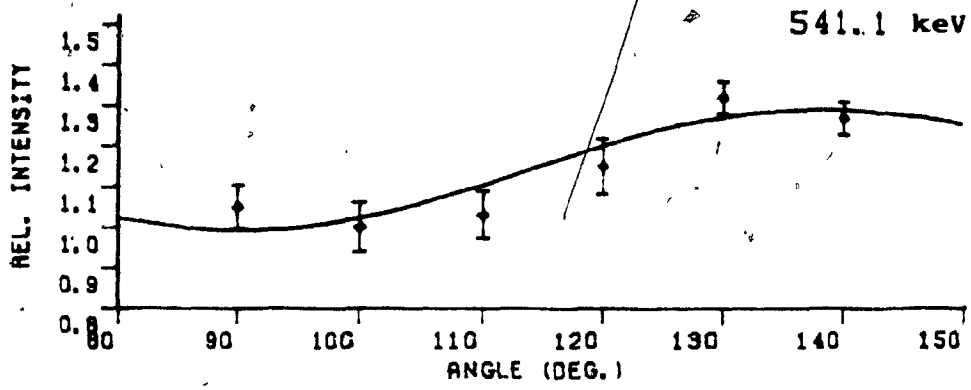
541.1 keV
REL. INTENSITY
1.5
1.4
1.3
1.2
1.1
1.0
0.9
0.8
80
90
100
110
120
130
140
150
ANGLE (DEG.)

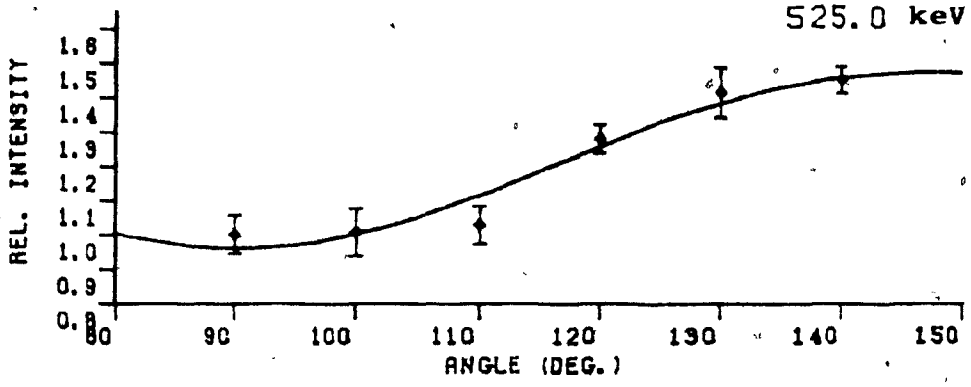
525.0 keV
REL. INTENSITY
1.6
1.5
1.4
1.3
1.2
1.1
1.0
0.9
0.8
80
90
100
110
120
130
140
150
ANGLE (DEG.)

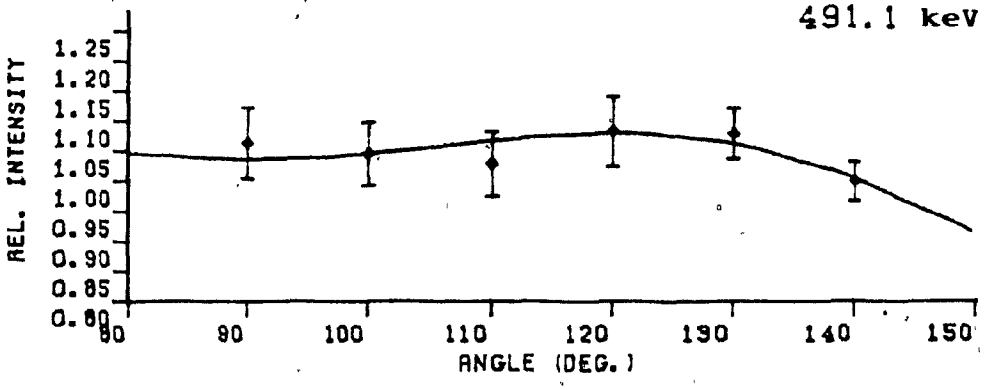
491.1 keV
REL. INTENSITY
1.25
1.20
1.15
1.10
1.05
1.00
0.95
0.90
0.85
0.80
80
90
100
110
120
130
140
150
ANGLE (DEG.)

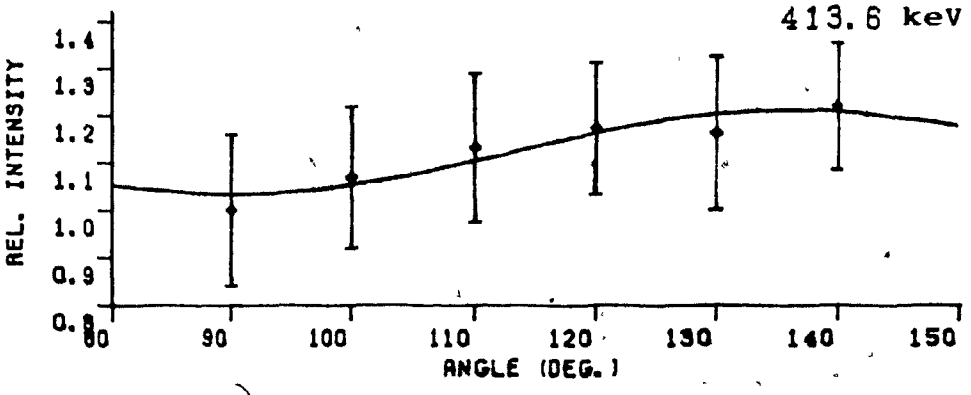
413.6 keV
REL. INTENSITY
1.4
1.3
1.2
1.1
1.0
0.9
0.8
80
90
100
110
120
130
140
150
ANGLE (DEG.)

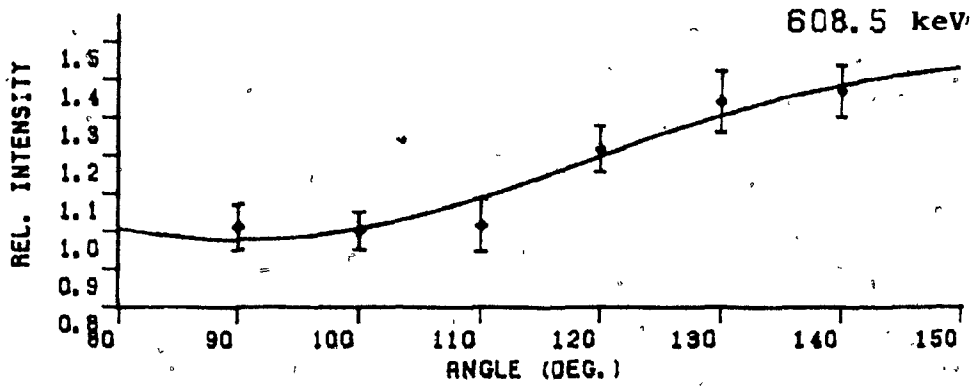
608.5 keV
REL. INTENSITY
1.5
1.4
1.3
1.2
1.1
1.0
0.9
0.8
80
90
100
110
120
130
140
150
ANGLE (DEG.)

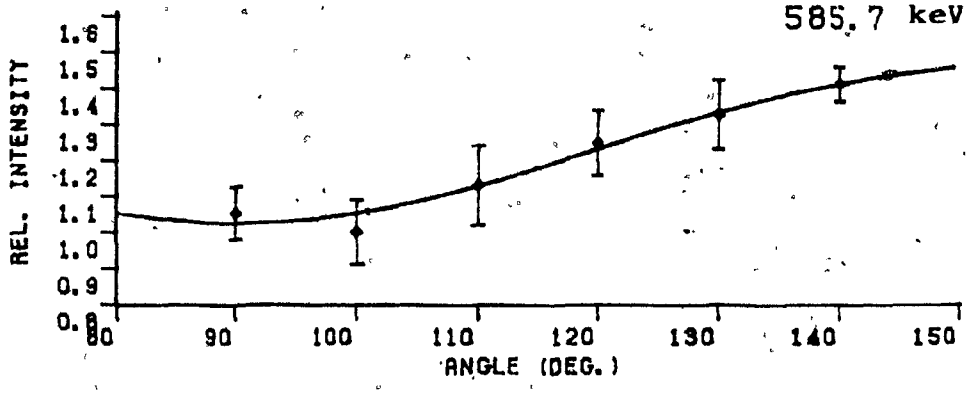
585.7 keV
REL. INTENSITY
1.6
1.5
1.4
1.3
1.2
1.1
1.0
0.9
0.8
80
90
100
110
120
130
140
150
ANGLE (DEG.)

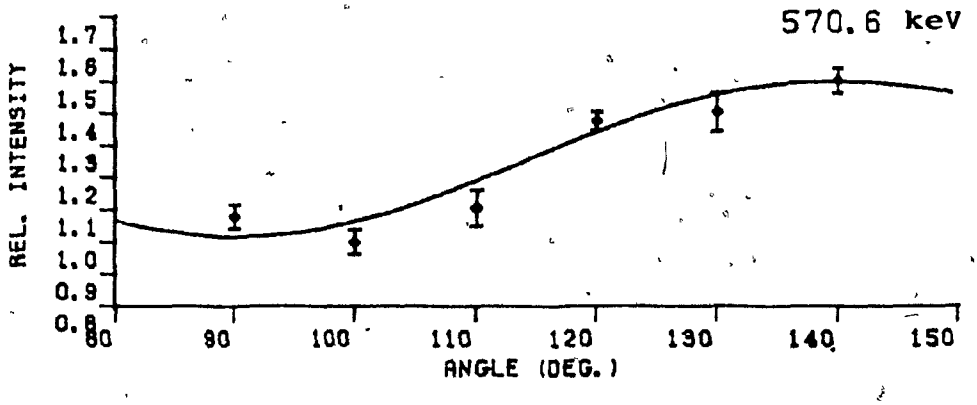
570.6 keV
REL. INTENSITY
1.7
1.6
1.5
1.4
1.3
1.2
1.1
1.0
0.9
0.8
80
90
100
110
120
130
140
150
ANGLE (DEG.)

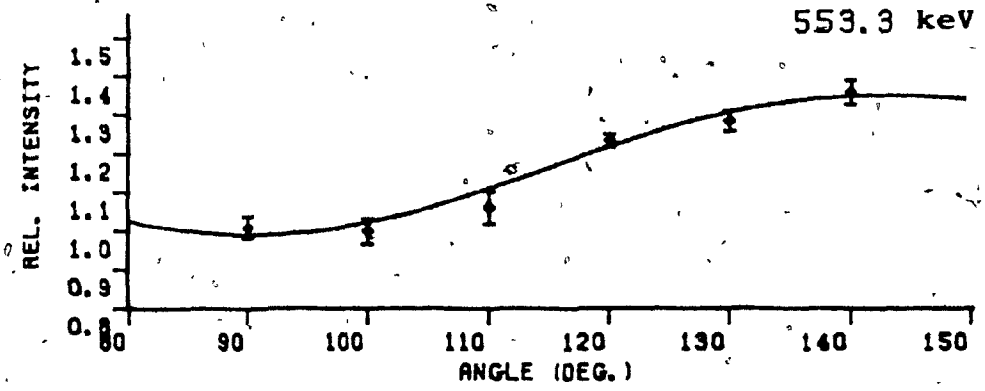
553.3 keV
REL. INTENSITY
1.5
1.4
1.3
1.2
1.1
1.0
0.9
0.8
80
90
100
110
120
130
140
150
ANGLE (DEG.)

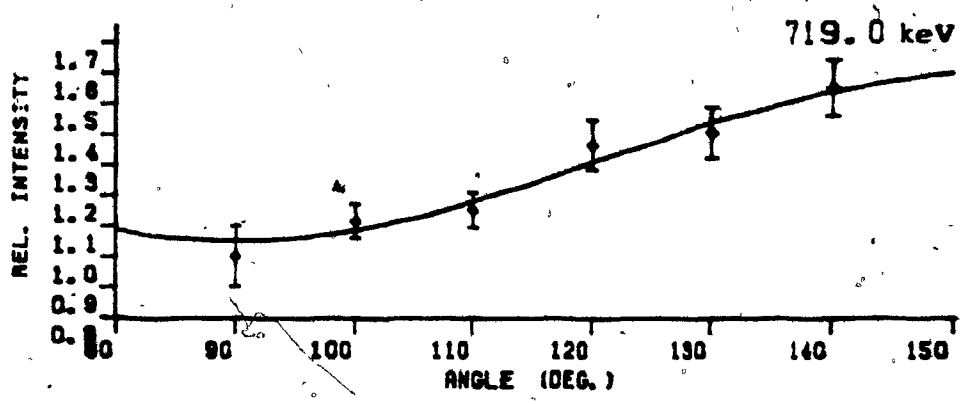
719.0 keV
REL. INTENSITY
1.7
1.6
1.5
1.4
1.3
1.2
1.1
1.0
0.9
0.
90
100
110
120
130
140
150
ANGLE (DEG.)

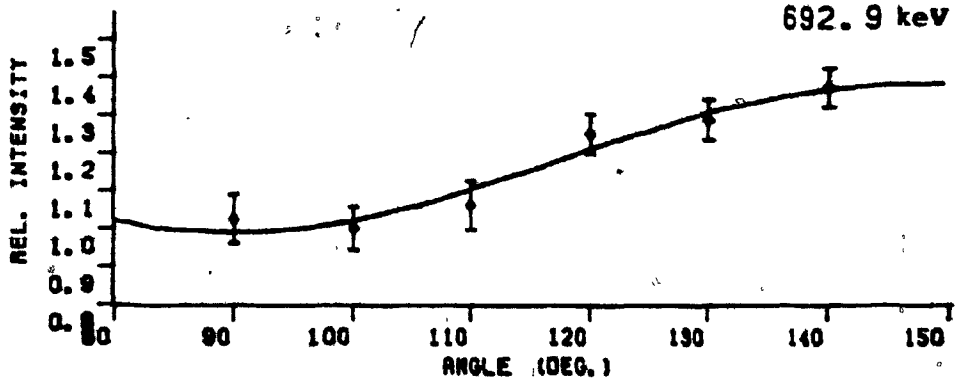
692.9 keV
REL. INTENSITY
1.5
1.4
1.3
1.2
1.1
1.0
0.9
0.
90
100
110
120
130
140
150
ANGLE (DEG.)

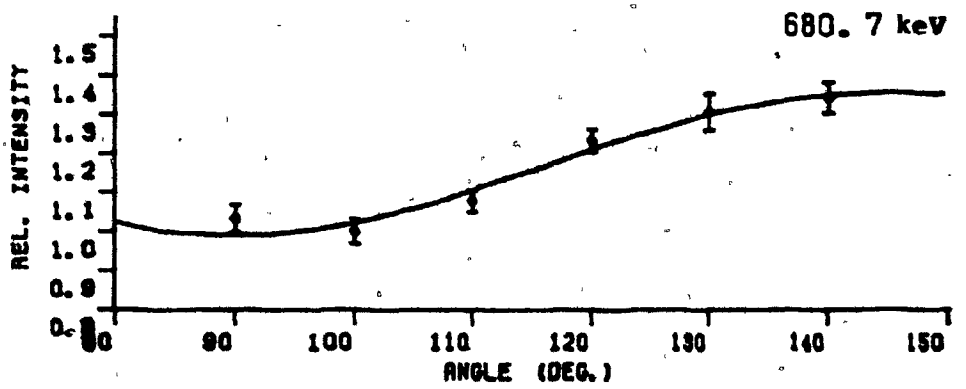
680.7 keV
REL. INTENSITY
1.5
1.4
1.3
1.2
1.1
1.0
0.9
0.
90
100
110
120
130
140
150
ANGLE (DEG.)

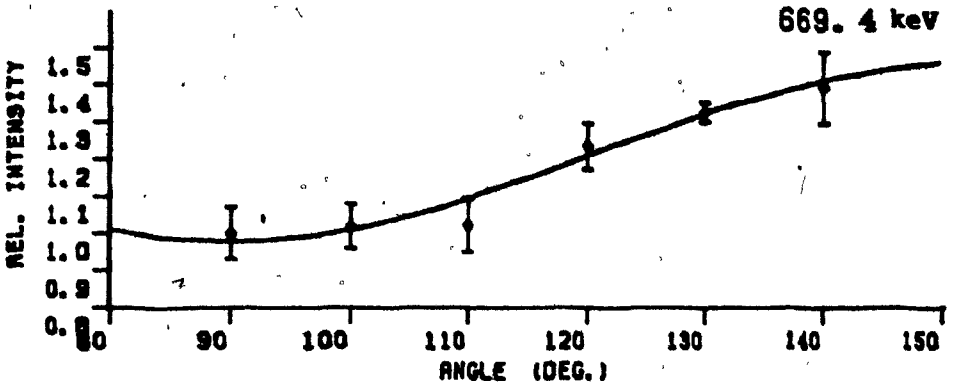
669.4 keV
REL. INTENSITY
1.5
1.4
1.3
1.2
1.1
1.0
0.9
0.
90
100
110
120
130
140
150
ANGLE (DEG.)

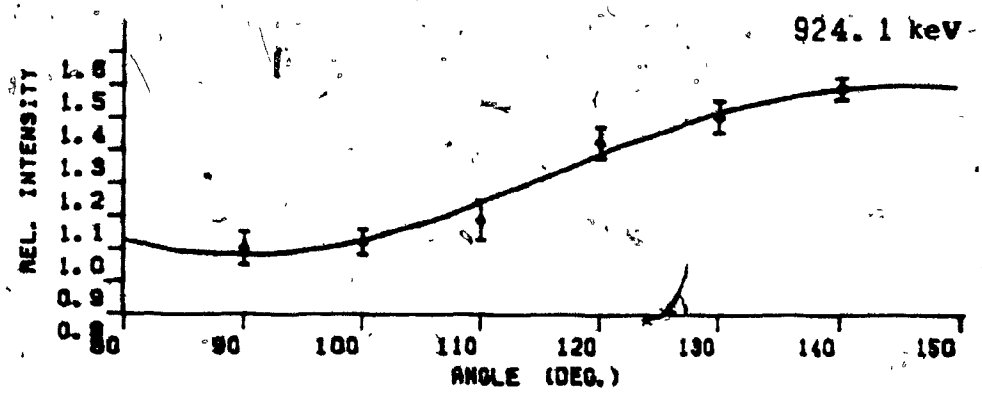
924.1 keV
REL. INTENSITY
1.6
1.5
1.4
1.3
1.2
1.1
1.0
0.9
0.
80
90
100
110
120
130
140
150
ANGLE (DEG.)

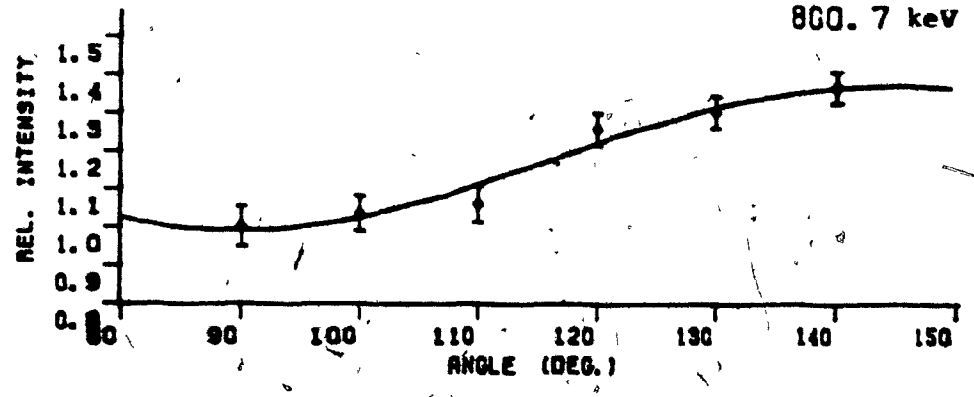
800.7 keV
REL. INTENSITY
1.5
1.4
1.3
1.2
1.1
1.0
0.9
0.
80
90
100
110
120
130
140
150
ANGLE (DEG.)

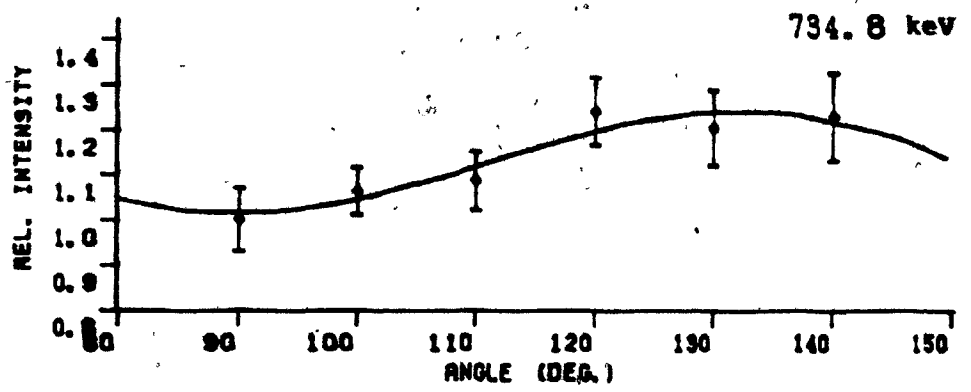
734.8 keV
REL. INTENSITY
1.4
1.3
1.2
1.1
1.0
0.9
0.
80
90
100
110
120
130
140
150
ANGLE (DEG.)

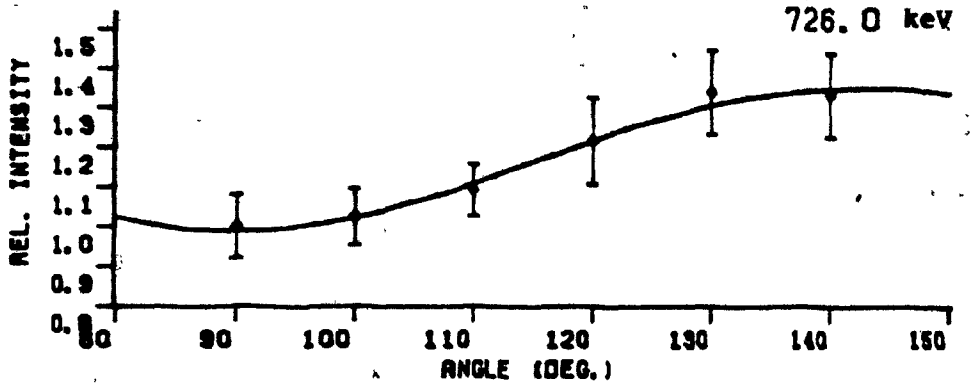
726.0 keV
REL. INTENSITY
1.5
1.4
1.3
1.2
1.1
1.0
0.9
0.
80
90
100
110
120
130
140
150
ANGLE (DEG.)

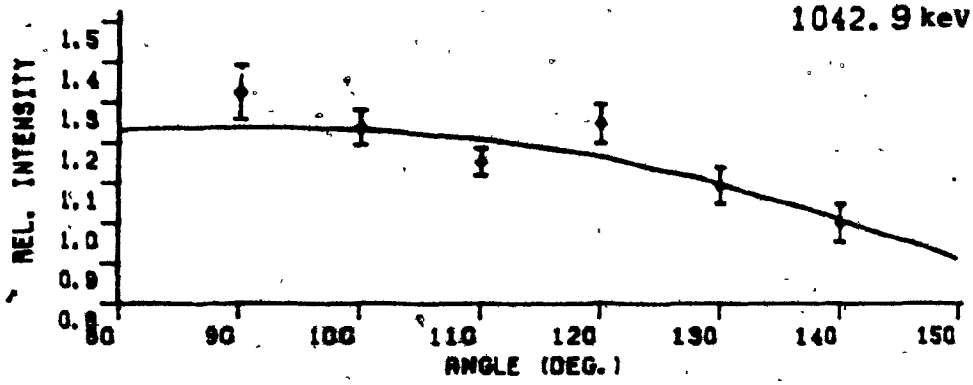
1042.9 kev
REL. INTENSITY
1.5
1.4
1.3
1.2
1.1
1.0
0.9
0.8
80
90
100
110
120
130
140
150
ANGLE (DEG.)

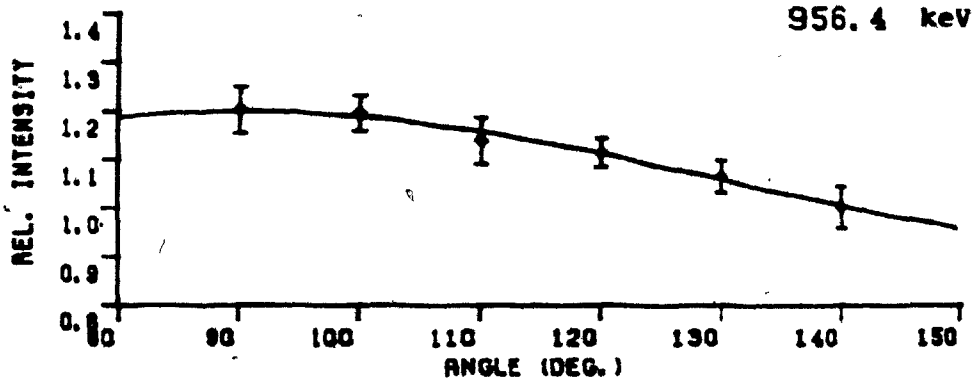
956.4 kev
REL. INTENSITY
1.4
1.3
1.2
1.1
1.0
0.9
0.8
80
90
100
110
120
130
140
150
ANGLE (DEG.)

Table 5

Table of Angular Distribution Results.

Energy (keV)	A2	A4	α_2	Assignment
166.8	-.304 ± .06	.169 ± .07	1	$8^+ \rightarrow 7^-$
306.1	-1.07 ± .13	0	---	$9^- \rightarrow 8^+$
388.62	.19 ± .05	.15 ± .07	.27	$2^+ \rightarrow 0^+$
413.6	---	---	---	$? \rightarrow 8^+$
437.8	---	---	---	$*3^+ \rightarrow 2^+$
472.9	.17 ± .2	.22 ± .2	.4	$9^- \rightarrow 7^-$
491.1	isotropic			$2_2^+ \rightarrow 2^+$
525.1	.314 ± .08	.2 ± .1	.78	$12^+ \rightarrow 10_2^+$
541.1	.142 ± .1	.2 ± .1		$(7,9)^\pm \rightarrow (5,7)^\pm$
553.3	.212 ± .06	-.18 ± .06	.42	$4^+ \rightarrow 2^+$
570.5	.233 ± .07	-.27 ± .08	.58	$12^+ \rightarrow 10^+$
585.7	.28 ± .14	-.1 ± .1	.58	$5^+ \rightarrow 3^+$
608.5	.306 ± .14	-.11 ± .16	.6	$4_2^+ \rightarrow 2_2^+$
669.4	.324 ± .2	-.11 ± .17	.75	$8_2^+ \rightarrow 6^+$
680.7	.226 ± .08	-.166 ± .09	.58	$16^+ \rightarrow 14^+$
692.9	.25 ± .1	-.15 ± .13	.55	$6^+ \rightarrow 4^+$
719.0	.343 ± .16	-.11 ± .11	.84	$11^- \rightarrow 9^-$
726.0	.211 ± .2	-.2 ± .2	.47	$6_2^+ \rightarrow 4_2^+$
734.8	.02 ± .2	-.23 ± .2	---	$14^+ \rightarrow 12^+$
800.7	.23 ± .09	-.17 ± .1	.53	$8^+ \rightarrow 6^+$
924.1	.304 ± .08	-.21 ± .1	.74	$10_2^+ \rightarrow 8^+$
956.4	.2 ± .1	0	.67	$7^- \rightarrow 6^+$
1042.9	-.29 ± .11	0		$(5,7)^\pm \rightarrow 6^+$

deduced spin, parity and the attenuation coefficients. The attenuation coefficients α_2 are calculated as the ratio of experimental and theoretical A2 coefficients assuming the assignments listed in the table. The theoretical values for A2 and A4 are taken from the tables by Yamazaki (37) and Der Mateosian and Sunyar (38). In determining the spin and parity of the levels the following assumptions were made: 1) All quadrupole transitions have a positive A2 coefficient and a small negative A4 coefficient. Since magnetic quadrupole transitions have a small transition amplitude, their occurence normally results in an isomeric state. Since none of the ^{126}Xe levels found in this work have any appreciable lifetimes, all quadrupole transitions are assumed electric. Further all E2 transitions are assumed to be of the stretched variety (i.e. $L = |\vec{J}i - \vec{J}f|$).

2) Transitions higher than quadrupole are assumed not to occur. 3) Pure dipole transitions have a negative A2 coefficient and zero A4 coefficient. Dipole transtitions are also assumed to be mostly of the stretched variety. Determination of the parity of the dipole transitions are determined, if at all, by other evidence, such as systematics, when possible. Levels which are not easily classified by the above scheme are either left undetermined or an attempt is made to determine them self-consistently by means of mixed radiative transitions.

The series of most intense gamma rays, up to the level at 3315.2 keV, were previously identified by Droste et al. (55), as being a cascade of E2 photons. The levels were thus assigned even spin and even parity values ending with the 3315.2 keV levl having a value of 10^+. The angular distributions in this work agrees definitely with these assignments. Further, the levels at 3359.6, 3884.7, 4620.5 and 5301.2 keV all display unambiguous E2 distributions and are assigned values of 10^+_2, 12^+, 14^+,

and 16^+ respectively. It must be pointed out, however, that for the 14^+ level at 4720.5 keV, the experimentally determined angular distribution of the 734.8 kev gamma-ray leaving that level is very poor. The A2 coefficient although positive, is very small (.02) and has a large error. The A4 coefficient is negative. The assignment of an E2 transition was thus not totally conclusive. However, the assignment of 14^+ to the 4720.5 kev level is very reasonable since the coincidence results indicate that the level is part of the ground band cascade. For the 10^+ level at 3315.2 keV the 879.7 keV gamma-ray depopulating this level is a doublet which could not be resolved by means of a non-linear least squares fit. No angular distribution for this gamma-ray was obtained and the 10^+ asignment to the 3315.2 keV level was made on the basis of the angular distribution of the gamma-ray feeding this level, the spin of the level above being known. Also, as in the case of the 14^+ level, the coincidence results indicate that the 3315.2 keV level is part of the ground band cascade.

The 956.4 keV gamma-ray coming from the level at 2591.2 keV and feeding the 6^+ level at 1634.8 keV, has a negative A2 coefficient and zero A4 coefficient. This indicates a dipole transition. The 956.4 keV gamma-ray is also the next most intense gamma-ray after the 800.7 keV gamma-ray in the $8^+ \rightarrow 6^+$ transition. Goettig et al. (57) report intense electric dipole transitions from 7^- to 6^+ in the ^{128}Xe and ^{130}Xe nuclei. Taking these facts into account the 2591.2 keV level is assigned the spin and parity of 7^-. The level which decays to the 2591.2 keV level also has a negative A2 coefficient and is assigned spin and parity 8^+. The level at 3064.1 keV decays either by the 306.1 keV gamma-ray to the level at 2758.1 keV or by the 472.9 keV gamma-ray to the level at 2591.2 keV. The 306.1 keV gamma-ray is identified as a dipole transition whereas the 472.9

keV gamma-ray shows a characteristic E2 distribution. Thus the 3064.1 keV level is assigned a value of 9^-. The 719.0 keV gamma-ray feeding the 3064.1 keV level comes from a level at 3783.1 keV and shows a stretched E2 pattern. Hence the 3783.1 keV level is assigned the value 11^-.

For the levels at 879.7, 1317.5, 1488.1, 1903.2 and 2214.2 keV, Kuskari et al. (53) in 1975 identified them as having spin and parities of 2_2^+, 3^+, 4_2^+, 5^+ and 6_2^+ respectively. For the case of the 2_2^+ to 2^+ transtion from the level at 879.7 keV, the transiting 491.1 keV gamma-ray has an isotropic angular distribution supporting the assignment. The other levels are also similarly verified by the angular distribution. One exception to this is the 3^+ assignment for the 1317.5 keV level. In this case the angular distribution obtained proved too ambiguous and had too large an error associated with it to make an assignment. Hence the assignment of 3^+ made by Kuskari is accepted as being correct without verification.

The 2717.8 keV level decays to a 2304.2 keV level by a 413.6 keV gamma-ray, the measured distribution of which has large errors and appears almost istropic. As a result no assignment could be made to the 2717.8 keV level. The 2304.2 keV level decays, in turn, to the 6^+ level at 1634.8 keV via a 669.2 keV gamma-ray. The angular distribution of this latter gamma-ray shows an E2 pattern and so the 2304.2 keV level is assigned a spin and parity value 8^+. The 6^+ level at 1634.8 keV is also fed by a 1042.9 keV gamma-ray, originating in a level at 2677.7 keV. The 1042.9 keV gamma-ray has a negative A2 coefficient which suggests an assignment of $(5,7)^\pm$ for the 2677.7 keV level. Finally the level at 3218.8 keV is assigned the value $(7,9)^\pm$ since it decays to the 2677.7 keV level via a 541.1 keV gamma-ray which has an E2 distribution.

Level Scheme

Figure 20 shows the level scheme of ^{126}Xe deduced in this work. Most of the previously reported levels have been observed and a number of new levels are reported. For example, the 16^+ level at 5301.2 keV is the highest spin yet reported for this isotope. The negative parity levels at 3064.1 and 3783.1 keV are also new. After the analysis of this isotope was completed a paper by Kusakari et al.(58 - Nuclear Physics June 1983) was published. That paper confirms the main features of the level scheme presented here but goes only to a spin of 14^+. Also the 9^- and 11^- levels are not reported in that paper although the 7^- level is.

In chapter V the level scheme will be discussed and the subject of back-bending will be dealt with there.

Figure 20

Level scheme for ^{126}Xe

(Energies are in keV)

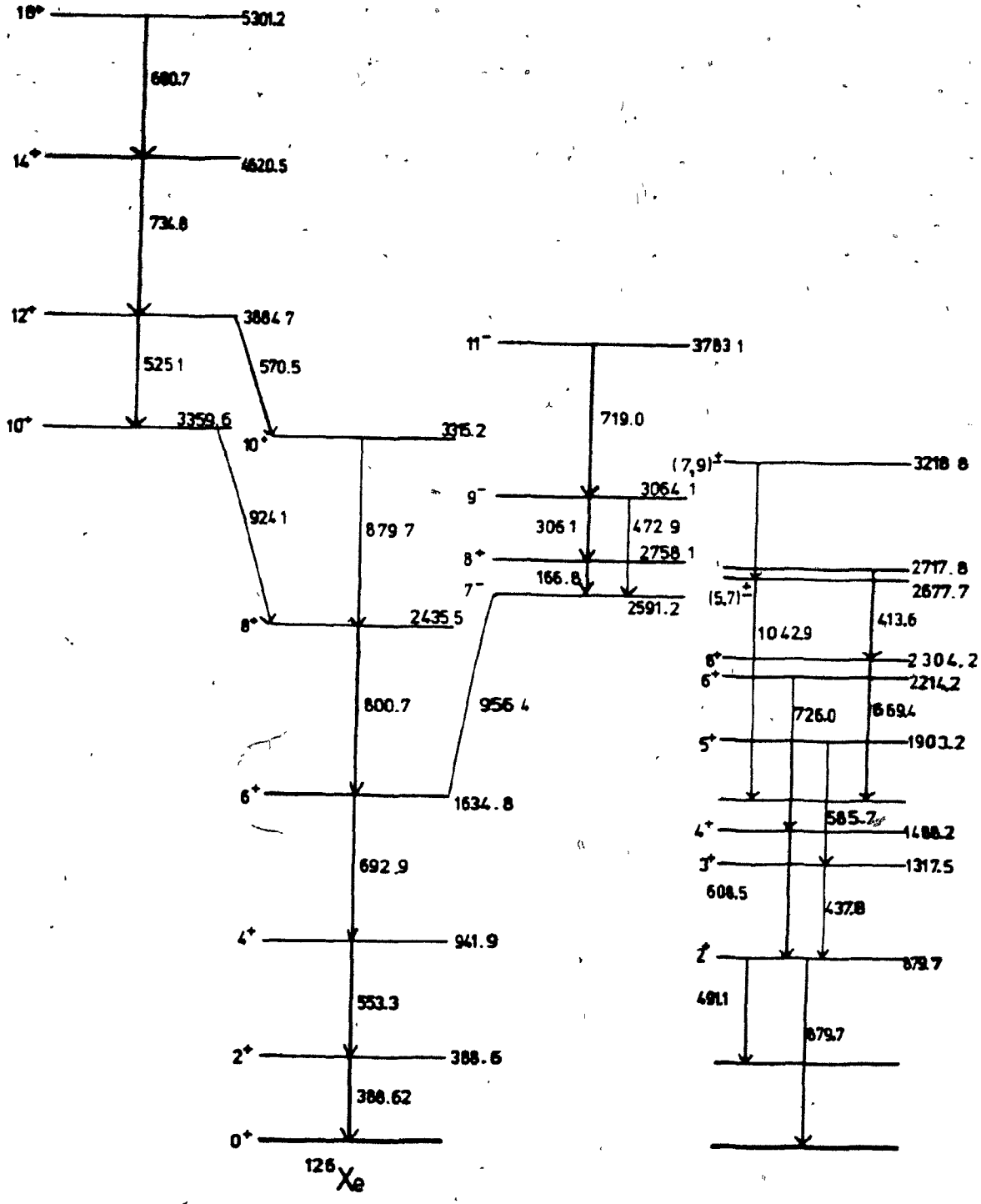
18+
5301.2
680.7
14+
4620.5
734.8
12+
3884.7
525.1
570.5
10+
3359.6
3316.2
10+
924.1
879.7
8+
2435.5
800.7
956.4
6+
1634.8
692.9
4+
941.9
553.3
2+
388.6
388.62
0+
126Xe
11−
3783.1
719.0
9−
3064.1
306.1
472.9
8+
2758.1
166.8
7−
2591.2
(7,9)+
3218.8
2717.8
2677.7
(5,7)+
1042.9
413.6
8+
2304.2
6+
2214.2
726.0
669.4
5+
1903.2
585.2
4+
1488.2
3+
1317.5
608.5
437.8
2+
879.7
491.1
879.7

B)The ^{128}Xe isotope:

Previous work

Morinaga and Lark(47) presented, in 1965, a level scheme for ^{128}Xe deduced from I.B.γ. studies. The target used was separated metallic Tellurium and the ^{128}Xe isotope was produced via ^{128}Te(α,4nγ)^{128}Xe and ^{128}Te(α,2nγ)^{128}Xe reactions. The incident energy of the alpha particles was 48 MeV. Ground band levels up to 10^+ were reported in that work. In 1967 Betigeri and Morinaga(49) published the first study of the level structure of ^{128}Xe using a Ge(Li) detector. The ^{128}Xe isotope was produced from the ^{128}Te(^{3}He,3nγ)^{128}Xe reaction with a maximum projectile energy of 19.3 MeV. Because of this low projectile energy, as compared to the projectile energy used in Ref. 47 above, the ground band levels were seen only up to a spin of 6. Bergstrom et al.(51), in 1969, were the next to publish data on the level scheme of ^{128}Xe. By bombarding ^{126}Te with 28 MeV alpha particles, they were able to produce ^{128}Xe and observe levels up to 10^+. They were also the first to carry out an angular distribution experiment on this isotope. A negative parity level of spin 5 at 2003 keV was tentatively reported. In 1971, Reierson et al.(59) used a bent-crystal spectrometer to obtain high precision gamma-ray energies and relative intensity values for the ^{128}Xe isotope. The ^{128}Xe isotope was produced via the decay of ^{128}I. Two levels were reported in that work, the $2^+ \rightarrow 0^+$ 442.9 keV level and the $2_2^+ \rightarrow 2^+$ 968.5 keV level. Gordon et al.(60), in 1975, populated the first 2^+ level in ^{128}Xe by Coulomb excitation. No further information regarding the level scheme was reported in that work. Helmer et al.(61) published, in 1977, the results of their investigation of the decay of ^{128}Cs. The ^{128}Cs was produced by 800 MeV proton induced spallation in praseodymium metal foils. The subsequent decay of ^{128}Cs to

^{128}Xe allowed the assigning of 57 gamma-rays to the ^{128}Xe nucleus. High spin states were not populated. In 1979 Shneider et al(62) presented their results on the decays of ^{128}Cs and ^{128}I to states in ^{128}Xe. As in Ref. 61, levels of spin higher than 4^+ were not populated. Also presented in 1979 were the results of the decay of ^{128}Cs as done by Singh et al.(63). The main thrust of that work was the assigning of an 0^+ excited state in ^{128}Xe. Finally, in 1980, Goettig et al.(57) published an in-depth I.B.γ. study of ^{128}Xe produced through the ^{128}Te(α,2nγ)^{128}Xe and ^{128}Te(^{3}H,3nγ)^{128}Xe reactions. Many new levels not in the ground band were reported. The highest spin assigned to a ground band level was 10^+ and a number of negative parity states were reported.

I.B.γ. Spectroscopy

The target used in this experiment was Tellurium 128 of 99.19% isotopic purity. AS in the case of the ^{126}Xe isotope an excitation function was obtained by bombarding the ^{128}Te target at energies of 42, 49, 54, 59, 64, 69 and 78 MeV and analysing the spectrum obtained at each energy. Figure 21 shows the excitation functions for six of the stronger peaks in ^{128}Xe. Except for the case of the 612.4 keV gamma-ray, all the peaks have their maximum intensity at 42 MeV. When the beam is degraded to 42 MeV it becomes very difficult to focus (Chapter II). Because of this latter difficulty and since we are interested in obtaining as high a spin as possible in the residual ^{128}Xe nucleus, the experiment was run at 49 MeV. This was made feasible by the fact that the intensity difference between gamma-rays emitted from the ^{128}Xe nucleus at 41 MeV is not that much greater than those emitted at 49 MeV. Figure 22 shows the singles spectrum obtained in the ^{128}Te(α,4n)^{128}Xe reaction at 49 MeV. The peaks identified as belonging to ^{128}Xe are labelled. Energy calibration was

Figure 21

Excitation Function for ^{128}Xe

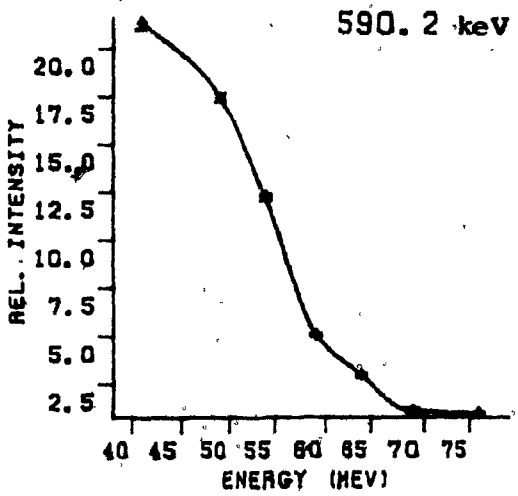
590.2 keV
REL. INTENSITY
20.0
17.5
15.0
12.5
10.0
7.5
5.0
2.5
40 45 50 55 60 65 70 75
ENERGY (MEV)

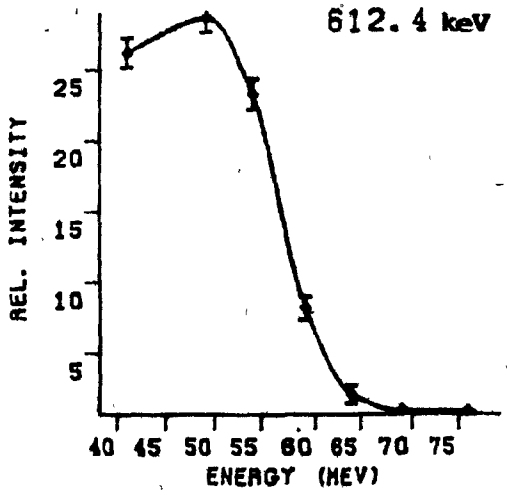
612.4 keV
REL. INTENSITY
25
20
15
10
5
40 45 50 55 60 65 70 75
ENERGY (MEV)

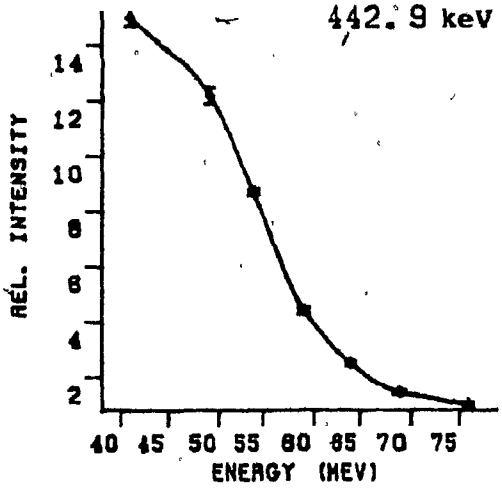
442.9 keV
REL. INTENSITY
14
12
10
8
6
4
2
40 45 50 55 60 65 70 75
ENERGY (MEV)

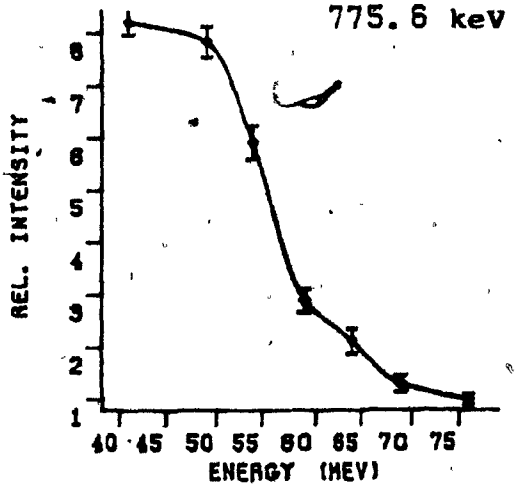
775.6 keV
REL. INTENSITY
8
7
6
5
4
3
2
1
40 45 50 55 60 65 70 75
ENERGY (MEV)

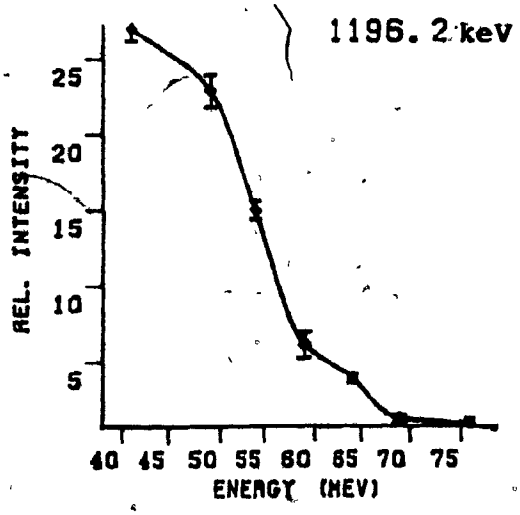
1196.2 keV
REL. INTENSITY
25
20
15
10
5
40 45 50 55 60 65 70 75
ENERGY (MEV)

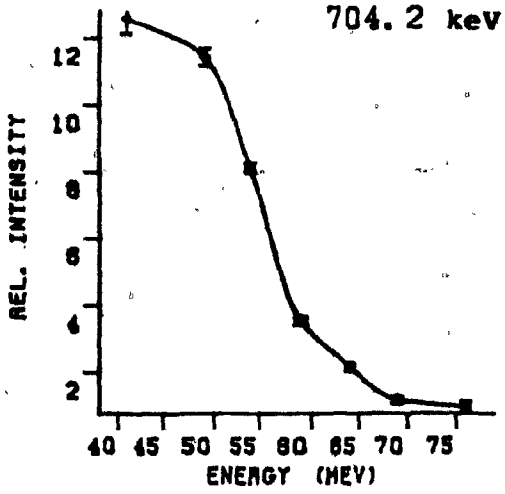
704.2 keV
REL. INTENSITY
12
10
8
6
4
2
40 45 50 55 60 65 70 75
ENERGY (MEV)

Figure 22

Singles Spectrum for ^{128}Xe

1196.2
953
887.1
852.1
846.0
808.4
775.6
704.2
683.9
656.8
625.0
612.4
590.2
570.6
550.0
531.9
526.6
491.1
460.6
442.9
429.1
353.8
286.4
273.8
204.1
ENERGY (keV)
RELATIVE INTENSITY
10⁶
10⁵
10⁴

performed by collecting spectra of ^{133}Ba and ^{152}Eu isotopes placed at the target site. Radiation spectra were collected after each experiment. In all, 25 gamma-rays have been assigned to the ^{128}Xe nucleus in this work. Table 6 lists all the gamma-rays assigned and their relative intensities.

For the multiplicity filter experiment, the procedure described in Chapter III was followed. A total of 68 gates were set, 35 of which were on peaks, the rest being set on the spectrum background. Figure 23 gives eight examples of background subtracted spectra with eight different gates. Table 7 shows the coincidence results for all the gamma-rays established as belonging to ^{128}Xe. From the coincidence results most of the gamma-rays previously assigned to the ^{128}Xe nucleus through I.B.γ. spectroscopy were confirmed. In addition three new levels at high spins have been found in this work.

The neutron multiplicity experiment was performed as described in Chapter III. If the neutron detection system was 100% efficient, then each spectrum accumulated would contain only those gamma-rays belonging to nuclei formed after one neutron emission, two neutron emission etc. For the case of the experiment actually performed, the overall efficiency of the neutron detection system was low, being certainly not greater than about 25%. As a result, the gamma-rays corresponding to xn reactions were seen in all spectra where the neutron multiplicity was $\leq$ x. Also, the intensities of the gamma-rays detected all decreased with increasing neutron multiplicity. To differentiate between the different reaction channels, the intensities of gamma-rays found in spectra of multiplicities of two and three neutrons were divided by the intensities of the same gamma-rays as found in the one neutron multiplicity spectrum. These ratios, designated I_{2n}/I_n , I_{3n}/I_n respectively, are unique for each

Table 6

Energies and relative intensities of gamma rays assigned to transitions in Xenon 128. The numbers in parentheses indicate the uncertainties in the last digit(s).

Energy (keV)	Rel. Intensity	Energy (kev)	Rel. Intensity
204.1 (1)	32 (4)	808.4 (1)	77 (5)
271.8 (1)	75 (6)	846.0 (1)	156 (12)
286.4 (1)	50 (2)	852.1 (1)	79 (20)
353.8 (2)	30 (2)	887.1 (2)	34 (4)
429.1 (1)	34 (2)	953 (1)	15 *
442.89 (5)	1000 (20)	1196.2 (1)	132 (2)
460.6 (4) D	41 (4)		
491.1 (1)	12 (2)		
526.6 (1)	41 (3)		
531.9 (1)	53 (4)		
550.0 (1)	68 (3)		
570.6 (1)	40 (2)		
590.2 (1)	893 (62)		
612.4 (1)	170 (9)		
625.0 (1)	75 (3)		
656.8 (2)	34 (2)		
683.9 (1)	266 (8)		
704.2 (1)	669 (13)		
775.6 (1)	441 (13)		

* = upper limit

D = doublet

Figure 23(in two parts)

Examples of Gamma Multiplicity Spectra

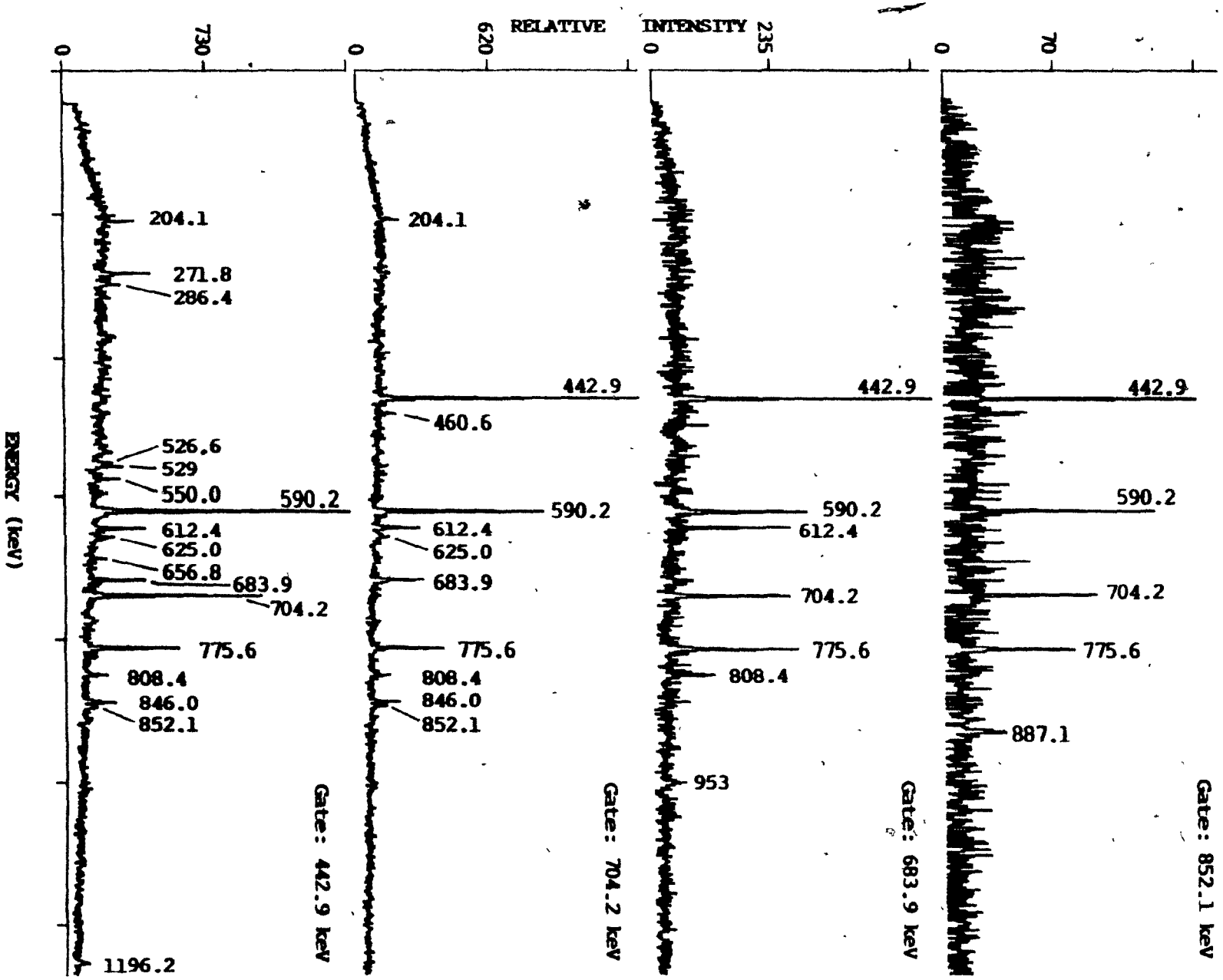
RELATIVE INTENSITY
0
730
620
235
70
ENERGY (keV)
204.1
271.8
286.4
526.6
529
550.0
590.2
612.4
625.0
656.8
683.9
704.2
775.6
808.4
846.0
852.1
1196.2
442.9
460.6
953
887.1
Gate: 442.9 keV
Gate: 704.2 keV
Gate: 683.9 keV
Gate: 852.1 keV

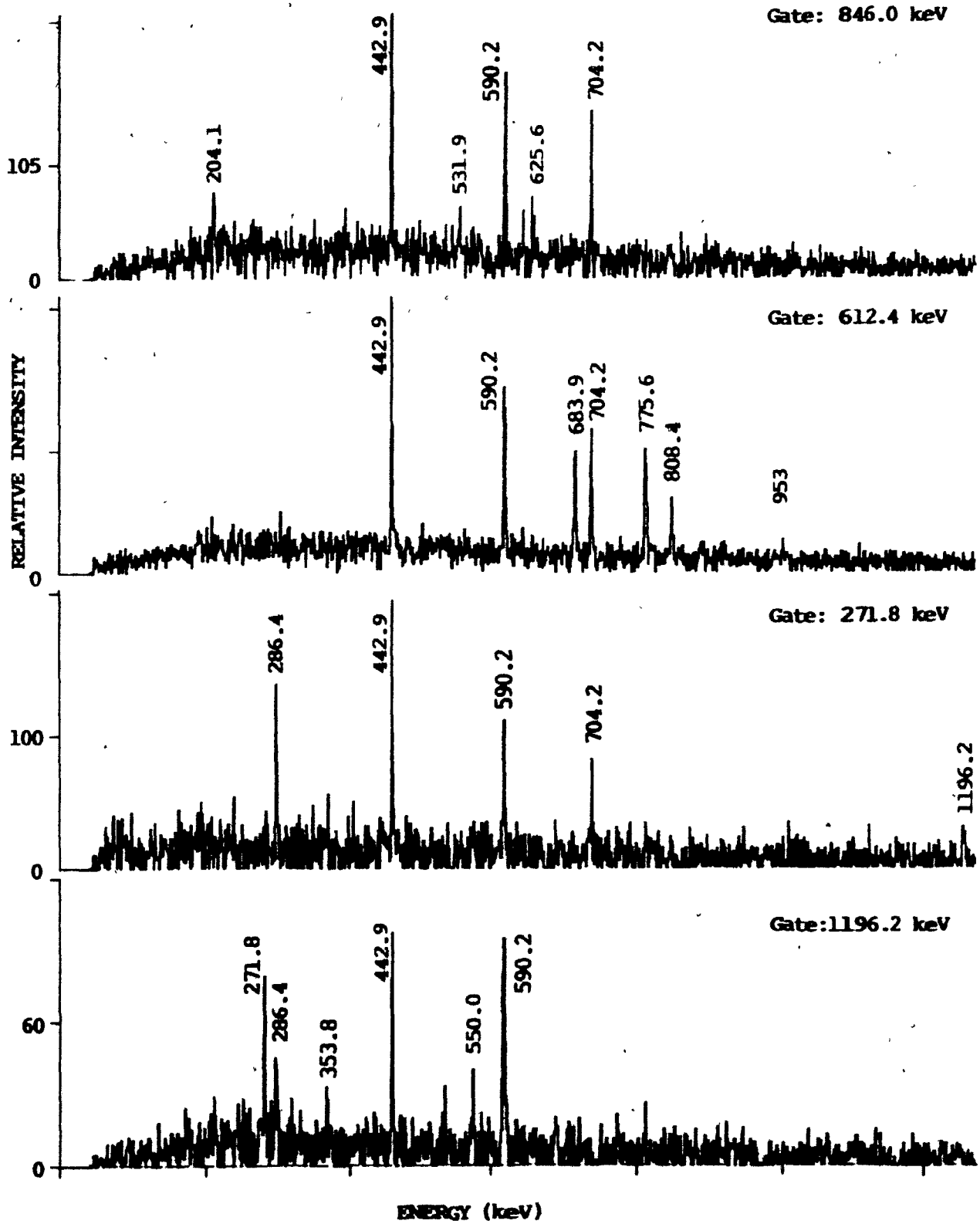
Gate: 846.0 keV
105
0
204.1
442.9
531.9
590.2
625.6
704.2
Gate: 612.4 keV
RELATIVE INTENSITY
0
442.9
590.2
683.9
704.2
775.6
808.4
953
Gate: 271.8 keV
100
0
286.4
442.9
590.2
704.2
1196.2
Gate:1196.2 keV
60
0
271.8
286.4
353.8
442.9
550.0
590.2
ENERGY (keV)

TABLE 7

Multiplicity Filter Results.

Gate (keV)	Coincident Gamma Rays (keV)
204.1	297*, 442.9, 590.2, 704.2
271.8	286.4, 442.9, 590.2, 704.2, 1196.2
286.4	271.8, 442.9, 590.2, 1196.2
353.8	(204.1), 442.9
429.1	271.8, 442.9, 590.2, 775.6
442.9	204.1, 271.8, 286.4, 353.8, 526.6, 529*, 550.0, 590.2, 612.4, 625.0, 656.8, 683.9, 704.2, 775.6, 808.4, 846.0, 852.1, 1196.2
460.6	442.9, 590.2, 704.2, 775.6
491.1	442.9, 590.2
526.6	442.9, 460.6
531.9	442.9, 590.2, 704.2, 766*, 846.0
550.0	271.7, 442.9, 590.2, (656.8)
570.6	442.9, 590.2
590.2	204.1, 271.8, 286.4, 353.8, 429.1, 442.9, (460.6), (526.6), (550.0), 612.4, 625.0, 656.8, 683.9, 704.2, 736*, 775.6, 808.4, 846.0, 852.1, 1196.2
612.4	442.9, 590.2, 683.9, 704.2, 775.6, 808.4, 953
625.0	201*, 271.8, (353.8), 442.9, 590.2, 704.2
656.8	271.8, 353.8, 442.9, 550.0, 590.2, (704), 737*,

Gate (keV)	Coincident Gamma Rays (keV) (cont'd)
	1196.2
683.9	442.9, 590.2, 612.4, 704.2, 775.6, 808.4, 953
704.2	204.1, 442.9, 460.6, 590.2, 612.4, 625.0, 683.9, 775.6, 808.4, 846.0, 852.1
775.6	271.8, 277*, 429.1, 442.9, 460.6, 590.2, 612.4, 683.9, 704.2, 808.4, 852.1
808.4	442.9, 590.2, 612.4, 704.2, 775.6
846.0	204.1, 442.9, 531.9, 590.2, 625.0, 704.2
852.1	442.9, 590.2, 704.2, 775.6, 887.1
887.1	442.9, 704.2
953	442.9
1196.2	271.8, 286.4, 353.8, 442.9, 550.0, 590.2

* = not placed in level scheme

( ) = possible coincidence

reaction channel. However, because of the low efficiency of the system, a peak coming from one reaction channel may be contaminated by a peak of similar energy coming from another reaction channel and the resulting intensity ratio would not be useful. In addition, because of poor statistics, it was found that the intensity ratios could not be accurately determined, if at all, for weak peaks. The peaks for which the intensity ratios could be accurately determined are listed in table 8. In the case of the 442.9 keV gamma-ray the intensity ratio is anomalously large. Examination of the radiation spectrum of the ^{128}Te target after bombardment reveals a radiation peak at 442 keV. The large value of the intensity ratio of the 442.9 keV gamma-ray is thus attributed to contamination by the latter radiation peak. The isotope emitting the radiation was not determined. In general, the neutron multiplicity results confirm the assignments of gamma-rays to the ^{128}Xe nucleus as determined from the gamma multiplicity data.

Angular Distribution Results

The spin and parities of the levels assigned to ^{128}Xe were deduced mainly from the gamma-ray angular distribution data. As for the ^{126}Xe isotope, the intensities of the peaks in the angular distribution spectra were analysed and then normalised to the intensities of the main transitions in ^{128}Xe as measured by a stationary detector placed at 125 degrees. These normalised intensities were fitted to fourth order Legendre polynomials as a function of detector angle. The A2 and A4 coefficients so obtained were then corrected for solid angle effects, the correction terms being calculated as Q2 = .94 and Q4 = .81. The plotted Legendre function for the gamma-rays in ^{128}Xe are shown in figure 24. Table 9 lists the solid angle corrected A2 and A4 coefficients, the deduced spin, parity and

the attenuation coefficients. In determining the spin and parity of the levels, the assumptions detailed in section A of this chapter are employed.

Most of the levels found in this work confirm the results published by Goettig et al.(57). The ground band levels all show the typical stretched E2 distributions. The level at 4617.6 keV is new for this isotope and is assigned a spin and parity of 14^+ on the basis of its angular distribution. The other new level reported, at 5570.6 keV, is perhaps the 16^+ level but the intensity of the 953 keV gamma-ray depopulating this level was too small for its angular distribution to be determined. Another new level, at 4252 keV is tentatively assigned a spin and parity of 12^+ . The level at 3365 keV, previously assigned a value 9^+, 10^+ by Goettig et al., is tentatively assigned a spin and parity of 10^+ here. Although the A2 coefficient is positive and the A4 coefficient is negative for the 852 keV gamma-ray depopulating this level, the coefficients have large errors assigned to them, making a definite assignment impossible. A number of levels have not been assigned any spin and parity because of the ambiguity in their angular distributions. The negative parity states reported by Goettig et al. at 2229.3, 2501.1, 2583.3 and 2720 keV are confirmed. For the level at 1430.1 keV Goettig et al. have the spin and parity of this level as being 3^+ . From the angular distribution of the 460.6 keV gamma-ray depopulating this level found in this work, the A2 coefficient is .21 and the A4 coefficient is -.14 indicating an E2 transition. Although this gamma-ray is a doublet with a 461.6 keV gamma-ray depopulating the 2974.5 keV level, the larger part of the intensity is due to the 460.6 keV gamma-ray depopulating the 1430.1 level. Hence, the 1430.1 keV level is tentatively assigned a value of 4^+ , contradicting the 3^+ value previously reported.

Table 8

Neutron Multiplicity Results

Energy (keV)	I_{2n} / I_n %	I_{3n} / I_n %
271.8	25 (2)	2.0 (2)
353.8	24 (4)	1.8 (8)
429.1	27 (2)	2.2 (2)
442.9	43 (2)	3.8(2)
460.6	22 (4)	2.7 (6)
550.0	24 (2)	5.4 (5)
570.6	27 (3)	1.5 (5)
590.6	24 (1)	2.1 (1)
612.4	24 (2)	2.6 (2)
625.0	21 (2)	2.6 (2)
683.9	23 (1)	2.5 (1)
704.2	24 (1)	2.1 (1)
775.6	24 (1)	2.2 (1)
808.4	25 (2)	2.0 (3)
846.0	25 (1)	2.3 (2)
852.1	29 (2)	2.4 (4)
887.1	33 (4)	2.9 (7)
953	24 (4)	3 (1)

Figure 24(in 6 parts)

Angular Distributions for ^{128}Xe

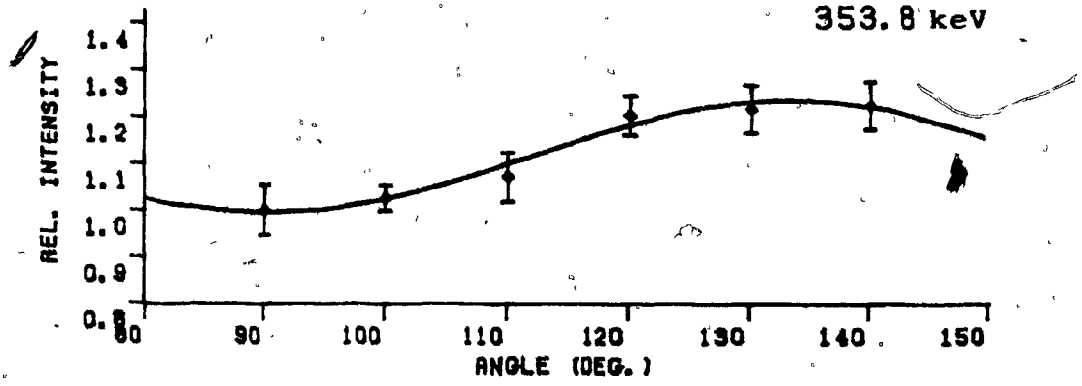
353.8 keV
REL. INTENSITY
1.4
1.3
1.2
1.1
1.0
0.9
0.8
80
90
100
110
120
130
140
150
ANGLE (DEG.)

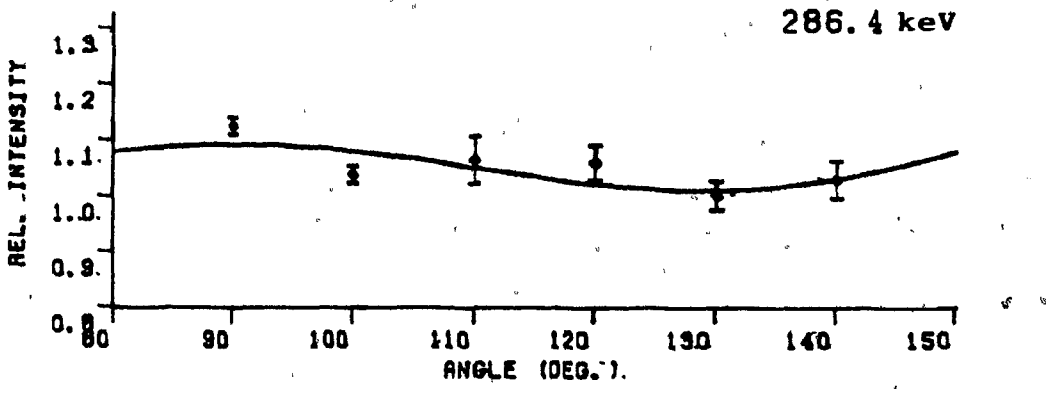
286.4 keV
REL. INTENSITY
1.3
1.2
1.1
1.0
0.9
0.8
80
90
100
110
120
130
140
150
ANGLE (DEG.)

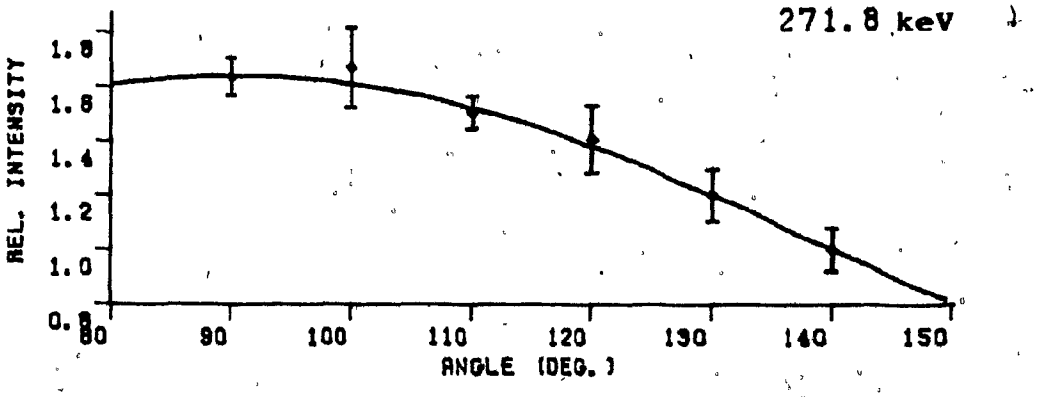
271.8 keV
REL. INTENSITY
1.8
1.6
1.4
1.2
1.0
0.8
80
90
100
110
120
130
140
150
ANGLE (DEG.)

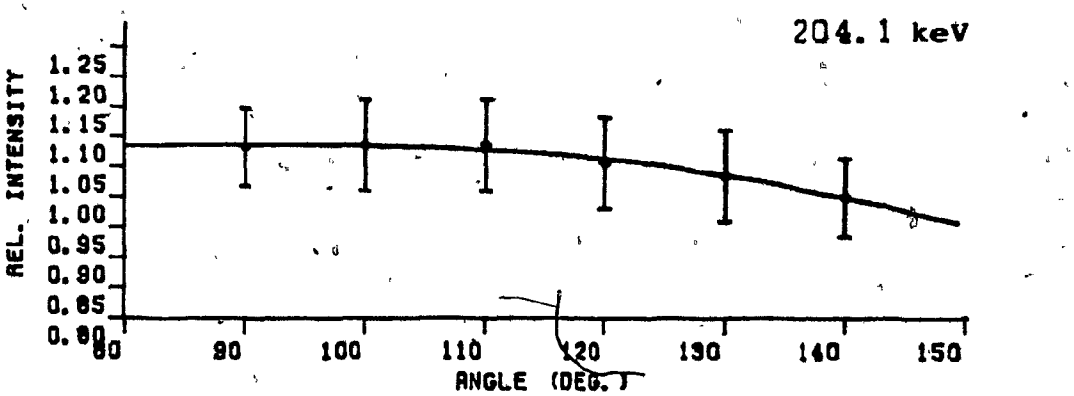
204.1 keV
REL. INTENSITY
1.25
1.20
1.15
1.10
1.05
1.00
0.95
0.90
0.85
0.80
80
90
100
110
120
130
140
150
ANGLE (DEG.)

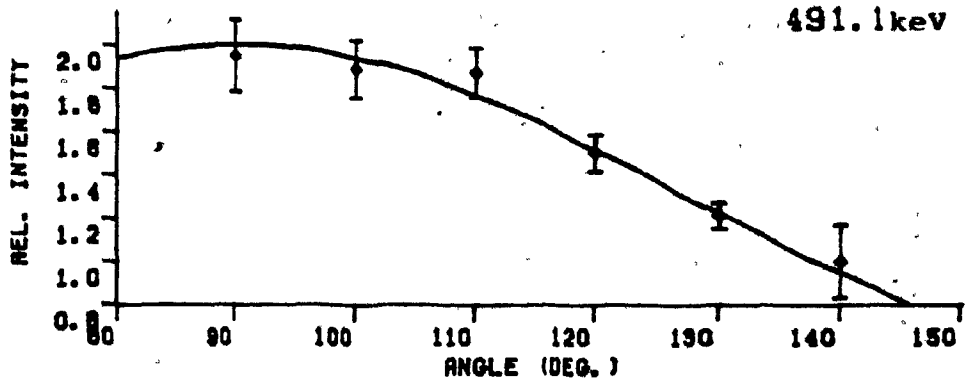
491.1kev
REL. INTENSITY
2.0
1.8
1.6
1.4
1.2
1.0
0.8
80
90
100
110
120
130
140
150
ANGLE (DEG.)

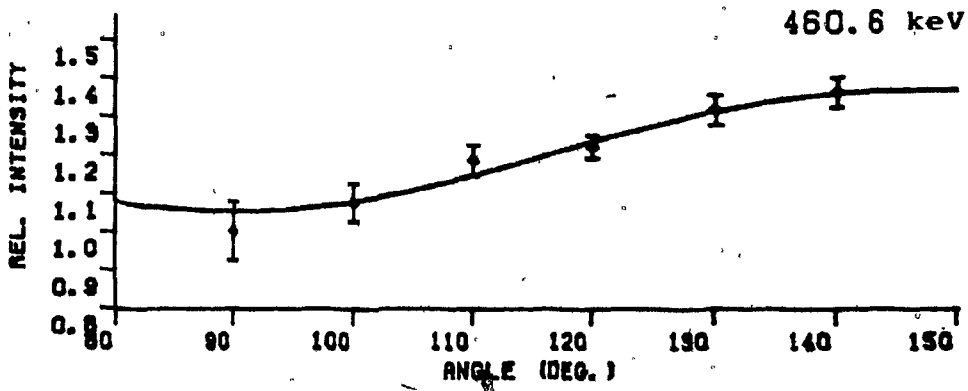
460.6 keV
REL. INTENSITY
1.5
1.4
1.3
1.2
1.1
1.0
0.9
0.8
80
90
100
110
120
130
140
150
ANGLE (DEG.)

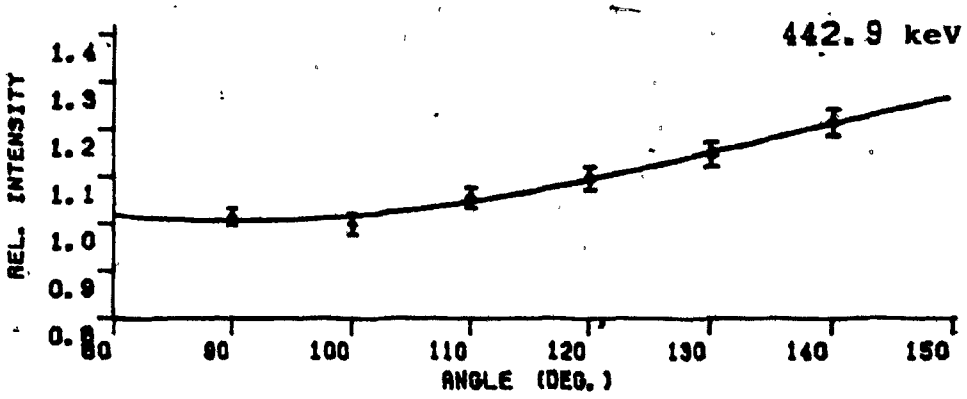
442.9 keV
REL. INTENSITY
1.4
1.3
1.2
1.1
1.0
0.9
0.8
80
90
100
110
120
130
140
150
ANGLE (DEG.)

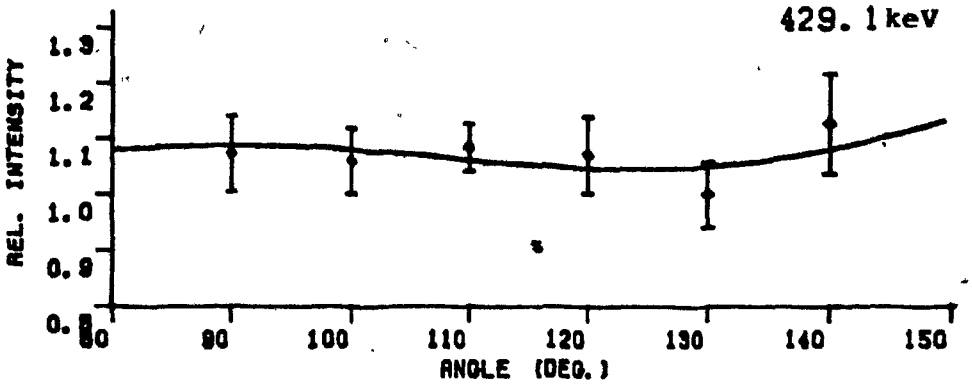
429.1kev
REL. INTENSITY
1.3
1.2
1.1
1.0
0.9
0.8
80
90
100
110
120
130
140
150
ANGLE (DEG.)

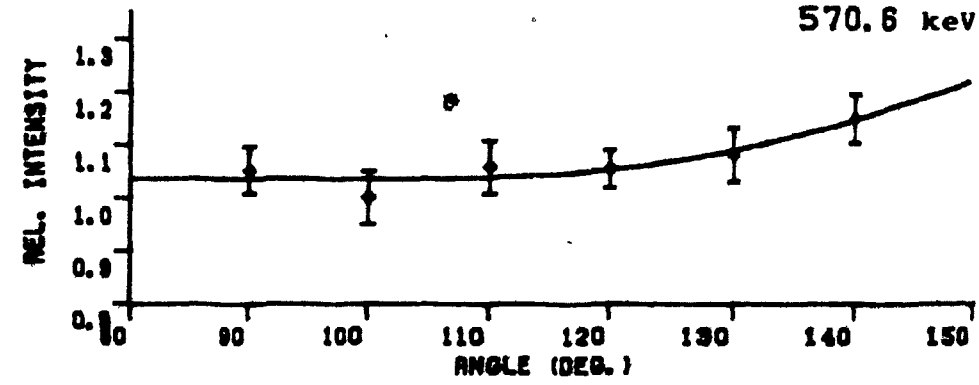
570.6 keV
REL. INTENSITY
1.3
1.2
1.1
1.0
0.9
0.8
80
90
100
110
120
130
140
150
ANGLE (DEG.)

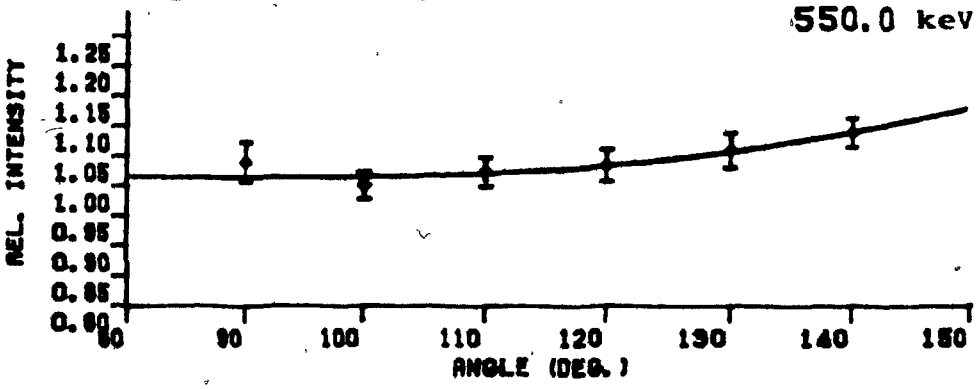
550.0 keV
REL. INTENSITY
1.25
1.20
1.15
1.10
1.05
1.00
0.95
0.90
0.85
0.80
80
90
100
110
120
130
140
150
ANGLE (DEG.)

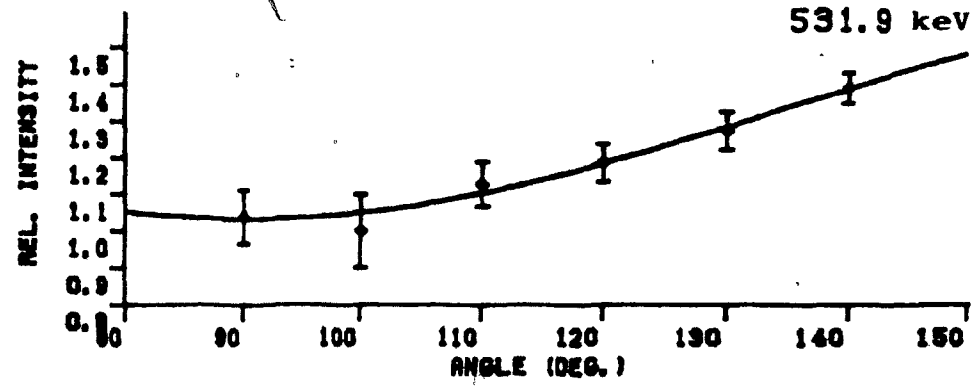
531.9 keV
REL. INTENSITY
1.5
1.4
1.3
1.2
1.1
1.0
0.9
0.8
80
90
100
110
120
130
140
150
ANGLE (DEG.)

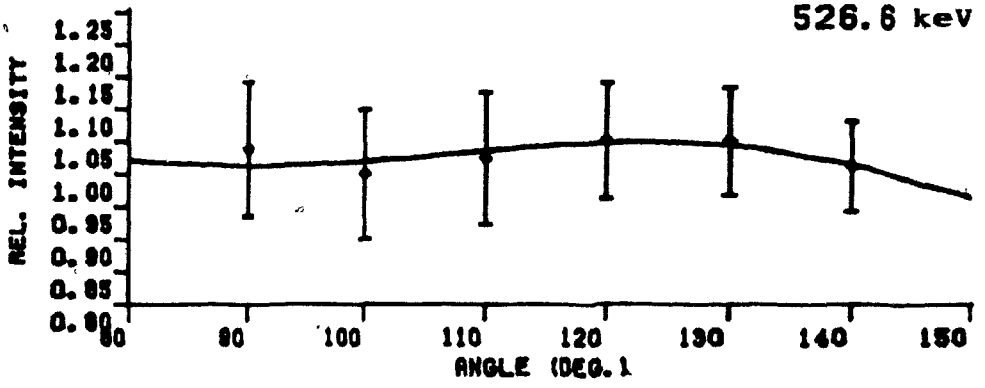
526.6 keV
REL. INTENSITY
1.25
1.20
1.15
1.10
1.05
1.00
0.95
0.90
0.85
0.80
80
90
100
110
120
130
140
150
ANGLE (DEG.)

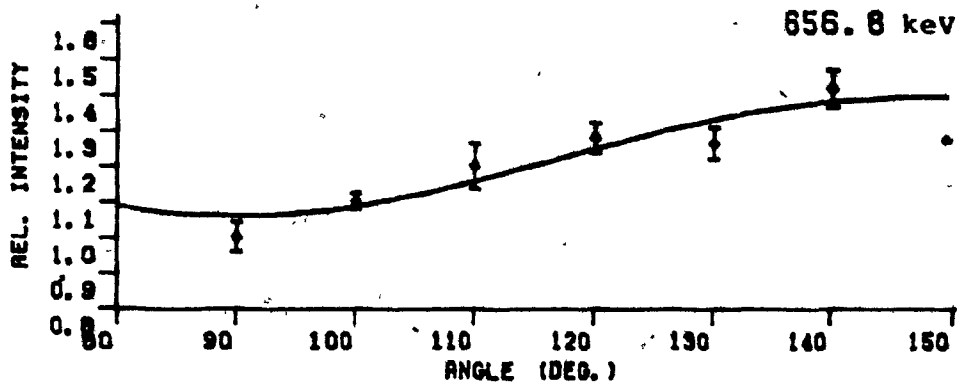
656.8 kev
REL. INTENSITY
1.6
1.5
1.4
1.3
1.2
1.1
1.0
0.9
0.8
80
90
100
110
120
130
140
150
ANGLE (DEG.)

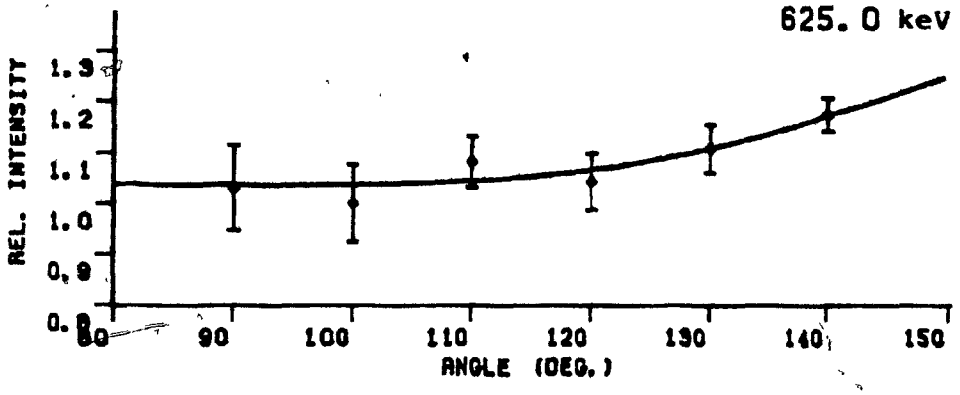
625.0 kev
REL. INTENSITY
1.3
1.2
1.1
1.0
0.9
0.8
80
90
100
110
120
130
140
150
ANGLE (DEG.)

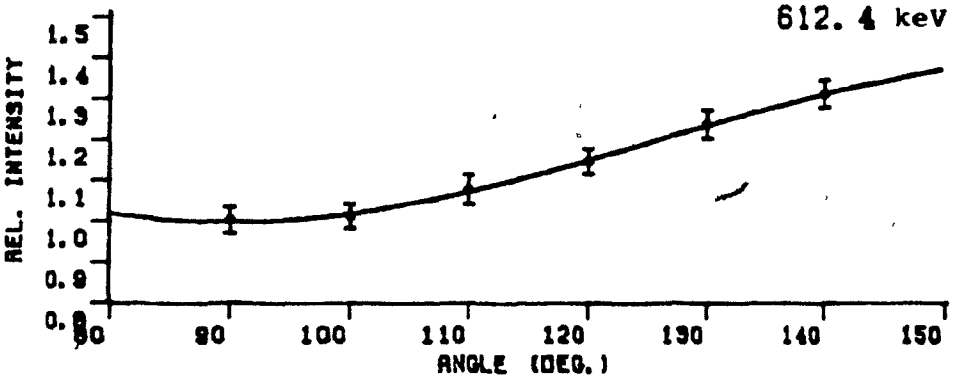
612.4 kev
REL. INTENSITY
1.5
1.4
1.3
1.2
1.1
1.0
0.9
0.8
80
90
100
110
120
130
140
150
ANGLE (DEG.)

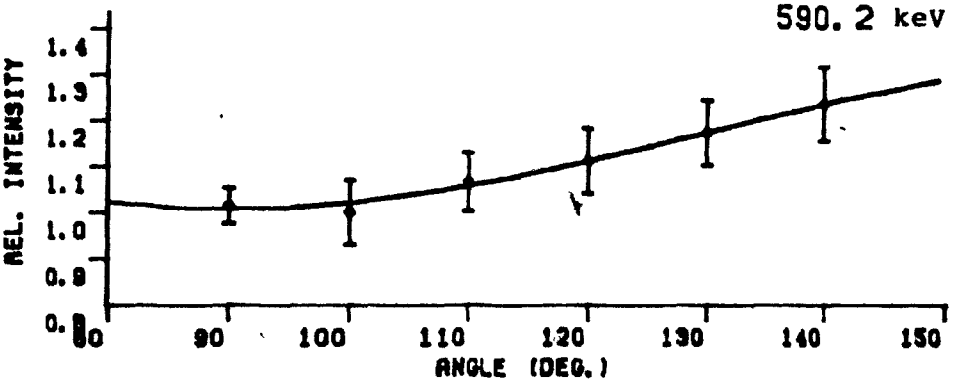
590.2 kev
REL. INTENSITY
1.4
1.3
1.2
1.1
1.0
0.9
0.8
80
90
100
110
120
130
140
150
ANGLE (DEG.)

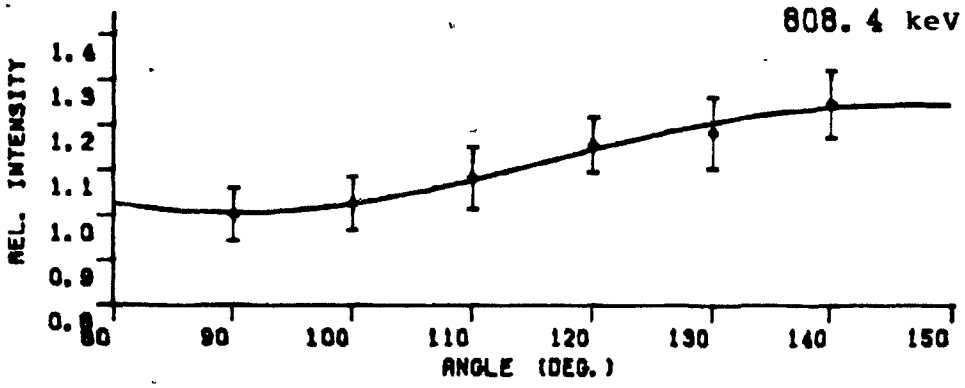
808.4 keV
REL. INTENSITY
1.4
1.3
1.2
1.1
1.0
0.9
0.8
80
90
100
110
120
130
140
150
ANGLE (DEG.)

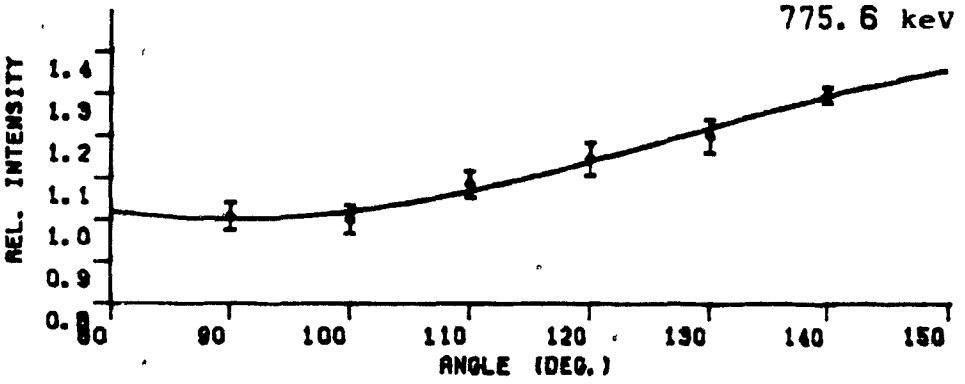
775.6 keV
REL. INTENSITY
1.4
1.3
1.2
1.1
1.0
0.9
0.8
80
90
100
110
120
130
140
150
ANGLE (DEG.)

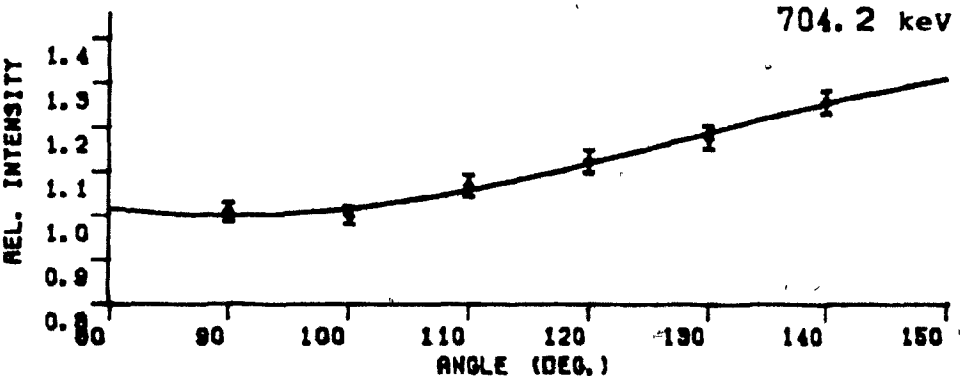
704.2 keV
REL. INTENSITY
1.4
1.3
1.2
1.1
1.0
0.9
0.8
80
90
100
110
120
130
140
150
ANGLE (DEG.)

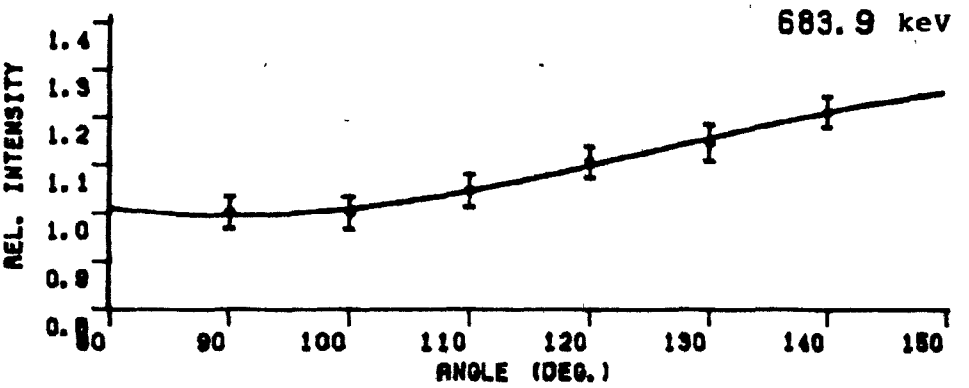
683.9 keV
REL. INTENSITY
1.4
1.3
1.2
1.1
1.0
0.9
0.8
80
90
100
110
120
130
140
150
ANGLE (DEG.)

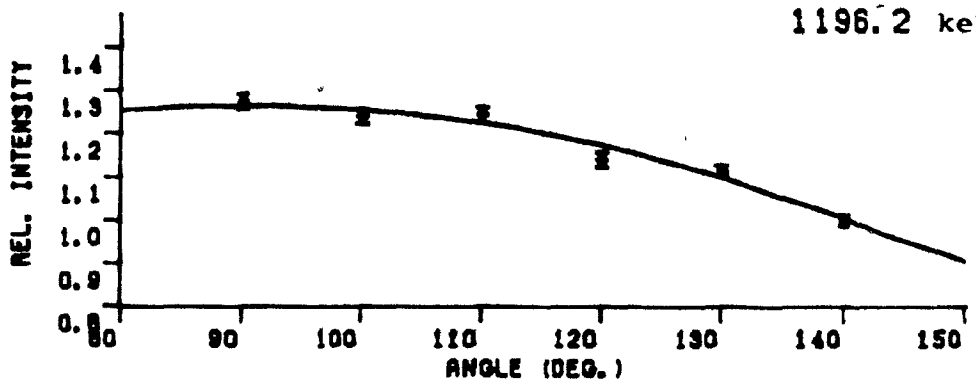
1196.2 keV
REL. INTENSITY
1.4
1.3
1.2
1.1
1.0
0.9
0.8
80
90
100
110
120
130
140
150
ANGLE (DEG.)

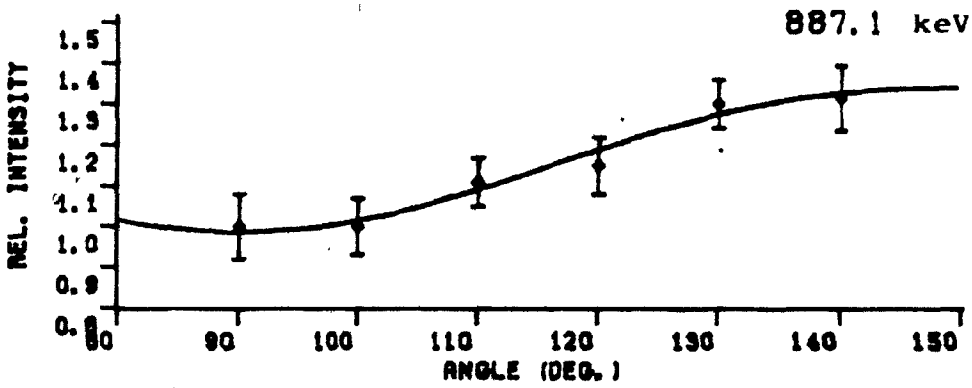
887.1 keV
REL. INTENSITY
1.5
1.4
1.3
1.2
1.1
1.0
0.9
0.8
80
90
100
110
120
130
140
150
ANGLE (DEG.)

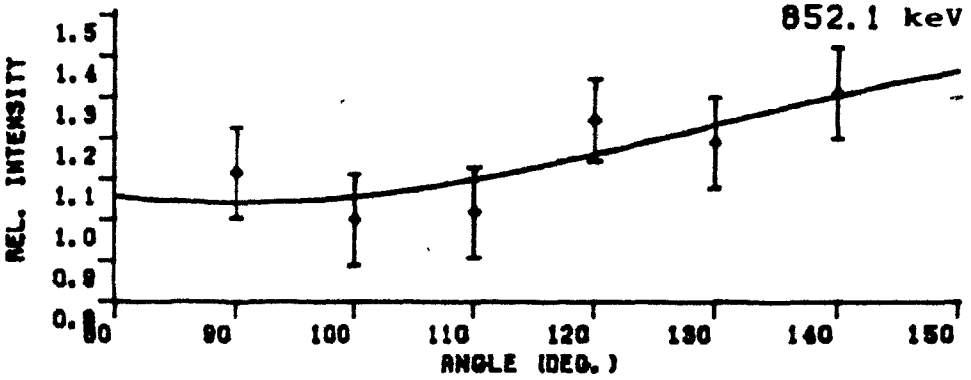
852.1 keV
REL. INTENSITY
1.5
1.4
1.3
1.2
1.1
1.0
0.9
0.8
80
90
100
110
120
130
140
150
ANGLE (DEG.)

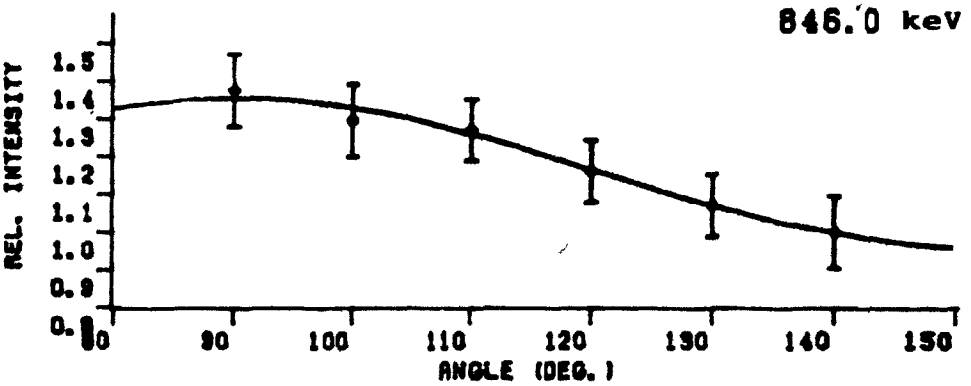
846.0 keV
REL. INTENSITY
1.5
1.4
1.3
1.2
1.1
1.0
0.9
0.8
80
90
100
110
120
130
140
150
ANGLE (DEG.)

Table 9

Table of Angular Distribution Results.

Energy (keV)	A2	A4	α 2	Assignment
204.1	-.13 ± .18	0	---	? → 14^+
271.8	-.62 ± .2	0	---	$(4^-,6^-) \rightarrow 5^-$
286.4	isotropic		---	? → $(4^-,6^-)$
353.8	.62 ± .1	-.27 ± .12	---	? → 6^+
429.1	isotropic		---	? → 8^+
442.9	.22 ± .08	-.004 ± .06	0.3	$2^+ \rightarrow 0^+$
460.6	.21 ± .08	-.14 ± .1	---	$(4_2^+) \rightarrow 2^+$
491.1	-.8 ± .3	0	---	$5^- \rightarrow 6^+$
526.6	isotropic		---	$2_2^+ \rightarrow 2^+$
531.9	.35 ± .09	-.03 ± .1	---	$(7^-,8^-,11^-) \rightarrow 5^-,6^-,7^-$
550.0	.11 ± .06	.04 ± .07	---	? → $4^-,6^-$
570.6	.18 ± .1	.09 ± .1	---	? → 4^+
590.2	.23 ± .07	-.02 ± .16	.45	$4^+ \rightarrow 2^+$
612.4	.29 ± .07	-.05 ± .08	.72	$12^+ \rightarrow 10^+$
625.0	.2 ± .09	.08 ± .1	---	? → $5^-,6^-,7^-$
656.8	.22 ± .1	-.14 ± .1	---	--
683.9	.21 ± .08	-.04 ± .08	.52	$10^+ \rightarrow 8^+$
704.2	.25 ± .06	-.03 ± .06	.55	$6^+ \rightarrow 4^+$
775.6	.28 ± .06	-.04 ± .08	.65	$8^+ \rightarrow 6^+$
808.4	.17 ± .16	-.12 ± .17	.43	$14^+ \rightarrow 12^+$
846.0	-.29 ± .2	.9 ± .2	---	$5^-,6^-,7^- \rightarrow 6^+$
852.1	.25 ± .23	-.02 ± .2	0.6	$10_2^+ \rightarrow 8^+$

Table of Angular Distribution Results (cont'd)

Energy (keV)	A2	A4	α2	Assignment
887.1	.26 ± .16	-.16 ± .17	---	$(12_2^+) \rightarrow 10_2^+$
953	---	---	---	$? \rightarrow 14^+$
1196.2	-.32 ± .04	0	.97	$5^- \rightarrow 4^+$

Level Scheme

The level scheme deduced in this work is shown in figure 25. The spin of 14^+ assigned to the 4617.6 keV level is the highest yet reported for this isotope. After the analysis of this isotope was completed, a paper by Kusakari et al.(58, Nuclear Physics June 1983) was published. This paper verifies the main features of the level scheme presented here but goes only to a spin of 12^+.

The level scheme will be further discussed in Chapter V where the topic of back-bending will be treated.

Figure 25

Level scheme for ^{128}Xe

(Energies are in keV)

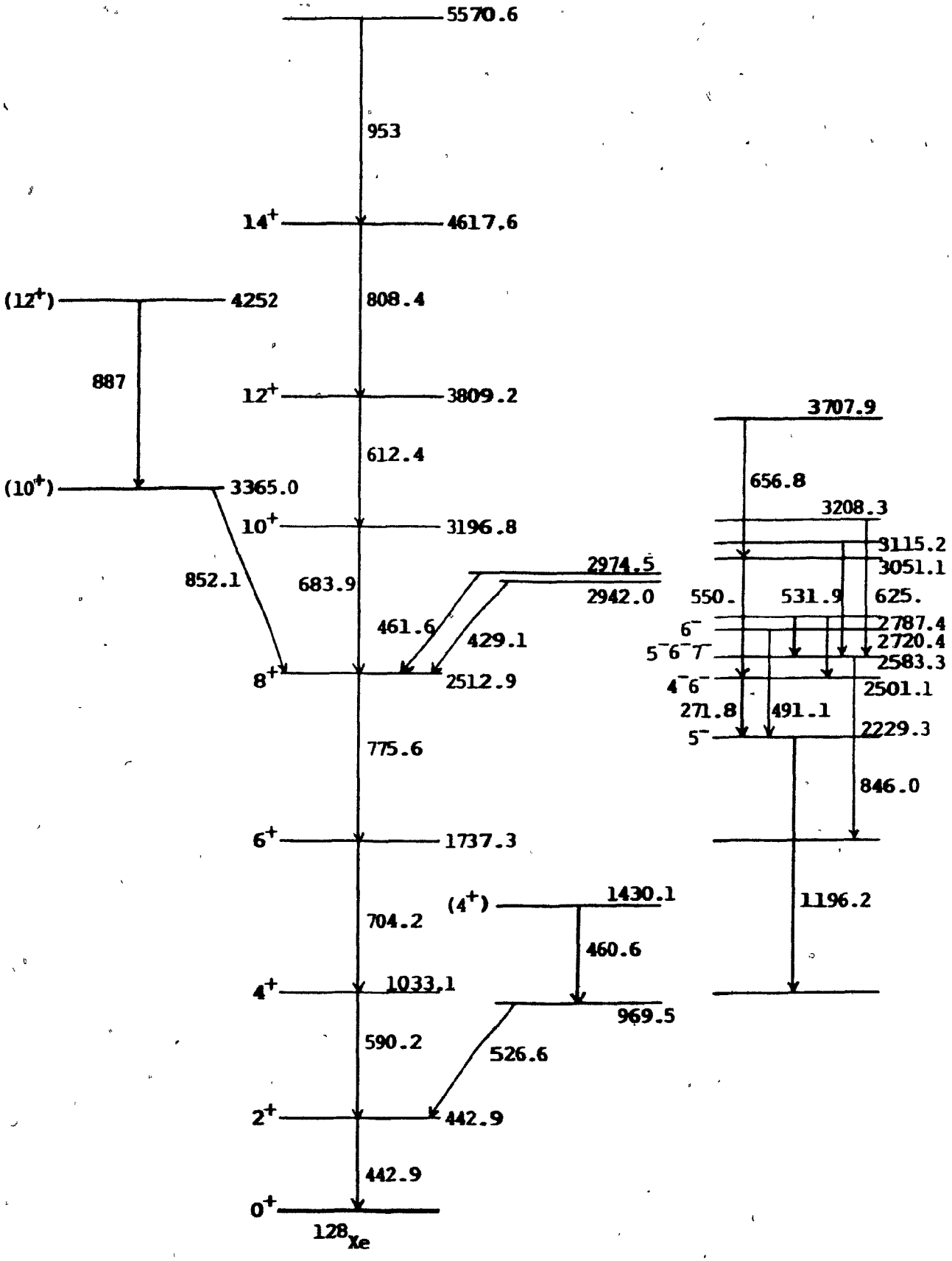
5570.6
953
14+
4617.6
(12+)
4252
808.4
887
12+
3809.2
612.4
(10+)
3365.0
10+
3196.8
852.1
683.9
2974.5
2942.0
461.6
429.1
8+
2512.9
775.6
6+
1737.3
(4+)
1430.1
704.2
460.6
4+
1033.1
969.5
590.2
526.6
2+
442.9
442.9
0+
128Xe
3707.9
656.8
3208.3
3115.2
3051.1
550.
531.9
625.
6-
2787.4
5-6-7-
2720.4
2583.3
4-6-
2501.1
271.8
491.1
5-
2229.3
846.0
1196.2

C)The ^{116}Te isotope

Previous Work

In 1967 Betigeri and Morinaga(49) proposed a level at 607 keV with a spin and parity of 2^+ for the ^{116}Te isotope. The ^{116}Te isotope was produced via the ^{116}Sn(^{3}He,3n)^{116}Te reaction, carried out at energies of 19.3, 17.5 and 15.0 MeV. Then, in 1969, Lukko et al.(64) published their study of the ^{116}Te nucleus as produced via the ^{114}Sn(α,2n)^{116}Te reaction at 33.5 MeV. They assigned four gamma rays to ^{116}Te. The 607 keV gamma-ray reported by Betigeri and Morinaga was not seen in that work. The four gamma-rays assigned by Lukko et al. were established as coming from the $2^+ \rightarrow 0^+, 4^+ \rightarrow 2^+$, $6^+ \rightarrow 4^+$ and $8^+ \rightarrow 6^+$ transitions with energies 678.8, 680.6, 643.0 and 770.8 keV respectively. Warner and Draper(65) in 1970 studied the excited states of ^{116}Te through (α,2n) and (α,4n) reactions, finding the same levels as reported by Lukko et al. and confirming the absence of a 607 keV gamma-ray as reported in Ref. 49. In 1973, in-beam electron conversion measurements were made by Wyckoff and Draper(66) on ^{116}Te produced in the reaction ^{114}Sn(α,2n)^{116}Te. This work confirmed the spin-parity assignments previously made for this nucleus. Gowdy et al.(67) in 1976 reported the first study of the decay of ^{116}I to ^{116}Te. The 679 keV doublet in ^{116}Te was seen along with a new 540 keV gamma-ray depopulating a level at 1.2191 MeV. This latter level was given the tentative assignment of $(0_2^+, 2_2^+)$. Gizon et al.(68) published in 1981 the results of their study of ^{116}Te produced through the ^{106}Cd + ^{12}C reaction. Two new levels were reported, one at 3575 keV and one at 4412 keV. The 3575 keV level was assigned spin and parity of 10^+ and the level at 4412 keV was given the tentative value of (12^+). Finally, in 1982, Chowdury et al.(69) published their findings on the excited states of ^{116}Te. The

reactions used were $^{114}Sn(\alpha,2n)^{116}Te$ and $^{106}Pd(^{12}C,2n)^{116}Te$. In the $(\alpha,2n)$ reaction the level at 3575 keV reported in Ref. 68 was confirmed but not the level at at 4412 keV. Above the 3575 keV level are two levels at 4346 keV and 5109 keV assigned tentative spins and parities of (12^+) and (14^+) respectively. A 1025 kev gamma-ray depopulating a level at 3028 keV was also found to feed the 6^+ level at 2003 keV. The 3028 keV level was tentatively assigned spin and parity (7^-). The 3028 keV level is in turn fed by a gamma-ray coming from a level at 3175 keV for which no spin assignment was made.

I.B.γ. Spectroscopy

For this experiment the target used was ^{116}Sn in the form of tin oxide of 95.6% isotopic purity. As in the case of the previous two isotopes, an excitation function was measured with spectra being taken at lab energies of 42, 49, 54, 59, 64, 69 and 78 MeV. Figure 26 shows the excitation function for the six strongest peaks in ^{116}Te. The graphs all have their peak at 59 MeV. so all subsequent experiments were performed at this energy. Figure 27 shows the singles spectrum obtained from the $^{116}Sn(\alpha,4n)^{116}Te$ reaction at 59 MeV. The peaks identified as belonging to ^{116}Te are labelled. Energy calibration was made by collecting spectra from ^{152}Eu, ^{133}Ba and ^{56}Co placed at the target site. The energies and intensities of all gamma-rays identified as belonging to ^{116}Te are listed in table 10.

The multiplicity experiment was conducted as described earlier in Chapter III. A total of 96 gates were set, 51 of which were on peaks, the remainder being gates set on the spectrum background. Fifty one spectra with background subtracted were then obtained. Figure 28 shows examples of background subtracted spectra with four different gates. Table 11 gives

Figure 26

Excitation Function for ^{116}Te

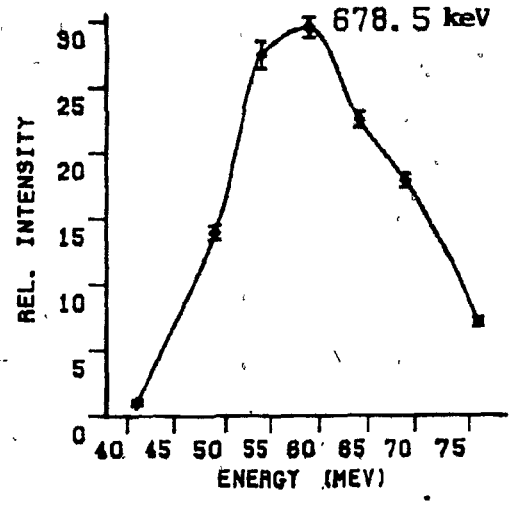
678.5 keV
REL. INTENSITY
ENERGY (MEV)

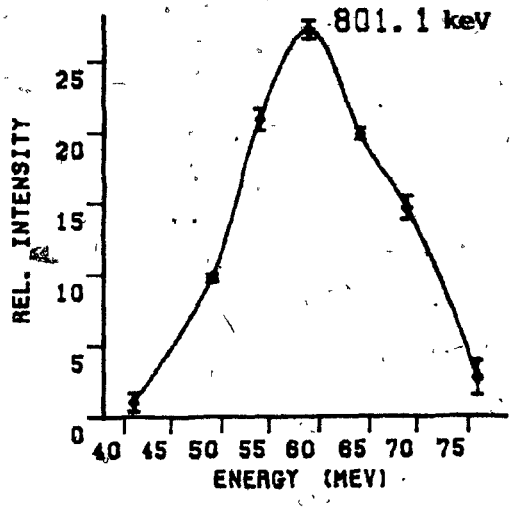
801.1 keV
REL. INTENSITY
ENERGY (MEV)

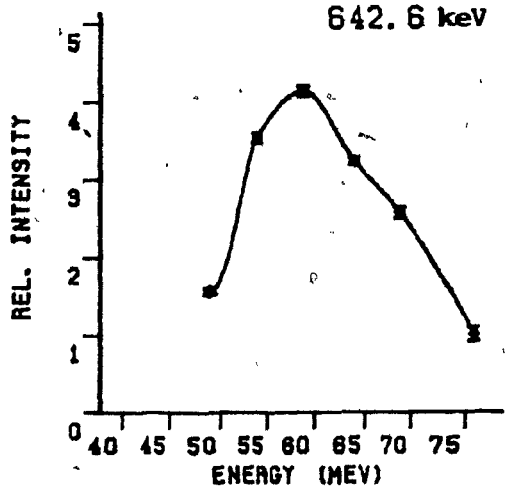
642.6 keV
REL. INTENSITY
ENERGY (MEV)

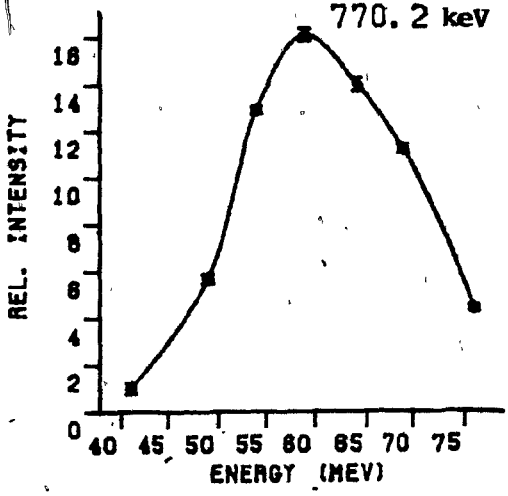
770.2 keV
REL. INTENSITY
ENERGY (MEV)

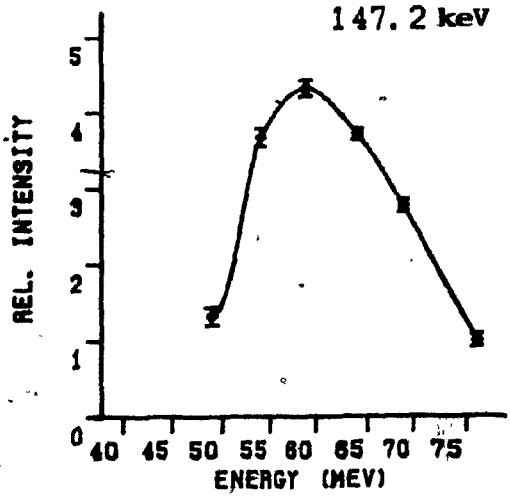
147.2 keV
REL. INTENSITY
ENERGY (MEV)

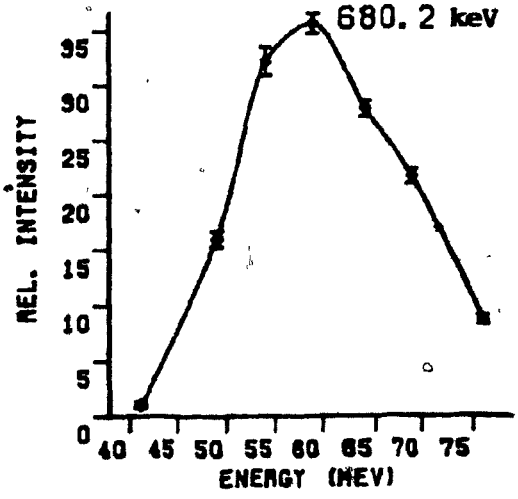
680.2 keV
REL. INTENSITY
ENERGY (MEV)

Figure 27

Singles Spectrum for ^{116}Te

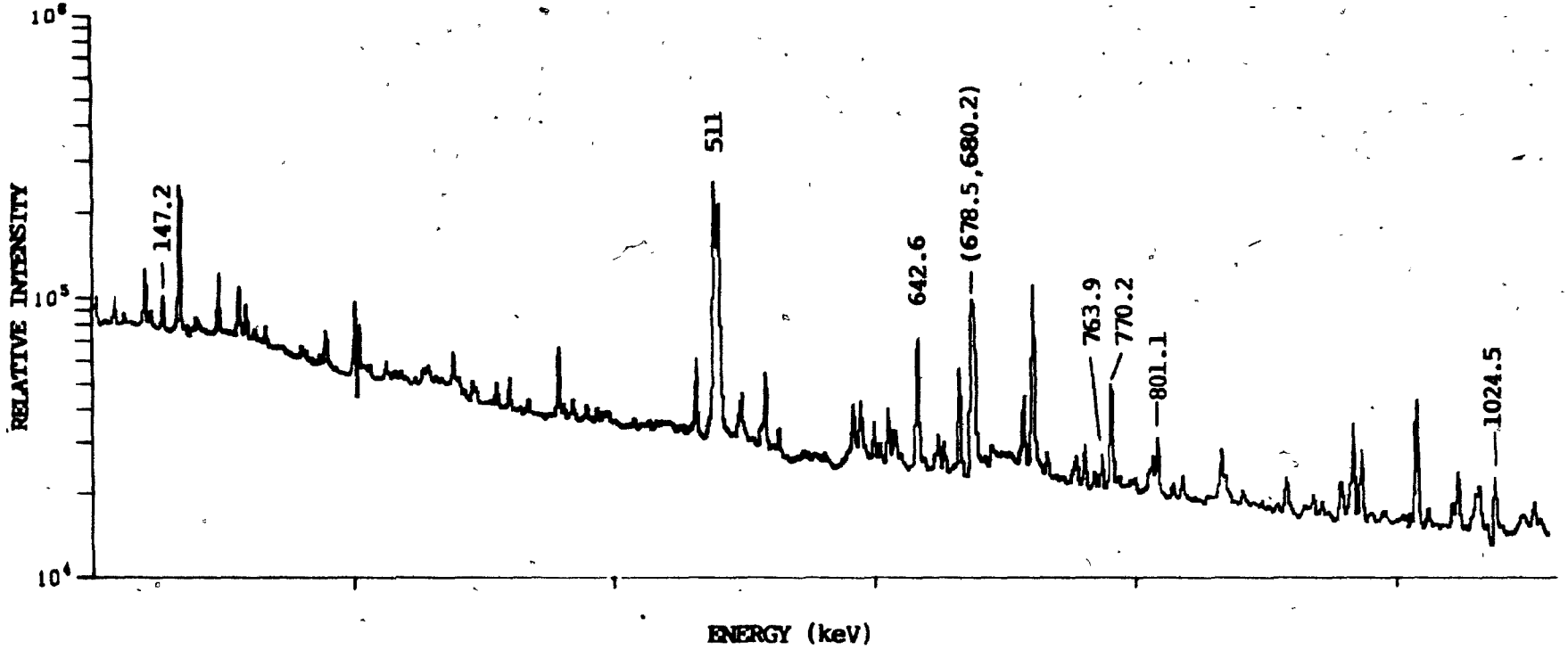
RELATIVE INTENSITY
10^6
10^5
10^4
147.2
511
642.6
(678.5,680.2)
763.9
770.2
801.1
1024.5
ENERGY (keV)

Table 10

Energies and relative intensities of gamma rays assigned to transitions in Tellurium 116. The numbers in parentheses indicate the uncertainties in the last digit(s).

Energy (keV)	Rel. Intensity
147.19(5)	88 (8)
493.1 (3) *	25 (5)
511 *	undetermined
642.6 (1)	760 (36)
678.5 (1)	1000 (30)
680.2 (1)	920 (55)
763.9 (1)	121 (8)
770.2 (1)	574 (25)
801.1 (1)	223 (12)
1024.5 (2)	162 (15)

* = tentative assignment

the coincidence results for all gamma-rays determined to belong to ^{116}Te.

The analysis of this isotope proved very difficult since the gamma-rays of interest are all very weakly produced. In an attempt to squeeze as much information as possible out of the coincidence data, each gate was analysed several times by projecting out spectra for which the number of gamma-rays in coincidence varied from two or more to four or more. This was done in the hope of detecting other possible gamma-rays that may have been present in a cascade of high multiplicity.

The level scheme was established on the basis of relative intensities. For the 678.5 and 680.2 keV doublet, the high resolution of the Ge. detector used made it possible to fit the peak with a non-linear least squares fitting routine and unambiguously determine the relative intensity of each component gamma-ray. With this information, the correct order of the peaks could be accurately determined. For the 770 keV doublet, the peak could not be resolved into its components. However, the relative intensity of 574 for the 770 keV peak compared to the relative intensity of 223 for the 801.1 keV gamma-ray indicates that one member of the doublet is below the 801.1 keV gamma-ray and the other above the 801.1 keV gamma-ray. The only ambiguity comes from the relative placement of the upper 770 keV peak and the 763 keV gamma-ray. The placement finally made was chosen on the basis of previous work.

Angular Distribution Results and Level Scheme

The spin and parity of the levels assigned to ^{116}Te were deduced from the angular distribution of the gamma-ray data. The intensities of the peaks in the angular distribution spectra were analysed and then normalised to the intensities of the main transitions in ^{116}Te as measured by a stationary detector set at 125°. The normalised intensities were then

Figure 28

Examples of Gamma Multiplicity Spectra

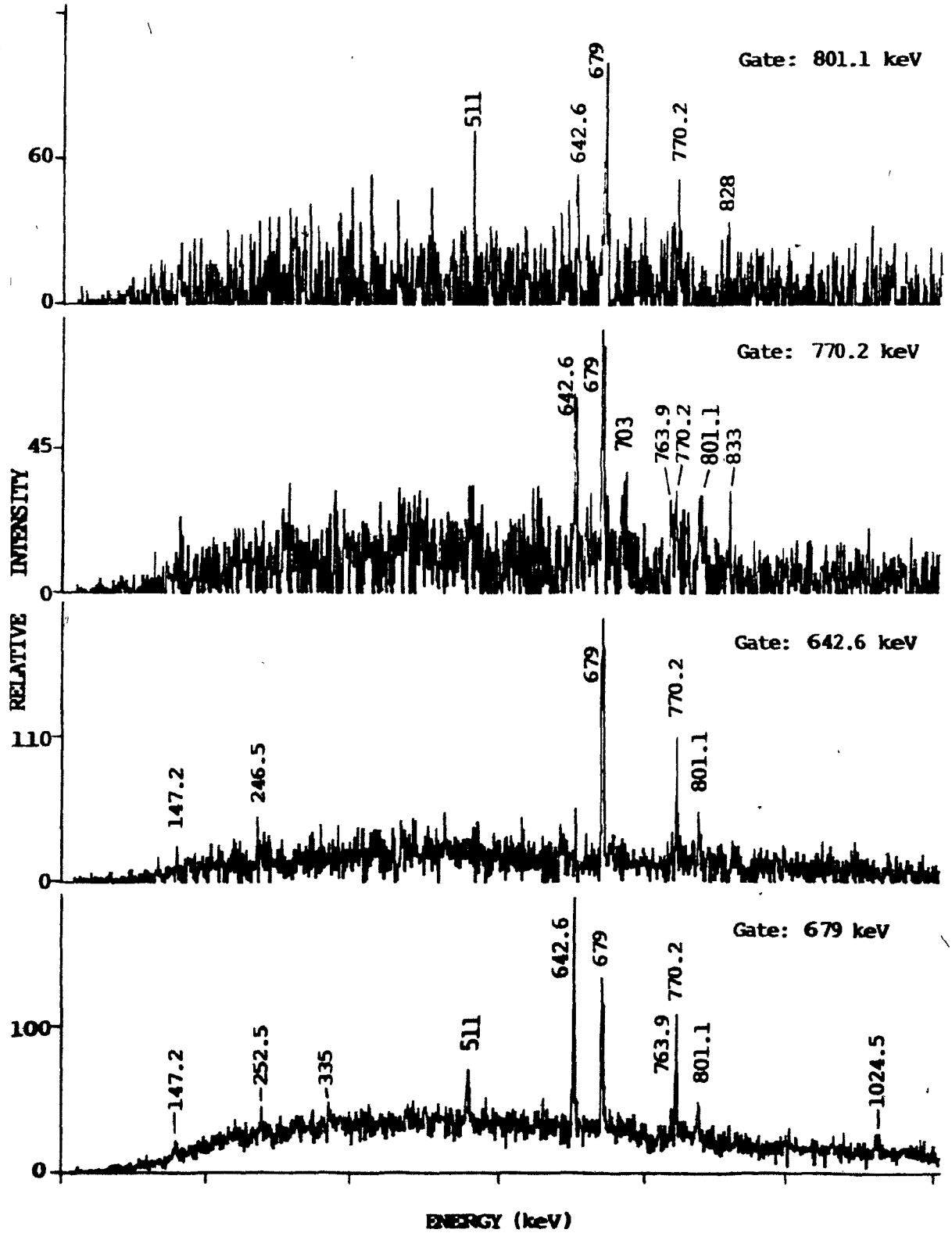
Gate: 801.1 keV
511
642.6
679
770.2
828
60
0
Gate: 770.2 keV
642.6
679
703
763.9
770.2
801.1
833
45
0
INTENSITY
Gate: 642.6 keV
679
770.2
801.1
147.2
246.5
110
0
RELATIVE
Gate: 679 keV
642.6
679
770.2
763.9
801.1
511
147.2
252.5
335
1024.5
100
0
ENERGY (keV)

TABLE 11

Multiplicity Filter Results.

Gate (keV)	Coincident Gamma Rays (keV)
147.2	678.5, 680.2
642.6	147.2, 246.5*, 678.5, 680.2, (763.9), 770.2, 801.1
679 D	147.2, 252.5*, 335*, 511, 642.6, 679 D, 763.9 770.2, 801.1, 1024.5
763.9	291.0*, 597*, 642.6, 674.4*, 678.5, 680.2, 801.1
770.2	642.6, 678.5, 680.2, 703*, 760*, 763.9, 770.2 801.1, 833*
801.1	511, 642.6, 678.5, 680.2, 770.2, 828*
1024.5	147.2, (493.1), 642.6, 678.5, 680.2

* = not placed in level scheme

( ) = possible coincidence

D = doublet

fitted to fourth order Legendre polynomials and the A2 and A4 coefficients so obtained corrected for solid angle. The calculated correction terms are Q2 = 0.94 and Q4 = 0.81. The Legendre functions for the gamma-rays in ^{116}Te are shown in figure 29. Table 12 lists the A2 and A4 coefficients, corrected for solid angle, the deduced spin and parity and the attenuation coefficients. In determining the spins and parities of the levels, the assumptions presented in section A of this chapter were applied. Figure 30 shows the level scheme deduced in this work. Except for the tentative levels at 5617.7 keV and 3666.1 keV, no new levels were found for this isotope. All the previously reported levels have been identified and placed in the level scheme in a manner consistent with the previous works. All previous spins and parities have also been confirmed. The level at 3173.0 keV is tentatively assigned here a value of $8^{\pm}$. The 147.2 keV gamma-ray depopulating this level exhibits a dipole transition with negative A2 coefficient and zero A4 coefficient. For the 511 keV and 493.1 keV gamma-rays depopulating the tentative levels at at 5617.2 keV and 3666.2 keV, no angular distributions were obtained because of the contamination of the 511 keV gamma-ray and the low intensity of the 493.1keV gamma-ray. The gamma-rays in the ground band cascade all show clear E2 angular distributions. One exception is the 763.9 keV gamma-ray depopulating the 5106.7 keV level. The A2 coefficient for this gamma-ray is very small (.08) and has a large error, making the 12^{+} assignment tentative. Without exception, the data point at 130° was found to be anomalously low for all the angular distributions of all the gamma-rays. This effect was found to be independent of the normalisation used. Hence it was assumed that some error in measurement must have been made at the time the experiment was executed. Trying to fit the data with the 130°

data point included was found to introduce large errors and poor fits. Hence, that data point was removed for all gamma-rays and the Legendre polynomial fitted to the remaining five points.

Figure 29(in 2 parts)

Angular Distributions for ^{116}Te

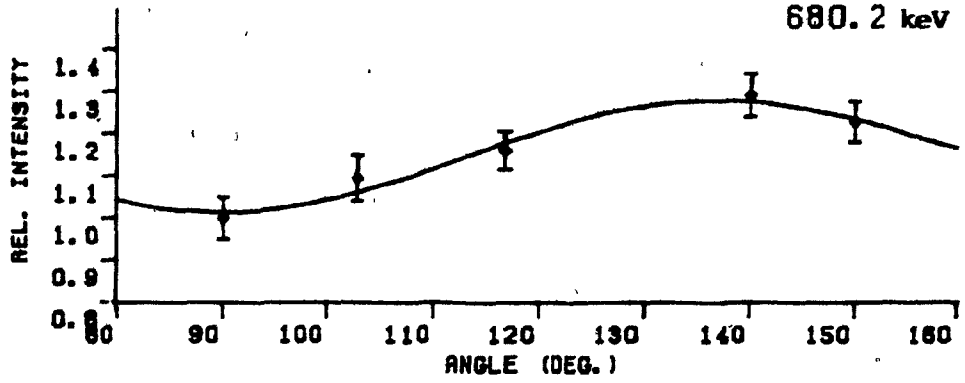
680.2 keV
REL. INTENSITY
1.4
1.3
1.2
1.1
1.0
0.9
0.8
80
90
100
110
120
130
140
150
160
ANGLE (DEG.)

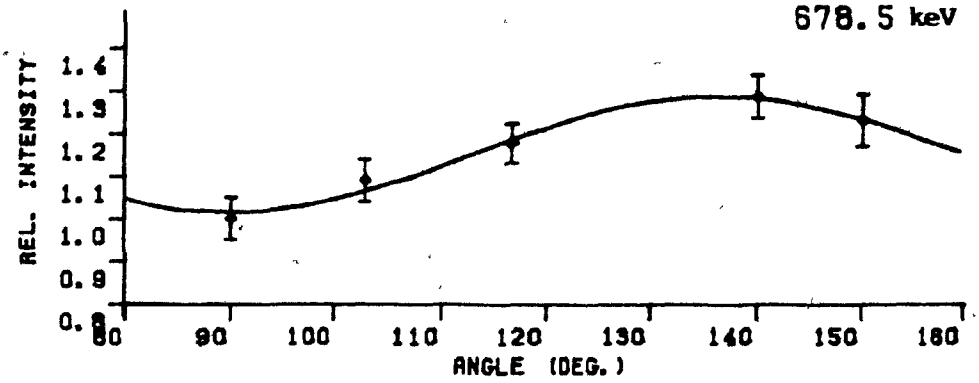
678.5 keV
REL. INTENSITY
1.4
1.3
1.2
1.1
1.0
0.9
0.8
80
90
100
110
120
130
140
150
160
ANGLE (DEG.)

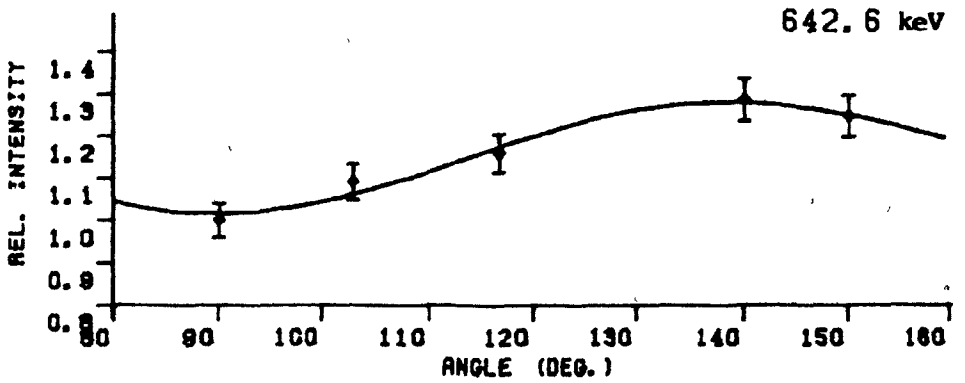
642.6 keV
REL. INTENSITY
1.4
1.3
1.2
1.1
1.0
0.9
0.8
80
90
100
110
120
130
140
150
160
ANGLE (DEG.)

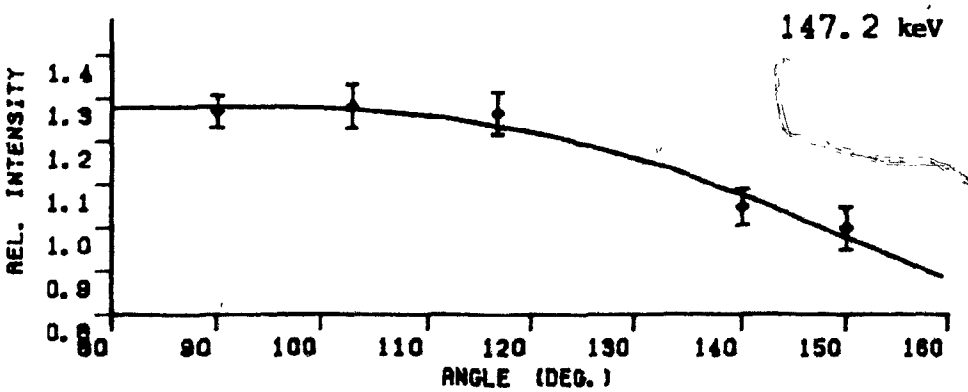
147.2 keV
REL. INTENSITY
1.4
1.3
1.2
1.1
1.0
0.9
0.8
80
90
100
110
120
130
140
150
160
ANGLE (DEG.)

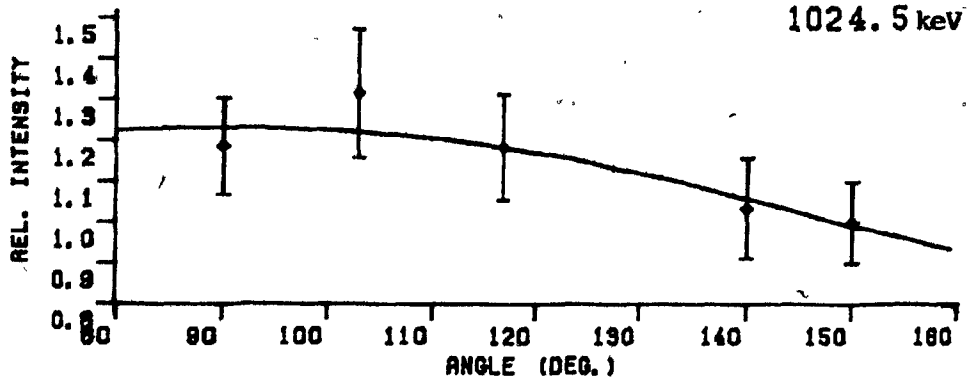
1024.5 keV
REL. INTENSITY
1.5
1.4
1.3
1.2
1.1
1.0
0.9
0.8
80
90
100
110
120
130
140
150
160
ANGLE (DEG.)

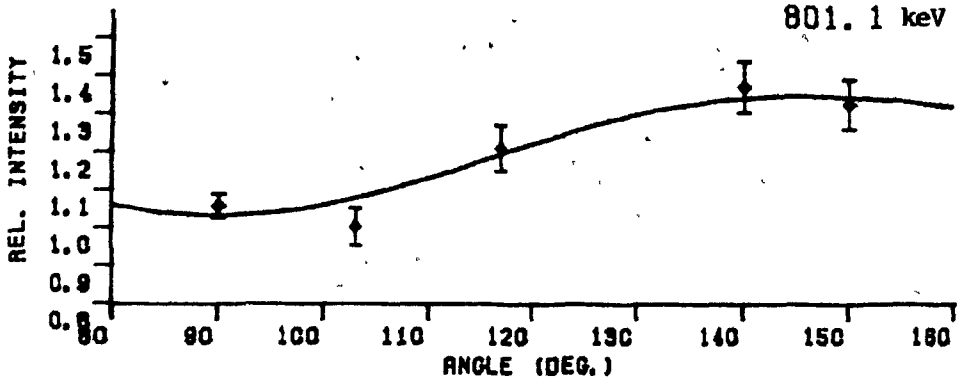
801.1 keV
REL. INTENSITY
1.5
1.4
1.3
1.2
1.1
1.0
0.9
0.8
80
90
100
110
120
130
140
150
160
ANGLE (DEG.)

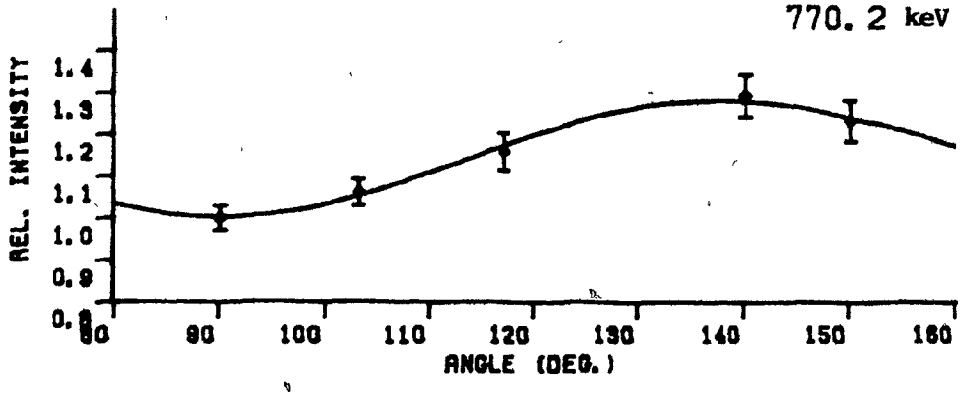
770.2 keV
REL. INTENSITY
1.4
1.3
1.2
1.1
1.0
0.9
0.8
80
90
100
110
120
130
140
150
160
ANGLE (DEG.)

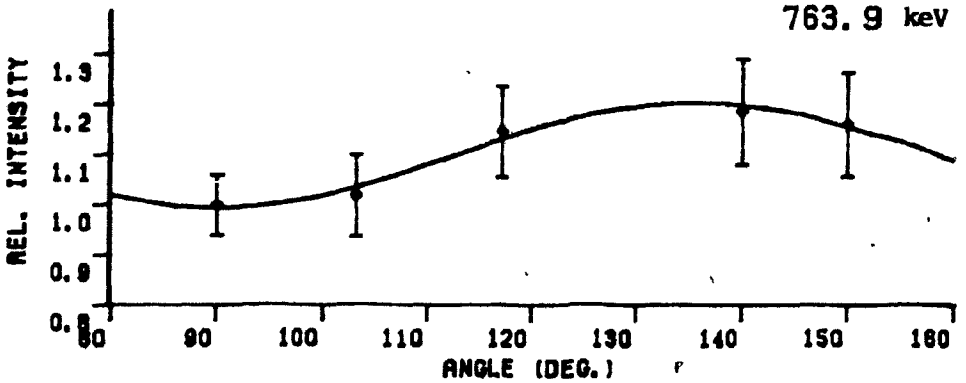
763.9 keV
REL. INTENSITY
1.3
1.2
1.1
1.0
0.9
0.8
80
90
100
110
120
130
140
150
160
ANGLE (DEG.)

Table 12

Table of Angular Distribution Results.

Energy (keV)	A2	A4	α 2	Assignment
147.2	-.27 ± .06	0	---	$(8^+) \rightarrow 7^-$
493.1	---	---	---	$? \rightarrow (8^+)$
642.6	.14 ± .05	-.2 ± .1	0.3	$6^+ \rightarrow 4^+$
678.5	.11 ± .06	-.2 ± .1	0.2	$2^+ \rightarrow 0^+$
680.2	.12 ± .06	-.2 ± .1	.23	$4^+ \rightarrow 2^+$
763.9	.08 ± .1	-.2 ± .2	---	$(14^+) \rightarrow 12^+$
770.2	.13 ± .05	-.2 ± .1	---	$8^+ \rightarrow 6^+, 12^+ \rightarrow 10^+$
801.1	.2 ± .06	-.4 ± .1	0.5	$10^+ \rightarrow 8^+$
1024.5	.2 ± .1	0	0.7	$7^- \rightarrow 6^+$

Figure 30

Level scheme for ^{116}Te

(Energies are in keV)

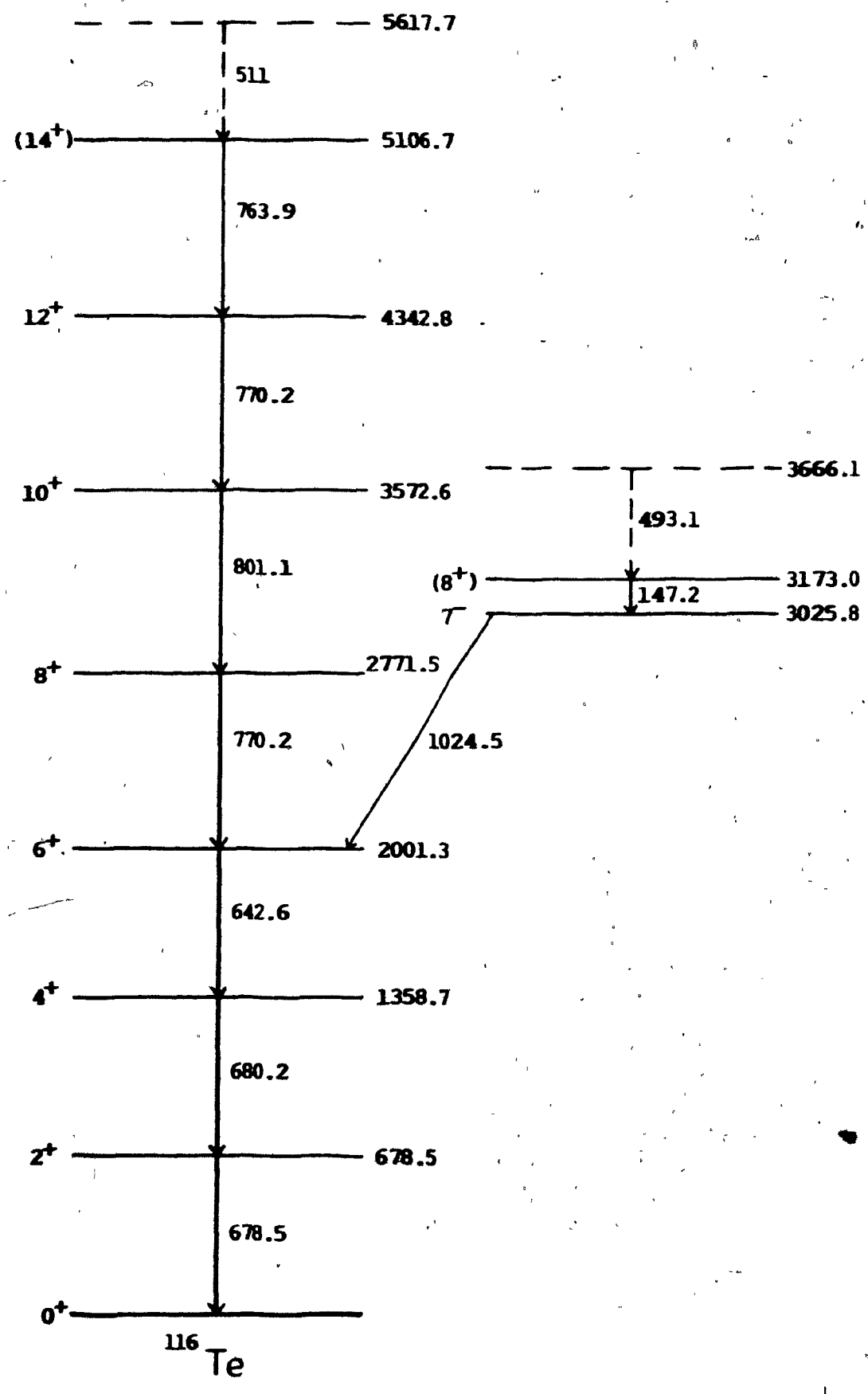
5617.7
511
(14+)
5106.7
763.9
12+
4342.8
770.2
10+
3572.6
3666.1
493.1
801.1
(8+)
3173.0
147.2
3025.8
8+
2771.5
770.2
1024.5
6+
2001.3
642.6
4+
1358.7
680.2
2+
678.5
678.5
0+
116 Te

Chapter V: Discussion and Conclusion

For many even-even nuclei, the energy levels in the ground band are found to follow very closely the simple formula:

$$E_I = AI(I + 1) + BI^2(I + 1)^2$$

where I is the spin of the level and the coefficients A and B are determined from the first two excited states. For the lower values of I, the first term in the above equation for E_I may be enough by itself to give fairly accurate values for the energy of the levels. In analogy to a rigid rotor, the coefficient A is expressed in terms of an effective moment of inertia defined by:

$$A = \hbar^2/2\mathcal{J}_I = (E_I - E_{I-2})/(4I - 2)$$

As a means of studying the behaviour of the effective moment of inertia as a function of increasing spin, one may make a plot of $2\mathcal{J}_I / \hbar^2$ versus the square of the rotational frequency $(\hbar\omega)^2$. This is done for the ^{128}Xe and ^{126}Xe isotopes and the graphs obtained are shown in figure 31. The numbers written beside each data point represents the spin of the level for which the moment of inertia is evaluated. The graphs exhibit the backbending behaviour discussed in Chapter I. The second backbend seen for ^{126}Xe is being reported here for the first time. The increase in the moment of inertia with I may be explained as being due to the Coriolis anti-pairing effect(70), but the backbending phenomenon itself seems to be a result of

Figure 31

Backbending in ^{126}Xe and ^{128}Xe

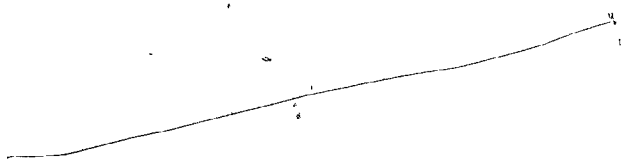

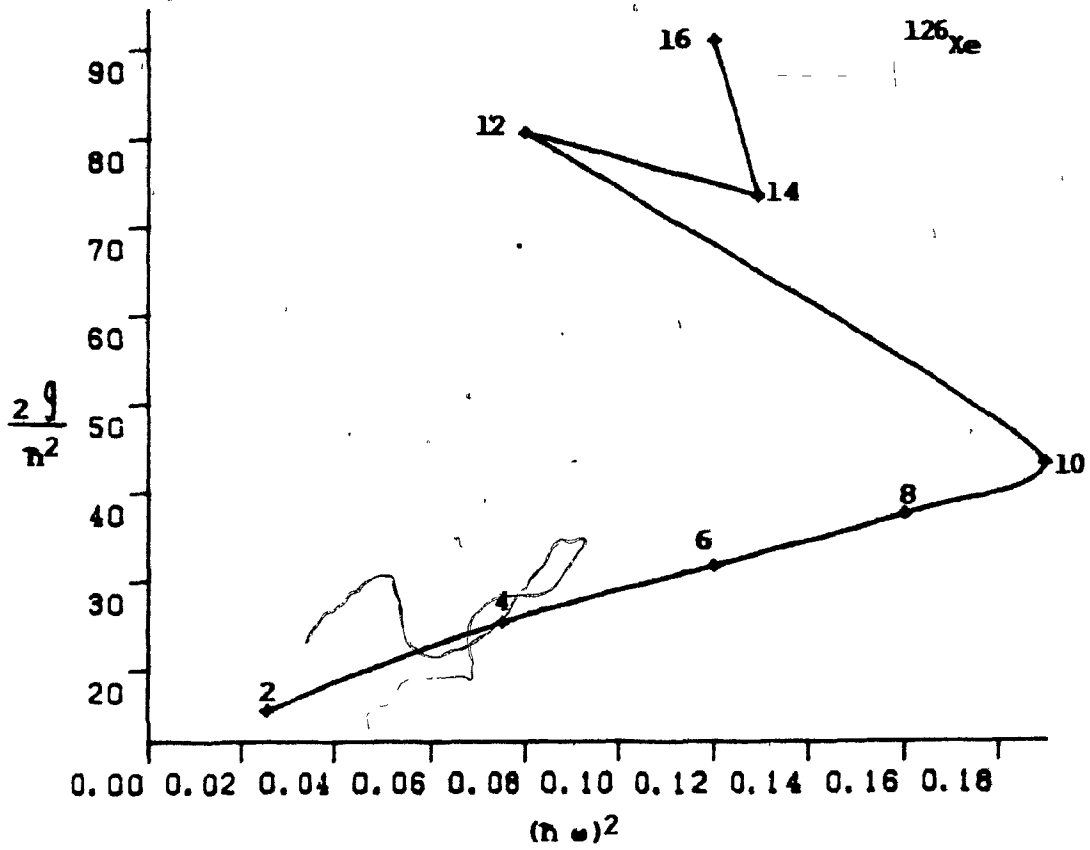
^{126}Xe
16
12
14
10
8
6
4
2
90
80
70
60
50
40
30
20
$\frac{2\mathcal{J}}{\hbar^2}$
0.00 0.02 0.04 0.06 0.08 0.10 0.12 0.14 0.16 0.18
$(\hbar\omega)^2$

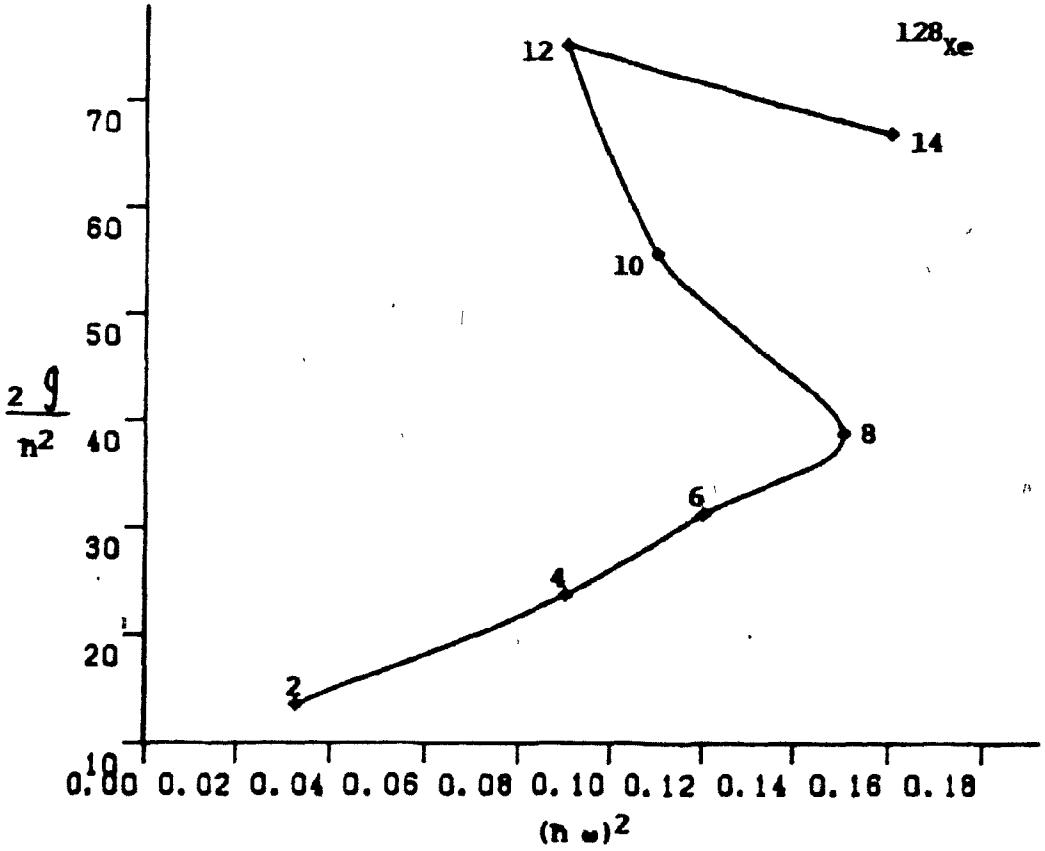
^{128}Xe
12
14
10
8
6
4
2
70
60
50
40
30
20
10
$\frac{2\mathcal{J}}{\hbar^2}$
0.00 0.02 0.04 0.06 0.08 0.10 0.12 0.14 0.16 0.18
$(\hbar\omega)^2$

band crossing(58).

In the ^{116}Te isotope it is found that the energy difference between successive levels is very similar in magnitude. This can be understood from the standpoint of vibrational motion. If the nucleus is considered in analogy to a liquid drop, then its vibration may be represented by harmonic vibrations about an equilibrium shape. Since the vibrations are those of a harmomic oscillator, the energy levels will be equally spaced with separation $\Delta E = h\omega$. The lowest quantum for this type of vibration, called a phonon, is the quadrupole type of deformation and carries an angular momentum of two units and positive parity. One thus expects a $J = 2^+$ first excited state for an even-even nucleus falling in this category.

In conclusion, the nuclei ^{128}Xe, ^{126}Xe and ^{116}Te have been studied using the techniques of I.B.Y. spectroscopy. For the Xenon nuclei new levels at high spin are reported and backbending is observed. For the Tellurium nucleus, the results of previous works have been verified and two tentative new levels are proposed.

REFERENCES

(1) DeShalit and Feshback, "Theoretical Nuclear Physics" - John Wiley & Sons Inc. 1974

(2) M.G. Mayer, Physical Review 75 (1949) 1969

(3) O. Haxel, J.H. Jensen and H.E. Suess, Physical Review 75 (1949) 1766

(4) N. Bohr, J.A. Wheeler, Physical Review 56 (1939) 426

(5) J. Rainwater, Physical Review 79 (1950) 432

(6) A. Bohr, Physical Review 81 (1951) 134

(7) A. Bohr, Dan. Mat. Fys. Medd. 26 (1952) no14

(8) D.L. Hill, J.A. Wheeler, Physical Review 89 (1953) 1102

(9) A. Bohr, B.R. Mottelson, Dan. Mat. Fys. Medd 27 (1953) no. 16

(10) S.G. Nilsson, Matt. Fys. Medd. Dan. Vid. Selsk. 29 (1955) no. 16

(11) F.S. Stephens, Review of Modern Physics, vol. 47, no. 1, Jan. 1975

(12) H. Morinaga, P.C. Gugelot, Nuclear Physics 46 (1963) 210

(13) A. Johnson, Z. Syzmanski, Physical Reports 7C (1973) 182

(14) J.M Blatt, V.F Weisskopf, "Theoretical Nuclear Physics", John Wiley and Sons, New York, (1952) 340-379

(15) H. Morinaga, "Nuclear Structure" , North-Holland Publ. Co., Amsterdam, (1967) 76

(16) H. Morinaga, T. Yamazaki, "In-Beam Gamma-Ray Spectroscopy", North-Holland Publ. Co., (1976) 300

(17) H. Morinaga, T. Yamazaki, "In-Beam Gamma-Ray Spectroscopy", North-Holland Publ. Co., (1976) 305-307

(18) A. Johnson, H. Ryde, J. Sztarkier, Phys. Lett. 34B (1971) 605

(19) A. Johnson, H. Ryde, S.A. Hjorth, Nuclear Phys. A179 (1972) 753

(20) P.M. Lieder, H. Beusher, W.F. Davidson, P. Jahn, H.J. Probst, C. Meyer-Boricke, Phys. Lett. 39B (1972) 196

(21) P. Thieberger, A.W. Sunyar, P.C. Rogers, N. Lark, O.C. Kistner E. der Mateosian, S. Cochavi, E.H Auerbach, Phys. Rev. Lett 19 (1972) 196

(22) L.D. Landau, J. Phys. U.S.S.R. 8, (1944) 201

(23) K.R. Symon, quoted by B. Rossi in "High Energy Particles" pg 32, Prentice Hall, New York, (1952)

(24) C.F. Williamson, J.P. Boujot, J. Picard, "Tables of Range and Stopping Power of Chemical Elements for charged Particles of Energy 0.5 to 500 MeV" Commissarat a L'Energie Atomique, France (1966) 1

(25) H. Ejiri, T. Itahashi, Y. Nagai, T. Shibata, S. Nakayama, T. Kishimato, K. Maeda, H. Sakai and M. Hoshi, Nuclear Physics A305 (1978) 167

(26) H. Sakai, H. Ejiri, T. Shibata, Y. Nagai and K. Okada, Phys. Rev C20 (1979) 464

(27) F.S. Goulding and R.H. Pehl, "Semiconductor radiation detectors." Nuclear spectroscopy and reactions Part A, ed. J. Cerny Vol 40A (1974) 289

(28) R. Hofstadter, Physical Review 74 (1948) 100

(29) M.T. Weber, R.R. Monchamp, J. Appl. Phys, 44 (1973) 5496

(30) H.W. Kraner, "Fast neutron damage in Germanium detectors." Nuclear Science Symposium (1979)

(31) T. Yamazaki, G.T. Evans Nuclear Physics A134 (1969) 81

(32) M. Blann, U.S. Atomic Energy Commision Report No. C00-3494-2 (1978)

(33) M. Blann, Ann. Rev. Nucl. Sci. 25 (1975) 123

(34) V.F. Weisskopf and D.H. Ewing Phys. Rev. 57 (1940) 472

(35) M. Blann, Nuclear Physics 80 (1966)223

(36) H. Morinaga and T. Yamazaki, "In-Beam Gamma-Ray Spectroscopy" North-Holland Publ. Co.(1976)

(37) T. Yamazaki, Nucl. Data A3 (1967) 1

(38) E. der Mateosian and A.W Sunyar, Nucl. Data 13 (1974)391

(39) R.M Diamond, E. Matthias, J.O. Newton and F.S. Stephens, Physical Review Letters 16 (1966) 1205

(40) M. Andersson and Z.P. Sawa, Research Institute of Physics, Stokholm, Ann. Rep. (1973) 9

(41) K.S. Krane, Nucl. Inst. and Meth. 98 (1972) 205

(42) P.R. Bevington, "Data Reduction and Analysis for the Physical Sciences", McGraw-Hill Book Company (1969)

(43) A.C.G. Mitchell, J.Y. Mei, F.C. Maienschein and C.L. Peacock Phys. Rev. 76 no. 10 (1949) 1450

(44) M.L. Perlman and G. Friedlander, Phys. Rev. 82, (1951) 449

(45) M.I. Kalkstein and J.M. Hollander, Phys. Rev. 96 (1954) 730

(46) L. Koerts, P. Macklin, B. Farrelly, R. van Lieshout and C.S. Wu, Physical Review 98 (1955) 1230

(47) H. Morinaga and N.L. Lark, Nuclear Physics 67 (1965) 315

(48) M. Sakai, T. Yamazaki and H. Ejiri, Nuc. Phys. 74 (1965) 81

(49) M.G. Betigeri and H. Morinaga, Nuclear Physics A95 (1967) 176

(50) H. Ejiri, M. Ishihara, M. Sakai, T. Inamura, K. Katori Nuclear Physics 89 (1966) 641

(51) I. Bergstrom, C.J. Herrlander, A. Kerek and A. Luukko, Nuc. Phys., A123 (1969) 99

(52) B. Singh and H.W. Taylor, Nuclear Physics A147 (1970) 12

(53) H. Kusakari, N. Yoshikawa, H. Kawakami, M. Ishihara, Y. Shida and M. Sakai, Nuclear Physics A242 (1975) 13

(54) B.P. Pathak, L. Lessard, L. Nikkinen and I.L. Preiss, Phys. Rev. 14 (1976) 14

(55) C. Droste, L. Goettig, T. Morek, J Srebrny, J. Bucka, J. Dobaczewski, S.G. Rohozinski, Zeitschrift fur Physik A 284 (1978) 297

(56) B. Singh, R. Iafigliola, K. Sofia, J.E. Crawford, J.K.P Lee Physical Review C 19 (1979) 19

(57) L. Goettig, Ch. Droste, A. Dygo, T. Morek, J. Srebrny, R. Broda J. Styczen, J. Hattula, H. Helppi, M. Jaaskelainen, Nuc. Phys. A357 (1981) 109

(58) H. Kusakari, K. Kitao, K. Sato, M. Sugawara, H. Katsuragawa Nuclear Physics A401 (1983) 445

(59) J.D.Reierson, G.C. Nelson, E.N. Hatch, Nuc. Phys. A153 (1971) 109

(60) D.M. Gordon, L.S. Eytel, H. deWaard, D.E. Murnick, Phys. Rev. 12 (1975) 628

(61) R.G. Helmer, C.W. Reich, R.J. Gehrke, R.C. Greenwood, R.A. Anderl Physical Review C 15 (1977) 1453

(62) E.W. Schneider, M.D. Glascock, W.B. Walters, R.A. Meyer Physical Review C 19 (1979) 19

(63) Same as reference 56.

(64) A. Lukko, A. Kerek, I. Rezanka, C.J. Herlander, Nuc. Phys. A95 (1967) 176

(65) R.A. Warner and J.E. Draper, Physical Review C, 1 (1970) 1069

(66) W.G. Wyckoff, J.E. Draper, Physical Review C, 8 (1973) 796

(67) G.M. Gowdy et al., Physical Review C 13 (1976) 1601

(68) A. Gizon et al., Z. Phys. 302 (1981) 79

(69) P. Chowdury, W.F. Piel, D.B. Fossan, Phys. Rev. C 25 (1982) 813

(70) H. Morinaga and T, Yamazaki, "In-Beam Gamma-Ray Spectroscopy" North-Holland Publ. Co. (1976) 349